15. Effect of expansion/shrinkage of crystal lattice on hydrogen isotopes behavior in body-centered cubic metals

Yamauchi Daisuke, Takuji Oda and Satoru Tanaka
Department of Nuclear Engineering and Management, The University of Tokyo,
Hongo 7-3-1, Bunkyo-ku, Tokyo 113-8656, Japan, azuma@flanker.q.t.u-tokyo.ac.jp

Abstract

Effects of shrinkage/expansion of crystal lattice on the diffusivity and the solubility of hydrogen isotopes in bcc-metals were investigated. In order to obtain systematic and detailed information, an energy was decomposed into two parts: *potential-energy-of-hydrogen* and *elastic-energy*. Both of the migration barrier and the solution energy of hydrogen were increased by lattice shrinkage and were decreased by lattice expansion, basically. Change of migration barrier was mainly subject to that of *elastic-energ.* However, when the crystal lattice was strongly shrunk, e.g. 5% shrinkage, the migration barrier was decreased due to an abrupt decrease of *potential-energy-of-hydrogen*, which resulted from increasing interaction between the hydrogen atom and the second-nearest neighbor metal atoms.

Keywords: hydrogen isotopes, DFT, bcc metals, solubility, diffusivity

1. Introduction

A part of bred tritium stays in fusion blanket materials, and causes increase of tritium inventory in materials [1]. In addition, leakage of tritium from the blanket have a risk that radioactive products diffuse out of the reactor, which are subjects not only for safety handling of tritium but also for establishing an economical fuel cycle [2]. In order to evaluate and reduce the amount of tritium inventory and leakage, it is important to understand how hydrogen isotopes stay and diffuse in materials under reactor conditions.

In previous works, hydrogen diffusivities and solubilities in bcc metals have been widely determined by experiments [3], and migration paths of hydrogen on the surfaces or in the bulk have been investigated in several bcc metals by computer simulations [4]. In realistic reactor conditions, it is anticipated that constitutional atoms of alloys or defects generated in materials induce a local shrinkage or expansion of crystal lattice, which may affect the tritium behavior in reactor conditions [5]. In the present paper, therefore, we studied the influence of lattice shrinkage/expansion on diffusion of hydrogen isotopes in bcc metals by using quantum mechanical calculations, in order to obtain fundamental knowledge on the behavior of hydrogen isotopes in reactor conditions. We conducted calculations mainly with bcc-W, which attracts attention as a promising candidate of the first wall material [6].

2. Calculation method

Quantum mechanical calculations were performed using VASP code [7] of density functional theory (GGA-PBE functional) with plane-wave basis set and PAW potential. All calculations were performed under a spin-polarized condition. Crystalline structures of body-centered cubic (bcc) metals were modeled by a 2×2×2 supercell (16 atoms in a unit cell) or a 3×3×3 supercell (54 atoms) with three-dimensional periodic boundary condition. Energy cut-off and k-point sampling point grid were set to 360 eV and 5×5×5, respectively.

At first, we optimized the lattice constants with fixing fractional coordinates of all the atoms contained in the unit cell. Then, the optimized lattice constants were isotropically changed by -5%, -2%, 0%, 2% and 5%. Hereafter, these shrunk/expanded cells are described as “0.95-cell”, “0.98-cell”, “1.00-cell”, “1.02-cell” and “1.05-cell”, respectively. After introduction of one H atom into certain sites of those cells, positions of all the atoms were optimized with fixing the cell parameters, in order to evaluate the migration barrier and the solution energy of hydrogen as a function of lattice shrinkage/expansion ratio.

3. Results

3.1. Typical sites of an interstitial hydrogen atom

Γ It is known that the most stable site for an interstitial H atom in bcc metals is tetrahedral site (T site) surrounded by four metal atoms, and that the transition site for diffusion of an interstitial H atom is trigonal site (Tri site) surrounded by three metal atoms [8]. The present calculation results agreed with them. The migration barrier corresponding to the difference of energies between a system of T site and a system of Tri site was evaluated as 0.21 eV.

The migration path through octahedral site (O site) surrounded by six metal atoms held a comparable energy

barrier (0.38 eV). Hence, the path through O site was also studied in the present paper. Note that these barriers calculated in the present study with PBE functional were well consistent with values calculated with PW91 functional [9].

3.2. Effects of lattice shrinkage/expansion on migration barrier of hydrogen

Fig. 1 shows change in migration barrier and solution energy of hydrogen due to shrinkage/expansion of crystal lattice. In the case of migration path through Tri site, the migration barrier was increased by lattice shrinkage and was decreased by lattice expansion. By 1% of lattice shrinkage/expansion, changes of the migration barrier were several tens meV, corresponding to several % of the original value.

In the case of migration path through O site, the same tendency was obtained for small shrinkage (-2~0%) and expansion (0~5%) of lattice. However, a larger shrinkage (> ~5%) induced an abrupt decrease of the migration barrier.

3.3. Effects of lattice shrinkage/expansion on solution energy of hydrogen

As shown in Fig. 1, the solution energy was increased by lattice shrinkage and was decreased by lattice expansion. By 1% of lattice shrinkage/expansion, changes in the solution energy were several hundreds meV, corresponding to 10~15 % of the original value. It was found that the solution energy is more strongly affected by lattice shrinkage/expansion than the migration barrier.

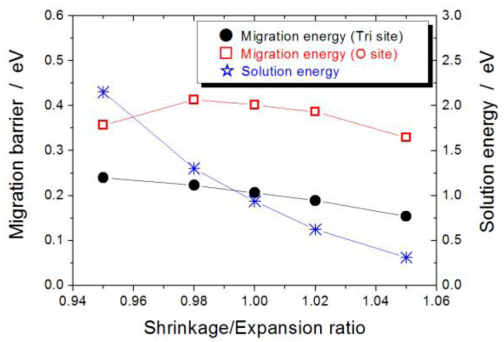

Fig. 1 The migration barrier and the solution energy of hydrogen as a function of shrinkage/expansion ratio. The left axis is for migration barrier and the right for solution energy.

4. Discussion

4.1. Energy decomposition into two parts

For further discussion, we divided an energy into two components as suggested by Fukai [8]: (i) potential energy of hydrogen atom in a metal lattice (*potential-energy-of-hydrogen*: ${}^{i}E_{0}^{j}$) and elastic energy of lattice deformation (*elastic-energy*: ${}^{i}E_{L}^{j}$). The superscripts *i* and *j* represents the system of *i*-cell (*i* is 0.95, 0.98, 1.00, 1.02 or 1.05) of *j*-site (*j* is T, Tri or O). Details have been given elsewhere [10].

4.2. *Potential-energy-of-hydrogen* (${}^{i}E_{0}^{j}$)

Potential-energy-of-hydrogen (${}^{i}E_{0}^{j}$) and its difference from that in the 1.00-cell (${}^{i}E_{0}^{j}$- ${}^{1.00}E_{0}^{j}$) are shown in Fig. 2. It has been reported that by introduction of a H atom into an interstitial site, metal atoms are displaced outer. Consequently, the valley of potential energy becomes deeper and wider, and thus the wave function of hydrogen spreads so that potential energy and kinetic energy of hydrogen are lowered [8]. This is the reason why ${}^{i}E_{0}^{j}$ generally took a negative value.

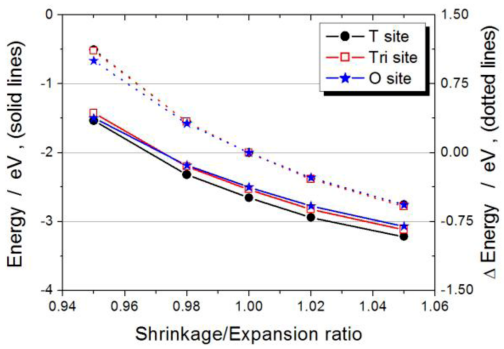

Fig. 2 Change of *potential-energy-of-hydrogen* as a function of shrinkage/expansion ratio. The plots connected by a solid line represents the absolute values (left axis), while those connected by a dotted line represents the difference from the value of 1.00-cell (right axis).

The distances from an interstitial H atom to adjacent metal atoms are given in Table 1. In any site, the distance between the H and the first-nearest neighbor W atom was lengthened by geometry optimization. This result indicates that the energetically most favorable H-W distance is longer than the initial H-W distance before geometry optimization, which is the reason why *potential-energy-of-hydrogen* was increased by lattice shrinkage and was decreased by lattice expansion.

When the crystal lattice is strongly shrunk, e.g. 5% shrinkage (0.95-cell), an abrupt decrease of the migration barrier was observed as shown in Fig. 1. This non-linear variation of the migration barrier seems to come from increasing interaction between the H atom and the second-nearest neighbor W atom. From H-W distances listed in

Table 1, it can be considered that an energetically favorable H-W distance is located at ~1.8 Å. In the case of O site, the distance between the H atom and the second-nearest neighbor W atom was 2.25 Å in the 1.00-cell. The distance was reduced when the lattice is shrunk, i.e. 2.12 Å in the 0.95-cell. Hence, it is expected that the interaction between the H atom and the second-nearest neighbor W atom was strengthened by shrinkage, which caused a decrease of *potential-energy-of-hydrogen*.

This effect should depend on the distance between the H atom and the second-nearest neighbor W atom. As shown in Table 1, the distance was the shortest in O site and the longest in T site among the three sites. This is the reason why *potential-energy-of-hydrogen* was significantly lowered by 5% lattice shrinkage (0.95-cell) in O site. Similarly, also in Tri site, *potential-energy-of-hydrogen* was reduced slightly in the 0.95-cell, although its degree was smaller than that in O site. This is because the distance between the H atom and the second-nearest neighbor W atom was longer in Tri site than that in O site.

Table 1 Distance between an interstitial hydrogen atom and the first-nearest/second earest neighbor W atoms before/after relaxation of atomic positions.

		Unrelaxed (eV)	Relaxed (eV)	
		1.00-cell	1.00-cell	1.05-cell
T site	1st	1.77	1.84	1.75
	2nd	2.86	2.87	2.72
Tri site	1st	1.68	1.78 1.81	1.68 1.74
	2nd	2.31	2.31	2.17
O site	1st	1.59	1.74	1.66
	2nd	2.24	2.25	2.12

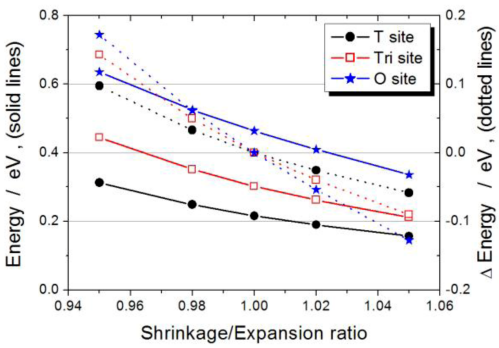

Fig. 3 Change of *elastic-energy* as a function of shrinkage/expansion ratio. The plots connected by a solid line represents the absolute values (left axis), while those connected by a dotted line represents the difference from the value of 1.00-cell (right axis).

4.3. *Elastic-energy*

Elastic-energy (${}^{i}E_{L}^{j}$) and its difference from the value of 1.00-cell (${}^{i}E_{L}^{j}$- ${}^{1.00}E_{L}$) are shown in Fig. 3. The values of ${}^{i}E_{L}^{j}$ were positive and the absolute values of ${}^{i}E_{L}^{j}$ were lower than those of ${}^{i}E_{0}^{j}$ by an order of magnitude. For example, the energy change by 1% lattice expansion was about 0.030 eV in O site, 0.025 eV in Tri site and 0.020 eV in T site.

Elastic-energy should depend on (i) the distance between H atom and the first-nearest neighbor W atom (W^{1st}), and (ii) the facility for W^{1st} to relax when H atom is inserted closely. If the distance between W^{1st} and a W atom (W') existing on the extension of line connecting the H atom and W^{1st} is short, it is difficult for W^{1st} to displace outer so as to reduce repulsive forces between H-W^{1st}. Hence, the effect of the point (ii) could depend mainly on W^{1st}-W' distance. Note that these distances should be the ones before optimization of atomic positions, because the values after geometry optimization are affected by both (i) and (ii). As listed in Table 1, H-W^{1st} distances before geometry optimization are 1.72 Å for O site, 1.77 Å for Tri site and 1.84 Å for T site. The W^{1st}-W' distance is 3.01 Å for O site, while it was not short for Tri site and T site. Therefore, it is anticipated that ${}^{i}E_{L}^{j}$ has the largest value in O site and the smallest value in T site, which was consistent with calculation results.

By the same consideration, it is clear that *elastic-energy* is increased by lattice shrinkage and is decreased by lattice expansion, because both H-W^{1st} and W^{1st}-W' distances before geometry optimization are totally proportional to shrinkage/expansion ratio.

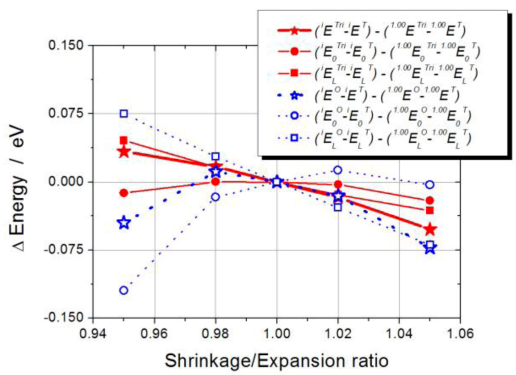

Fig. 4 Change in Migration barrier and the terms of *potential-energy-of-hydrogen* and elastic-energy contributing to the migration barrier due to lattice shrinkage/expansion.

4.4. Migration barrier

The difference of the barrier for hydrogen migration through *j*-site between *i*-cell and 1.00-cell are shown in Fig. 4, together with the two components.

In the case of small shrinkage (<2%) and expansion (< 5%) of lattice, the migration barrier was almost linearly increased and decreased by lattice shrinkage and expansion, respectively. In this shrinkage/expansion range, as *potential-energy-of-hydrogen* has almost the same value, the linear response mainly comes from a linear variation in *elastic-energy*. However, when the crystal lattice was strongly shrunk, e.g. 5% shrinkage (0.95-cell), the migration barrier was decreased due to the abrupt decrease of *potential-energy-of-hydrogen*.

5. Conclusion

Effects of shrinkage/expansion of crystal lattice on the diffusivity and the solubility of hydrogen isotopes in bcc-metals were investigated. In order to obtain systematic and detailed information, an energy was decomposed into two parts: *potential-energy-of-hydrogen* and *elastic-energy*. Both of the migration barrier and the solution energy of hydrogen were increased by lattice shrinkage and were decreased by lattice expansion, basically. Change of the migration barrier was mainly subject to that of *elastic-energy.* However, when the crystal lattice was strongly shrunk, e.g. 5% shrinkage, the migration barrier was decreased due to an abrupt decrease of *potential-energy-of-hydrogen*.

References

[1] P. Jung, J. Nucl. Mater. 258–263 (1998) 124.
[2] M. Rubel, Fusion Sci. Technol. 49 (2006) 465-473.
[3] H. Addach, P. Bercot et al., Mater. Letters 59 (2005) 1347-1351.
[4] D.C. Sorescu, Catalsys Today 105 (2005) 44-65.
[5] S. Mori, S. Yamazaki, J. Adachi et al., Fus. Eng. Des. 18 (1991) 249.
[6] J. Xu et al., Nucl. Inst. Meth. B, in press.
[7] G. Kresse, J. Furthmüller, Phys. Rev. B 54 (1996) 11169.
[8] Y. Fukai, The Metal-Hydrogen System, Springer, Berlin (2005).
[9] Y.L. Liu et al., J. Nucl. Mater. 390-391 (2009) 1032-1034.
[10] D. Yamauchi, T. Oda, Y. Oya, S. Tanaka, submitted to Proceedings of ICFRM-14.

Effect of expansion/shrinkage of crystal lattice on stability of hydrogen isotopes in bcc metals

Daisuke Yamauchi[1], Takuji Oda[1], Yasuhisa Oya[2], Satoru Tanaka[1]

[1]*Department of Nuclear Engineering and Management: The University of Tokyo, Tokyo, Japan*

[2]*Radioscience Research Laboratory, Faculty of Science: Shizuoka University, Shizuoka, Japan*

A part of bred tritium stays in the blanket of fusion reactor, and causes decrease of fuel recovery and embrittlement of materials. In addition, permeability and leakage of tritium from constructual materials have a risk that radioactive products diffuse out of the reactor. In order to evaluate and reduce the amounts of tritium inventory and leakage, it is inevitable to understand how hydrogen isotopes stay and diffuse in materials under the reactor conditions. In the reactor conditions, it is anticipated that defects generated in the materials induces local expansion or shrinkage of crystal lattice. Therefore, we analyze the influence of expansion/shrinkage of materials on diffusion of hydrogen isotopes using quantum mechanical calculations, in order to obtain fundamental knowledge with respect to modeling of the diffusion behavior of hydrogen isotopes in metal materials.

Quantum mechanical calculations were performed by VASP code based on density functional theory (GGA-PBE functional). Body-centered cubic metals (Fe, Cr, Mo, W, etc) were modeled with three-dimension periodic boundary condition. Total energies were evaluated on structures whose lattice constants were isotropically expanded or shrunk by -2%, -1%, 1% or 2% from those of the optimized structure. The stability of hydrogen isotopes around metal atoms was investigated.

It is known that the most stable site for hydrogen atom is the tetrahedral site of four coordinates in body-centered cubic metals. This fact was reproduced properly in the calculations. The trigonal site of three coordinates was evaluated as the transitional state of hydrogen atom migrating between two neighboring tetrahedral sites. The total energies of structures increased when the crystal lattices were expanded or shrunk. This tendency was observed whether hydrogen atom exists at the tetrahedral site or at the trigonal site. However, the increment in the trigonal site was larger when the crystal lattices were expanded, and smaller when they were shrunk, than that in the tetrahedral site. Diffusion barriers of hydrogen decreased by lattice expansion and increased by lattice shrinkage. We discussed the mechanism in the decrease of diffusion barriers by separating the stability of hydrogen into two parts: the solution energy of hydrogen in the relaxed lattice and the elastic energy of the surrounding lattice.

The University of Tokyo

Effect of expansion/shrinkage of crystal lattice on hydrogen isotopes behavior in body-centered cubic metals

Daisuke Yamauchi[*1], Takuji Oda[*1], Yasuhisa Oya[*2], Satoru Tanaka[*1]
[*1] The University of Tokyo
[*2] Shizuoka University

The University of Tokyo

Background

< Understanding of tritium behavior in metal material for fusion reactor >

<issues for engineering>
- ✓ permeation, leakage
- ✓ retention
- ✓ contamination

⟷

<elementary processes>
- ✓ ad/ab/de-sorption
- ✓ solution
- ✓ trap/detrap
- ✓ diffusion

In most issues, elementary processes are common.
⇒ Understanding of elementary processes enables to approach to several issues at once.

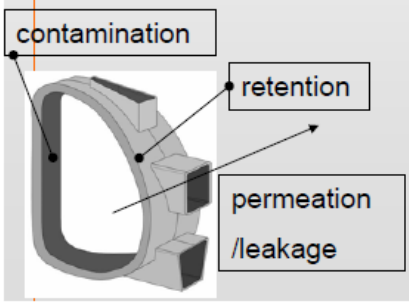

◆ Solubilities and diffusivities of H in alloys have not been systematically understood.

◆ Modeling to connect "issues for engineering" and "elementary processes" have not been well established.

The University of Tokyo

Method for tritium behavior modeling

◆ For approaching to issues of practical materials, continuous evaluation over micro, mezzo and macro scales is important.

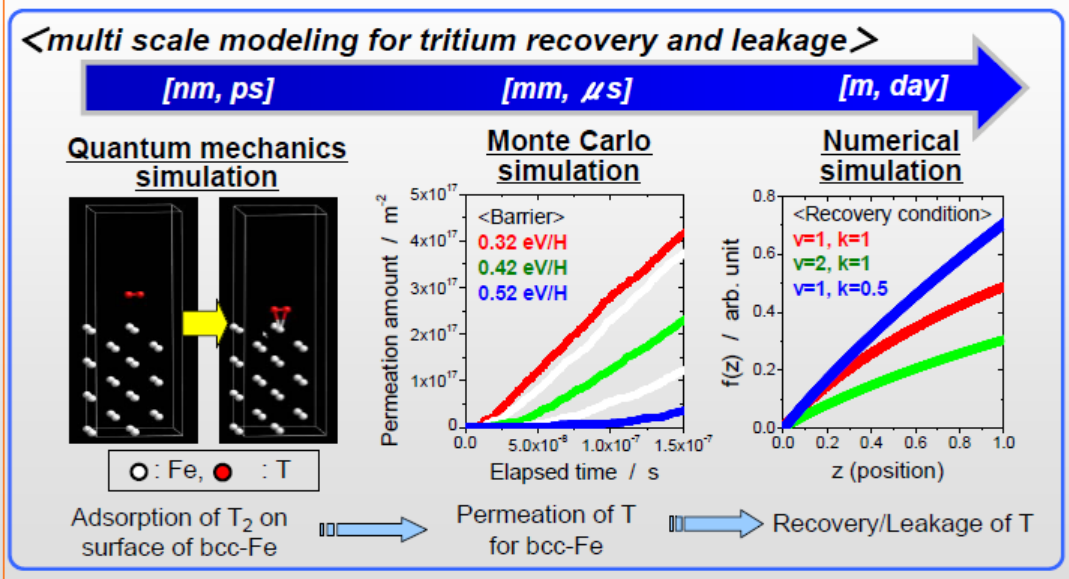

◆The present study aims to deepen understandings of T diffusion and solution behaviors in bcc metals.

The University of Tokyo

Research objective

Focused on bcc metals:

- ◆ bcc-Fe: base material of some alloys like F82H
- ◆ W: first wall material
- ◆ V alloys: advanced structural materials

✓ Alloy elements

✓ Impurities

✓ Defects induced by irradiation damage.

⇒ Locally expanded/shrunk structure

Effect of expansion/shrinkage on hydrogen solution and diffusion behaviors

<Objective>

Understanding and modeling solution and diffusion behaviors of hydrogen in expanded/shrunk crystal lattice of bcc metals, by using quantum mechanical calculation.

The University of Tokyo

Contents

Procedure of quantum mechanical calculation

① Nature of hydrogen in bcc metals

1.Benchmark	Lattice constant and solution energy of H
2.Benchmark	Stable state and transition state for diffusion of H
3.Result	H stable position (anti-bonding orbitals)
4.Discussion	Reason of difference in diffusion barrier

② Effect of expansion/shrinkage of crystal lattice

1.Result	Change of solution energy and diffusion barrier
2.Discussion	Dividing an energy into 2 components
3.Discussion	Solution energy
4.Discussion	Diffusion barrier
5.Discussion	Elastic energy
6.Disscusion	Potential energy of H

Conclusions

The University of Tokyo

Procedure of quantum mechanical calculation

VASP code
- ✓ **Density functional theory (DFT)**
- ✓ **GGA-PBE functional**
- ✓ **Plane wave basis set + PAW potential**
- ✓ **3D periodic boundary condition**
  :3×3×3 supercell (54 metal atoms)

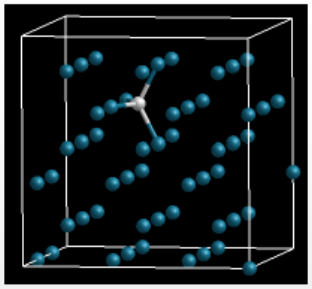

$M_{54}H_1$

(1) bcc metals (Fe,V,Ta,Cr,W,Mo)

1. Optimization of lattice constants
2. Geometry optimization of all atoms including an interstitial H
3. Evaluation of solution energy and diffusion barrier

(2) expanded/shrunk W

1. Geometry optimization of $W_{54}H$ whose lattice constants were expanded or shrunk (−5%, −2%, 2%, 5%).
2. Evaluation of solution energy and diffusion barrier

The University of Tokyo

Contents

Procedure of quantum mechanical calculation

① Nature of hydrogen in bcc metals

1.Benchmark Lattice constant and solution energy of H
2.Benchmark Stable state and transition state for diffusion of H
3.Result H stable position (anti-bonding orbitals)
4.Discussion Reason of difference in diffusion barrier

② Effect of expansion/shrinkage of crystal lattice

1.Result Change of solution energy and diffusion barrier
2.Discussion Dividing an energy into 2 components
3.Discussion Solution energy
4.Discussion Diffusion barrier
5.Discussion Elastic energy
6.Disscusion Potential energy of H

Conclusions

The University of Tokyo

Benchmark Lattice constant and solution energy of H

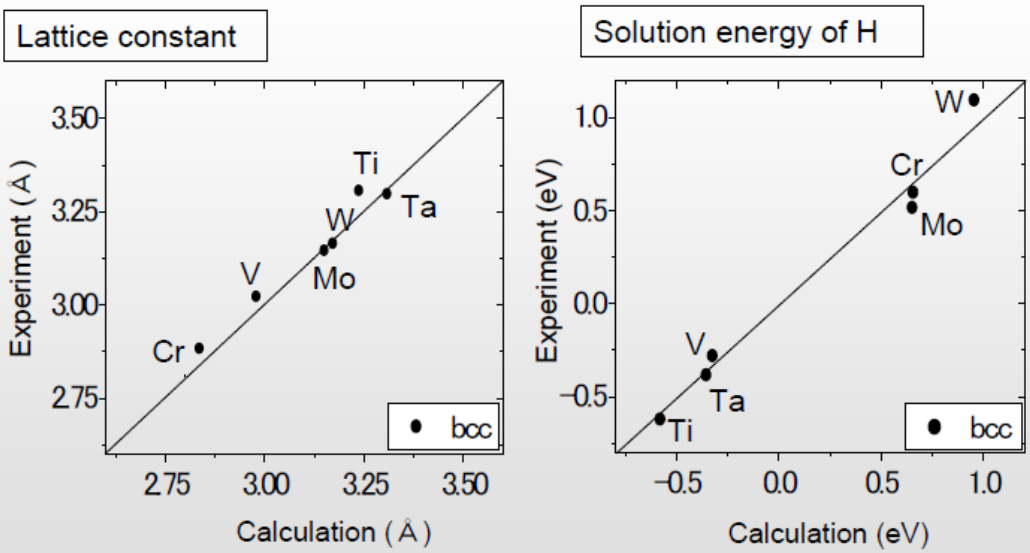

Calculation results corresponded to experimental date well.

*metal date book 2nd edition

The University of Tokyo

Benchmark Stable state and transition state for diffusion of H

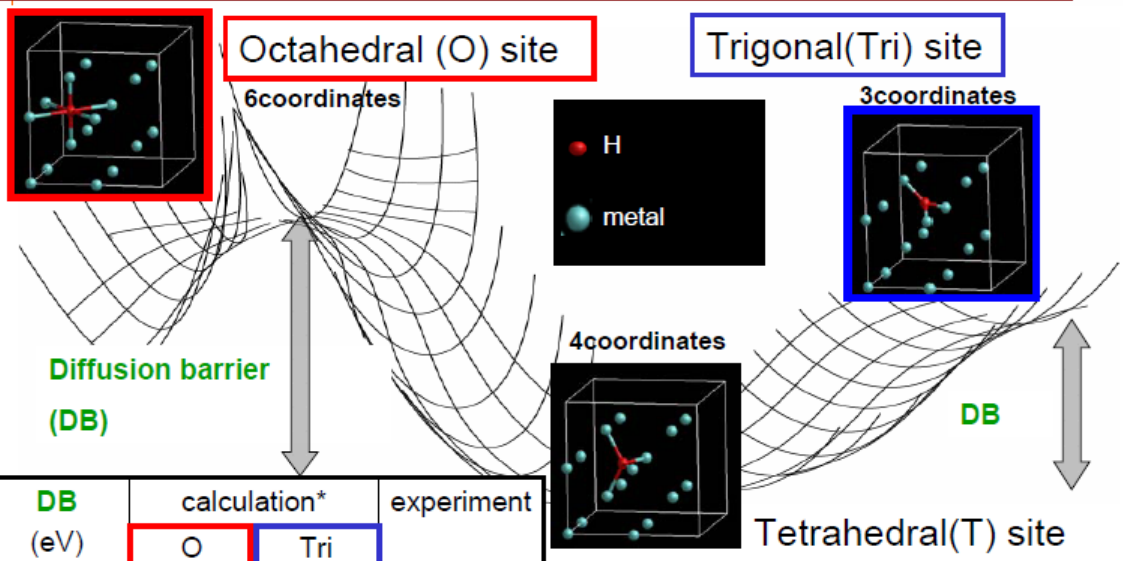

DB (eV)	calculation*		experiment
	O	Tri	
Fe	0.14	0.09	0.04-0.06
V	0.17	0.08	0.05-0.11
Ta	0.36	0.18	0.04-0.17
W	0.38	0.21	0.25-0.40

*Barriers were overestimated due to no counting of zero-point vibrational energy.

This method is available for metal-H system.

*D.E.Jiang, et al ,Physical Review B 70 (2004) 064102

The University of Tokyo

Contents

Procedure of quantum mechanical calculation

① Nature of hydrogen in bcc metals

1.Benchmark Lattice constant and solution energy of H
2.Benchmark Stable state and transition state for diffusion of H
3.Result Stable position of H (anti-bonding orbitals)
4.Discussion Reason of difference in diffusion barrier

② Effect of expansion/shrinkage of crystal lattice

1.Result Change of solution energy and diffusion barrier
2.Discussion Dividing an energy into 2 components
3.Discussion Solution energy
4.Discussion Diffusion barrier
5.Discussion Elastic energy
6.Disscusion Potential energy of H

Conclusions

The University of Tokyo

Stable position of H (anti-bonding orbitals)

Anti-bonding oribital

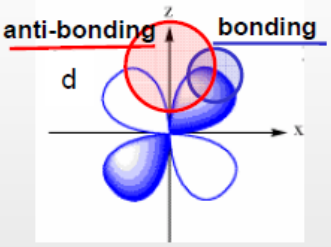

Some bonding with d-orbital has anti-bonding nature.
>> W 5d and H 1s form anti-bonding orbitals.

Electronic density in W

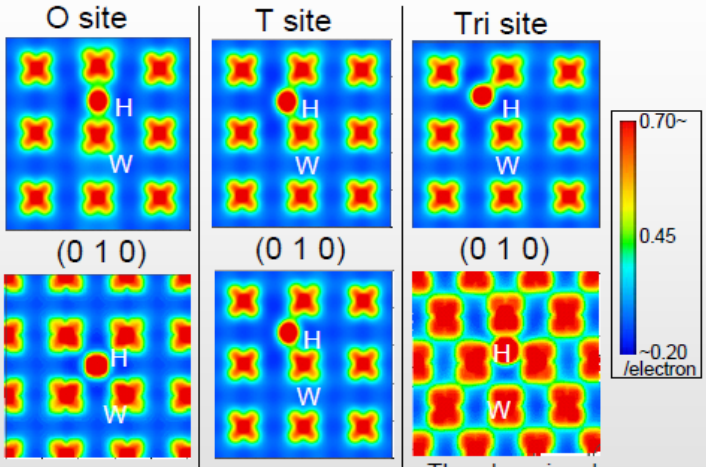

anti 2 | anti 0 | anti 1

The plane involves 3 coordinate atoms

O site occupies 2 anti-bonding orbitals, T site 0 and Tri site 1.
Hence, T site is the most stable position of H.

The University of Tokyo

Reason of difference in Diffusion barrier

Electronic density of O site in Fe(3d), Mo(4d) and W(5d)

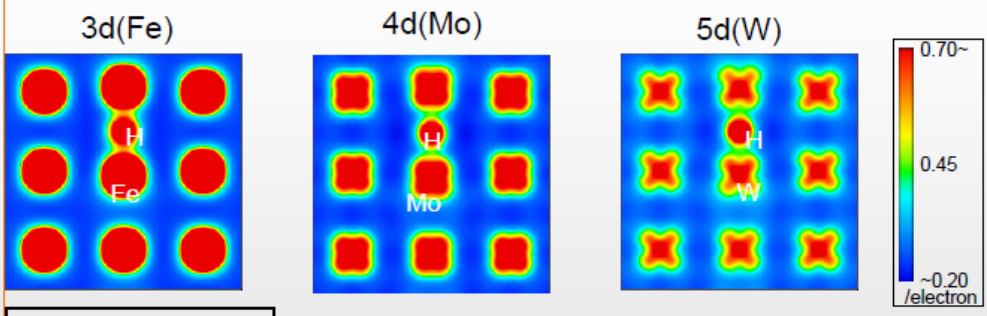

Diffusion barrier

DB (eV)	calculation* O	calculation* Tri	experiment
Fe	0.14	0.09	0.04-0.06
V	0.17	0.08	0.05-0.11
Ta	0.36	0.18	0.04-0.17
W	0.38	0.21	0.25-0.40

The electronic density of 5d-orbital is more directional than 3d and 4d, which may induce:

✓a stronger anti-bonding nature, and thus

✓a larger diffusion barrier.

The University of Tokyo

Contents

The University of Tokyo

1.Result Change of solution energy and diffusion barrier

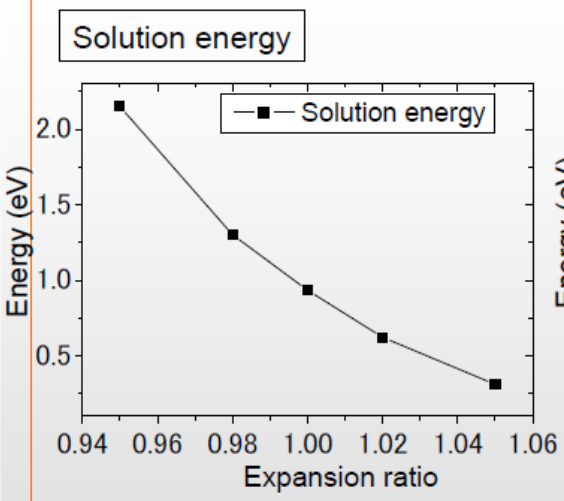

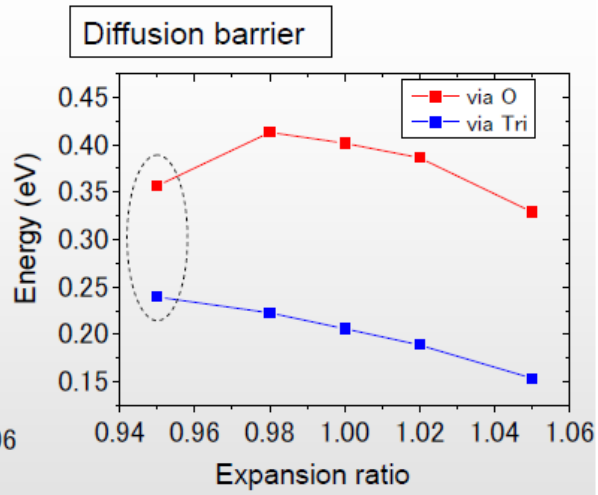

- Solution energy and diffusion barrier were decreased by lattice expansion and increased by lattice shrinkage, basically.
- Diffusion barrier via O site in 5% shrunk lattice was reduced abruptly.

The University of Tokyo

Contents

Procedure of quantum mechanical calculation

① Nature of hydrogen in bcc metals

1.Benchmark	Lattice constant and solution energy of H
2.Benchmark	Stable state and transition state for diffusion of H
3.Result	H stable position (anti-bonding orbitals)
4.Discussion	Reason of difference in diffusion barrier

② Effect of expansion/shrinkage of crystal lattice

1.Result	Change of solution energy and diffusion barrier
2.Discussion	Dividing an energy into 2 components
3.Discussion	Solution energy
4.Discussion	Diffusion barrier
5.Discussion	Elastic energy
6.Disscusion	Potential energy of H

Conclusions

The University of Tokyo

2.Discussion Dividing an energy into 2 components

E_0 : decrease in potential energy of H atom due to interaction with metal lattice (potential energy of H)

$$= E\left[\mathrm{M}_{54}\,(\mathrm{relaxed})\,\mathrm{H}_1\right] - \left(E\left[\mathrm{M}_{54}\,(\mathrm{relaxed})\right] + E\left[\mathrm{H}_1\right]\right)$$

E_L :elastic energy of lattice deformation (elastic energy)

$$= E\left[\mathrm{M}_{54}\,(\mathrm{relaxed})\right] - E\left[\mathrm{M}_{54}\,(\mathrm{unrelaxed})\right]$$

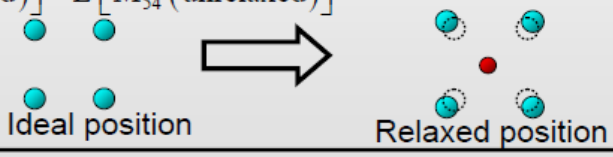

Solution energy (H) and diffusion barrier (DB) are followed by

$$H = E_0^T + E_L^T + \tfrac{1}{2}E\left[\mathrm{H\text{-}H}\right] \qquad DB = \left\{E_0^{Tri} - E_0^T\right\} + \left\{E_L^{Tri} - E_L^T\right\}$$

Reference: metal hydrogen system Yuh Fukai et al

The University of Tokyo

3.Discussion Solution energy

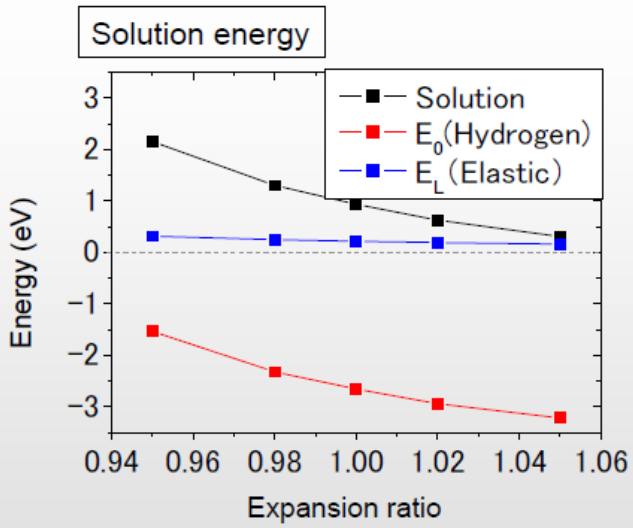

Solution energy= E_0(Hydrogen) + E_L(Elastic)+1/2E[H-H](binding energy)

Solution energy is mainly subject to potential energy of H.

The University of Tokyo

Contents

Procedure of quantum mechanical calculation

① Nature of hydrogen in bcc metals

1.Benchmark Lattice constant and solution energy of H
2.Benchmark Stable state and transition state for diffusion of H
3.Result H stable position (anti-bonding orbitals)
4.Discussion Reason of difference in diffusion barrier

② Effect of expansion/shrinkage of crystal lattice

1.Result Change of solution energy and diffusion barrier
2.Discussion Dividing an energy into 2 components
3.Discussion Solution energy
4.Discussion Diffusion barrier
5.Discussion Elastic energy
6.Disscusion Potential energy of H

Conclusions

The University of Tokyo

4.Discussion Diffusion barrier

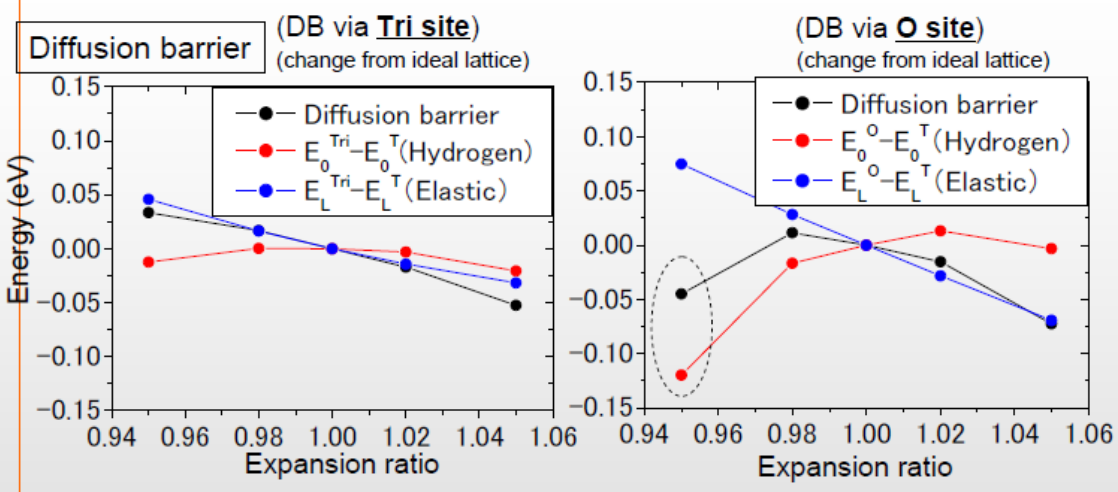

◆The change of diffusion barrier is almost the same with that of elastic energy in the case of expansion or small shrinkage(<2%) of lattice.

◆ In 5% shrunk lattice, diffusion barrier through O site decreased due to a decrease of potential energy of H.

The University of Tokyo

5.Discussion Elastic energy (E_L)

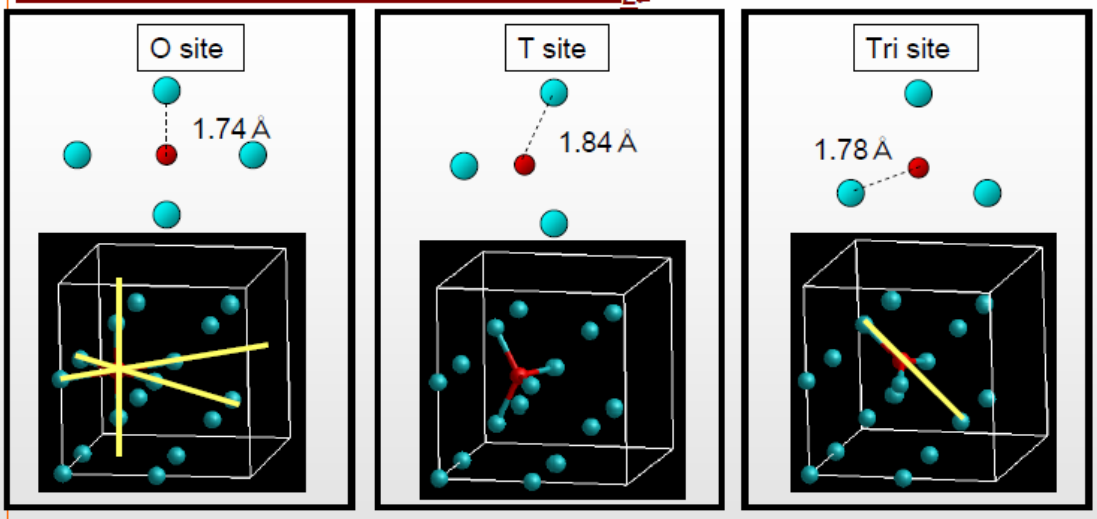

Elastic energy should depend on two points.

✓ Interatomic distance between the H atom and the first-nearest neighbor W.

✓ Facility of relaxation (outer displacement) of the first-nearest neighbor W.

O site > Tri site > T site

The University of Tokyo

6.Disscusion Potential energy of H (E_0)

Why potential energy of H for O site migration decreased by 5% shrinkage?

Distance from H to and the adjacent atoms

		ideal(Å)	5%shrunk(Å)
T site	1st	1.84	1.75
	2nd	2.87	2.72
Tri site	1st	1.78	1.68
	2nd	1.81	1.74
	3rd	2.31	2.17
O site	1st	1.74	1.66
	2nd	2.25	2.12

✓In T site, the distance between the H atom and the first-nearest neighbor W is ~1.8 Å, which could be a energetically favorable interatomic distance.

✓By 5% shrinkage, the distance between the H atom and the second-nearest neighbor W is shortened (~2.1 Å). Consequently, an additional interaction with the second-nearest neighbor W emerges, and thus the potential energy of H is lowered.

The University of Tokyo

Conclusions

The solution and diffusion behaviors of hydrogen isotopes in expanded/shrunk crystal lattice of bcc metals were studied using quantum mechanical calculation.

- The difference in stabilities of T/Tri/O sites could come from the anti-bonding nature in interaction between metal d-orbital and H 1s orbital.
- The anti-bonding nature is stronger when the d-orbital is more directional: i.e. 5d > 4d > 3d. A stronger directionality of electronic density in d-orbital would induce a larger diffusion barrier: W,Ta > Fe,V
- Effects of lattice shrinkage/expansion on solution energy of H is mainly subject to potential energy of H.
- Effects of lattice shrinkage/expansion on diffusion barrier of H is:
  - ✓ mainly subject to elastic energy, for expansion or small shrinkage (< ~2%)
  - ✓ However, a large shrinkage (~ 5%) causes a decrease of diffusion barrier, because interaction between H atom and the second-nearest neighbor W atoms are strengthened due to decrease of interatomic distance.

16.

Analysis of tritium in-pile release measurements in Exotic irradiation experiments

Alexander Fedorov
Lida Magielsen
Marcel Stijkel

NRG, Petten
The Netherlands

Outline of the talk

- Introduction
- Design of EXOTIC experiments
- Tritium residence time measured in temperature transition experiments
  - Definitions
  - Temperature reconstruction
  - Fitting procedure
- Conclusions

2

EXOTIC- EXtraction Of Tritium In Ceramics

- The EXOTIC program, started in 1985, aims at characterization of tritium release properties and mechanical stability of lithium containing ceramics
- Li containing ceramic materials irradiated in the Exotic program varied in composition, ^{6}Li abundance, production method and supplier

3

Test Breeder Modules for ITER

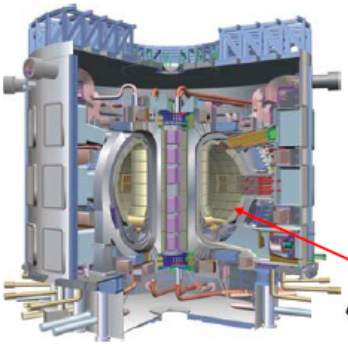

Fusion reaction:
$D + T \rightarrow {}^{4}He + n$ (Q = 17.6 MeV)

Required tritium is produced in the breeder
$n + {}^{6}Li \rightarrow T + {}^{4}He$

Li_2TiO_3 pebbles

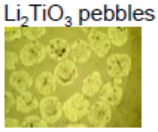

or Li_4SiO_4 pebbles

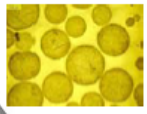

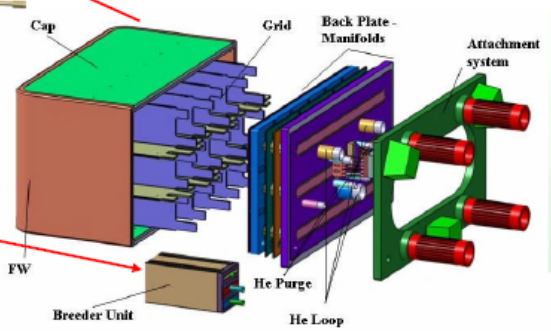

Helium Cooled Pebble Bed EU concept

4

Ideal breeder

- Absorb neutrons (as many as possible)
  - → generation of tritium (high ^{6}Li concentration)
  - → extraction of heat suitable for generation of electricity
- Low tritium inventory
- Mechanical and structural stability
- High and stable thermal conductivity

For the EU TBM two concepts are considered:

- HCPB: Helium Cooled Pebble Bed with ^{6}Li containing ceramics Li_2TiO_3, Li_4SiO_4
- HCLL: Helium Cooled Lithium Lead eutectic: Pb17Li

5

Design of EXOTIC experiment

One ring design

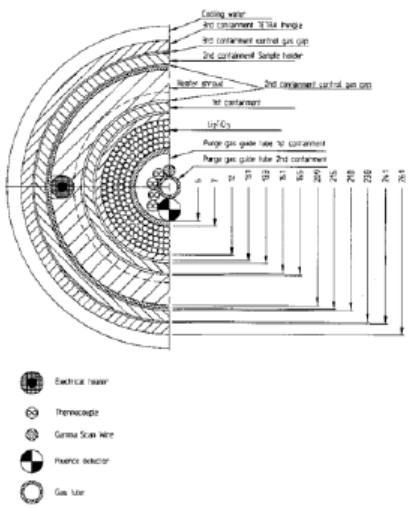

Three rings design

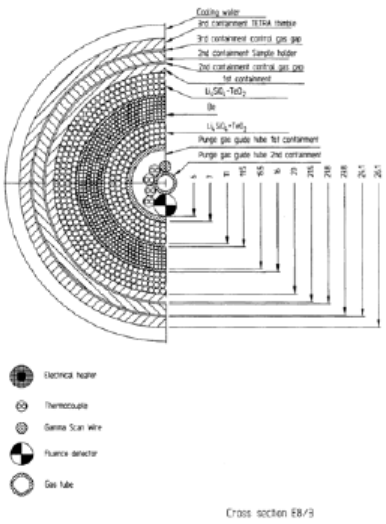

6

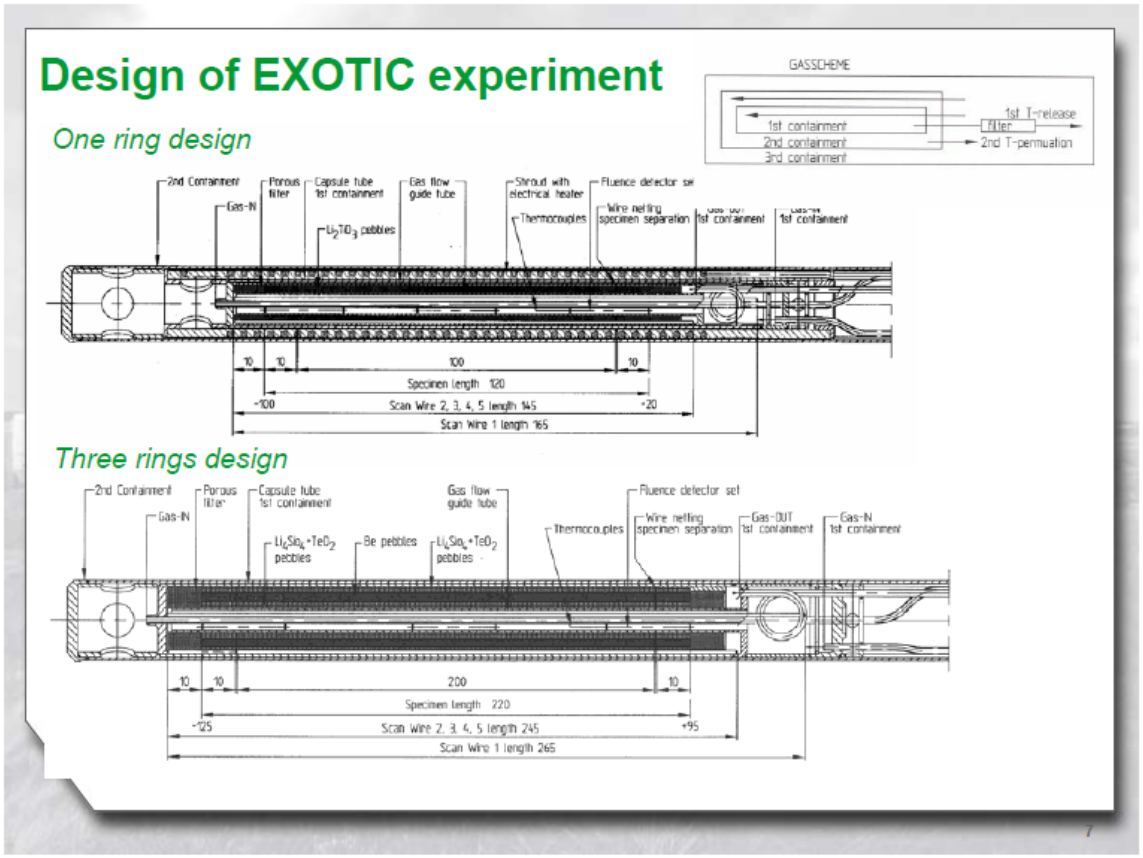
Design of EXOTIC experiment
One ring design
GASSCHEME
1st containment
2nd containment
3rd containment
1st T-release
filter
2nd T-permuation
2nd Containment
Gas-IN
Porous filter
Capsule tube 1st containment
Gas flow guide tube
Shroud with electrical heater
Fluence detector set
Thermocouples
Wire netting specimen separation
1st containment
Specimen length 120
Scan Wire 2, 3, 4, 5 length 145
Scan Wire 1 length 165
Three rings design
Be pebbles
Specimen length 220
Scan Wire 2, 3, 4, 5 length 245
Scan Wire 1 length 265

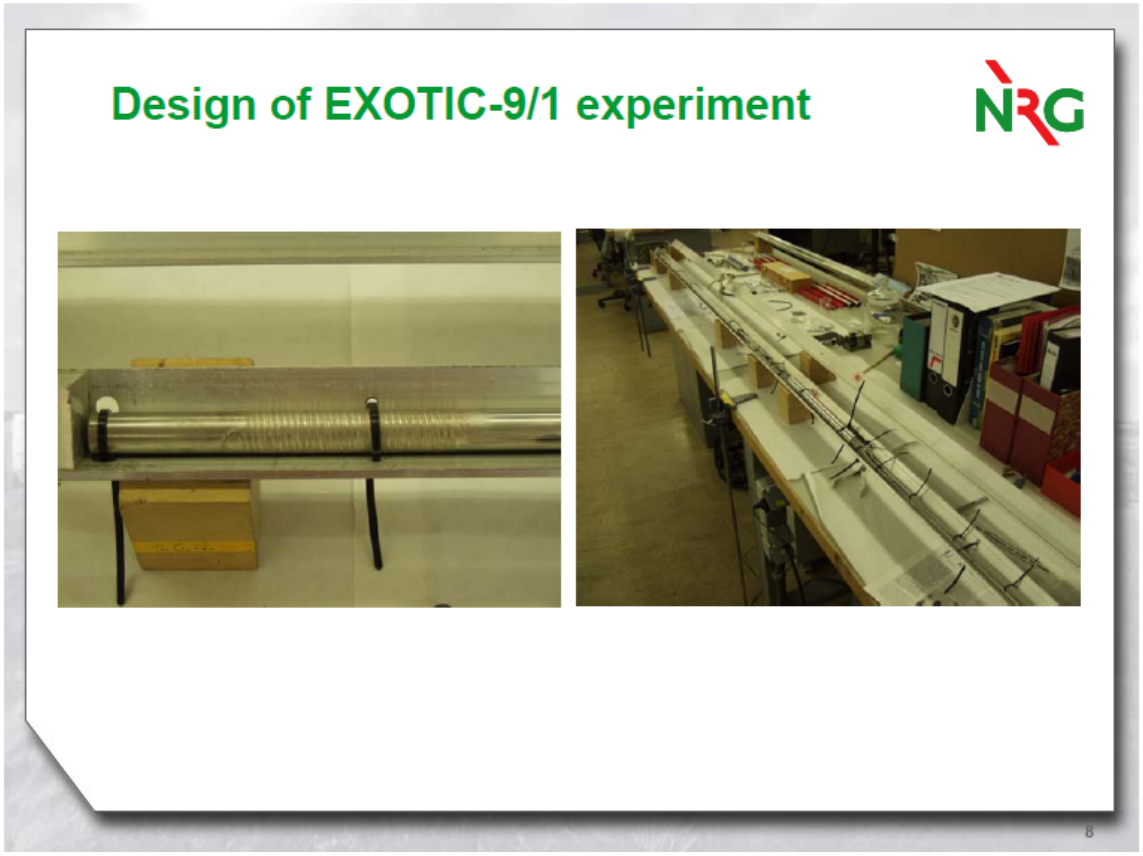
Design of EXOTIC-9/1 experiment
NRG

Filling of the pebble bed of EXOTIC 9/1

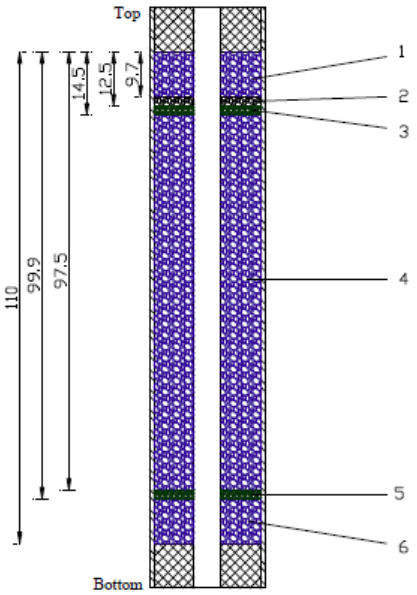

Ceramic materials:

1. Same as 4, 1.2 g
2. Li_4SiO_4 , 20 % ^6Li (FZK), 0.2 g
3. Li_4SiO_4 , 7.5% ^6Li (FZK), 0.2 g
4. **Li_2TiO_3 , 7.5% ^6Li (CEA) 12.8 g** *(extrusion-spheroidisation-sintering)*
5. Li_2TiO_3 , 29,5 % ^6Li (CEA), 0.2 g
6. Same as 4, .2 g

9

Materials irradiated in EXOTIC-9/1

table 1 Characteristics of irradiation specimens after assembly of the test elements

	bulk material	Piggyback 1	Piggyback 2	Piggyback 3	Piggyback 4
Material	Li_2TiO_3	Li_2TiO_3	Li_4SiO_4	Li_4SiO_4	Be
Supplier	CEA	CEA	FZK	FZK	FZK(NGK)
NRG ID	NRG 130	NRG 131	NRG 129	NRG132	NRG 2010
^6Li enrichment	7.5 %	30%	7.5 %	20 %	--
measured density ($g \cdot cm^{-3}$) by He pycnometry technique	3.280	3.246	2.34	not meas.	not meas.
open porosity (%)	1.7	2	3.5	not meas.	not meas.
closed porosity (%)	5.3	5.8	2.7	not meas.	not meas.
Smear density ($g \cdot cm^{-3}$)	1.84	1.84	1.44	1.44	not meas.
Theoretical density ($g \cdot cm^{-3}$)	3.43	3.43	2.25	not meas.	not meas.
Weight (g)	12.8	0.2	0.2	0.2	0.2
Pebble diameter (mm)	0.6-0.8	0.6-0.8	0.25-0.63	not meas.	0.85-1
grain size (µm)	1-3	1-4		not meas.	not meas.

10

Li_2TiO_3, 7.5% 6Li (NRG130)

reference

irradiated

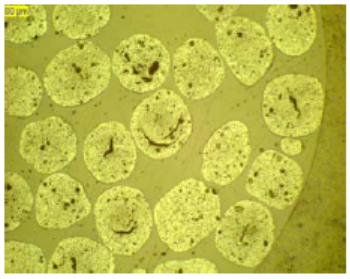

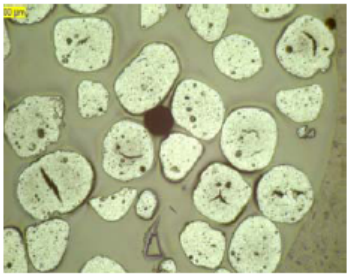

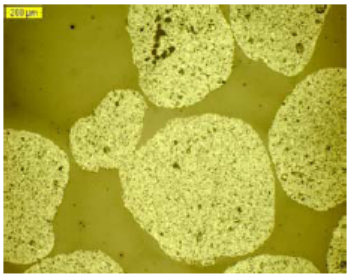

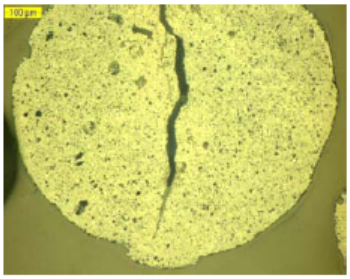

11

Li_2TiO_3, 30% 6Li (NRG131)

reference

irradiated

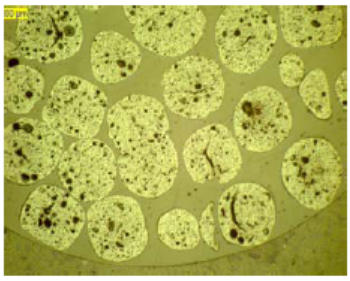

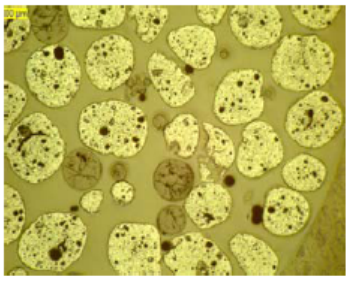

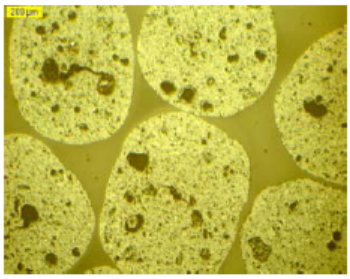

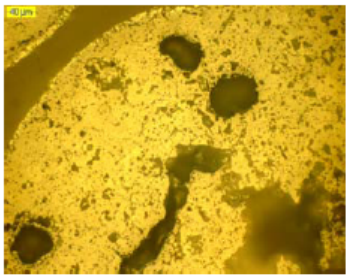

12

Li_4SiO_4, 7.5% 6Li (NRG129)

reference

irradiated

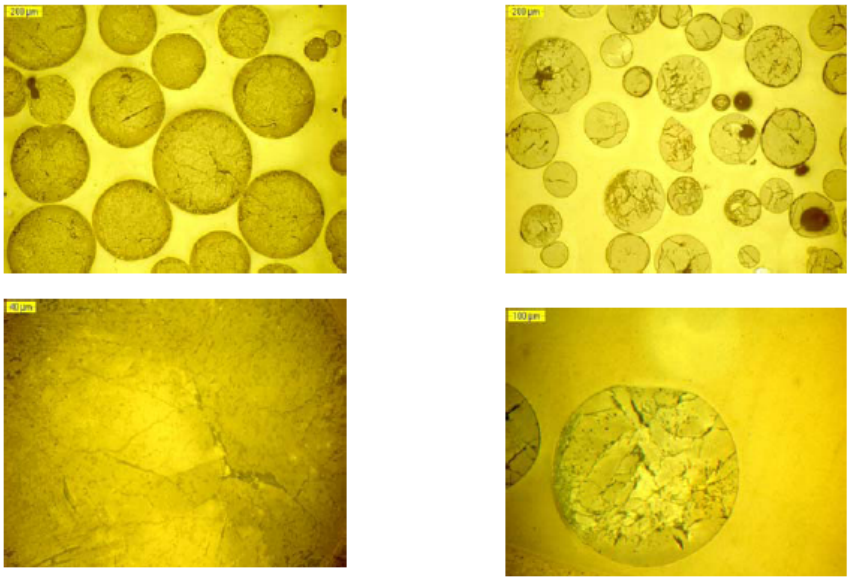

13

Li_4SiO_4, 30% 6Li (NRG132)

reference

irradiated

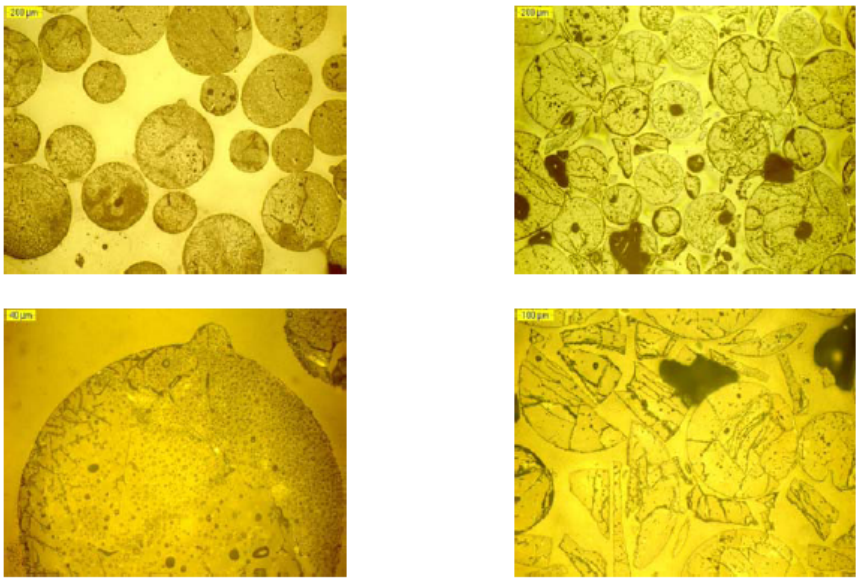

14

Irradiation in High Flux Reactor, Petten

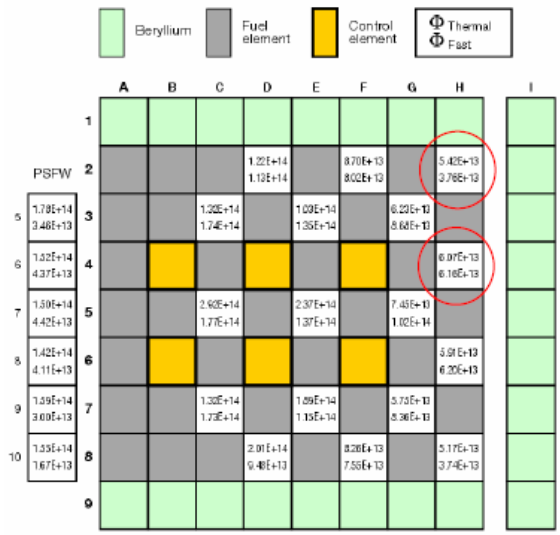

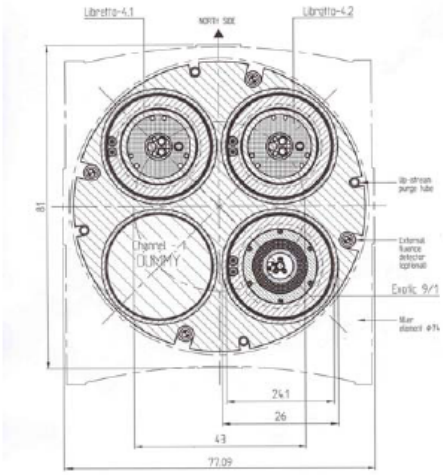

15

Irradiation history of Exotic 9/1

Cycle	units	05-04	05-05	05-06	05-07	05-09	05-10	05-11	05-12	06-01	06-02	06-03	06-05	total	measured	units
Power	MW	44.7	44.5	44.4	44.5	44.5	44.97	44.96	43.93	43.94	44.88	44.95	44.92			
FPD	days	25.67	25.22	24.26	25.19	25.60	23.16	22.67	25.26	26.77	24.58	25.99	27.46	301.85		days
E > 1.0 MeV	10^{18} m^{-2} s^{-1}	0.36	0.39	0.39	0.41	0.39	0.33	0.30	0.31	0.30	0.32	0.35	0.33	0.91	0.86	10^{25} m^{-2}
E > 0.1 MeV	10^{18} m^{-2} s^{-1}	0.77	0.81	0.79	0.84	0.83	0.71	0.66	0.68	0.65	0.70	0.77	0.72	1.94	1.89	10^{25} m^{-2}
^{54}Fe(n,p)^{54}Mn	10^{18} m^{-2} s^{-1}	0.38	0.42	0.42	0.44	0.41	0.34	0.32	0.33	0.31	0.34	0.37	0.35	0.96	0.92	10^{25} m^{-2}
^{59}Co(n,γ)^{60}Co	10^{18} m^{-2} s^{-1}	0.51	0.48	0.46	0.42	0.60	0.62	0.58	0.54	0.57	0.62	0.57	0.54	1.41	1.83	10^{25} m^{-2}
BU per cycle	%	0.40	0.34	0.30	0.32	0.40	0.31	0.27	0.26	0.28	0.26	0.24	0.22	3.62	3.25	%
BU comul	%	0.40	0.74	1.04	1.36	1.76	2.07	2.34	2.60	2.89	3.15	3.39	3.62			
damage steel	dpa	0.13	0.14	0.13	0.14	0.14	0.10	0.09	0.10	0.10	0.10	0.12	0.12	1.38	1.22	dpa

16

EXOTIC- Instrumentation

- In-pile monitoring (during irradiation)
  - Thermocouples
  - TMS – Tritium Measuring Station

    Tritium residence time measurements

- Out of pile, PIE – Post Irradiation Examination
  - TPD – Temperature Programmed Desorption
  - Cross-section Microscopy (optical and electron)
  - Neutron Fluence Detectors and gamma scan wires

17

Tritium residence time

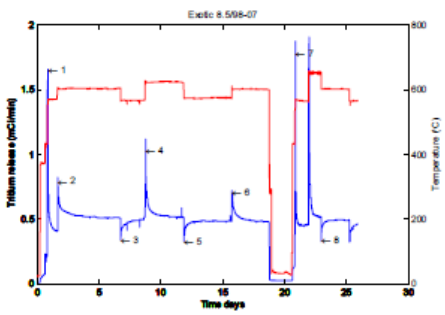

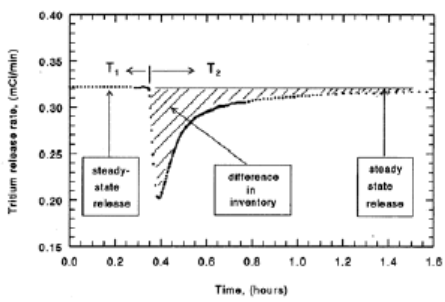

Tritium residence time: $\tau = \frac{I(T)}{G}$

Differential tritium residence time: $\Delta\tau = |\tau_2 - \tau_1| = \frac{|\Delta I|}{G}$

Model: $\tau = 10^{A+B\times 1000/T}$

18

Radial (left) and axial (right) temperature distributions

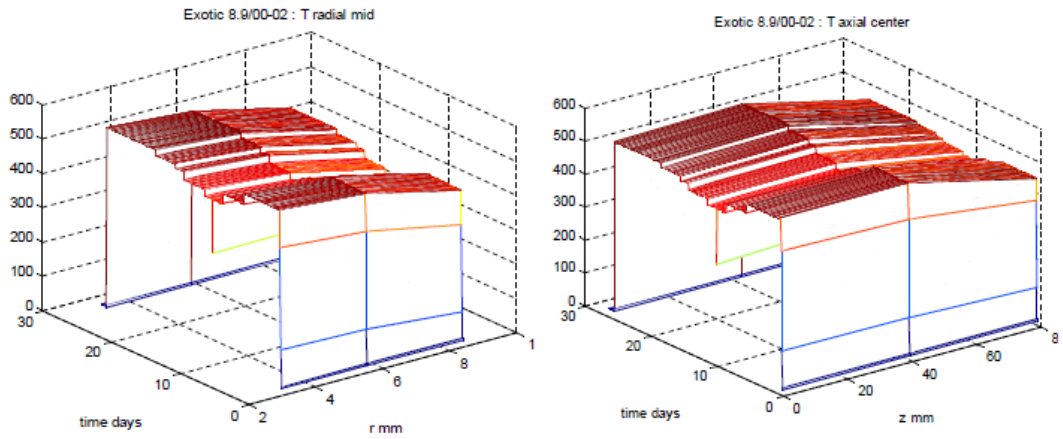

19

Pebble bed thermal conductivity derived from the experiments E8/9 (left) and E8/10 (right).

$$k_{eff} = k_0 - 0.08 \times BU(\%)$$

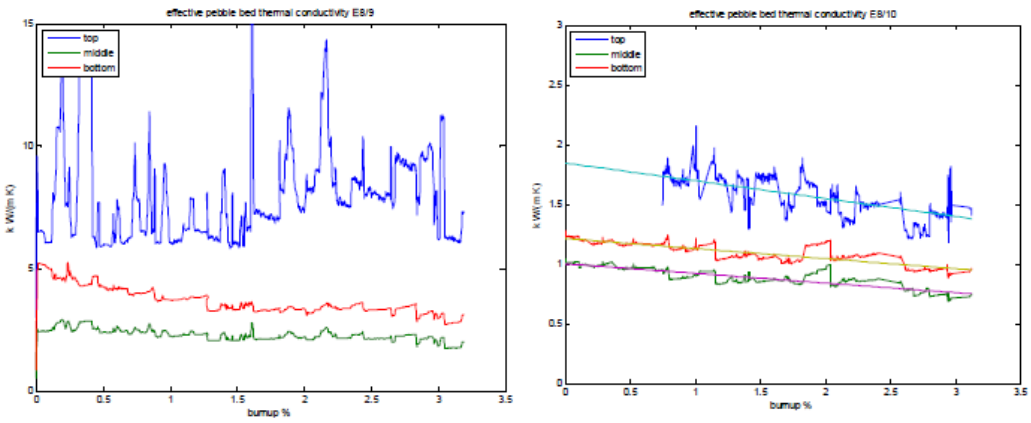

20

Temperature reconstruction

$$T(r,z) = T_{cen}(z) - \frac{q}{4k}\left(r^2 - R_1^2 - 2R_1^2 \ln(r/R_1)\right)$$

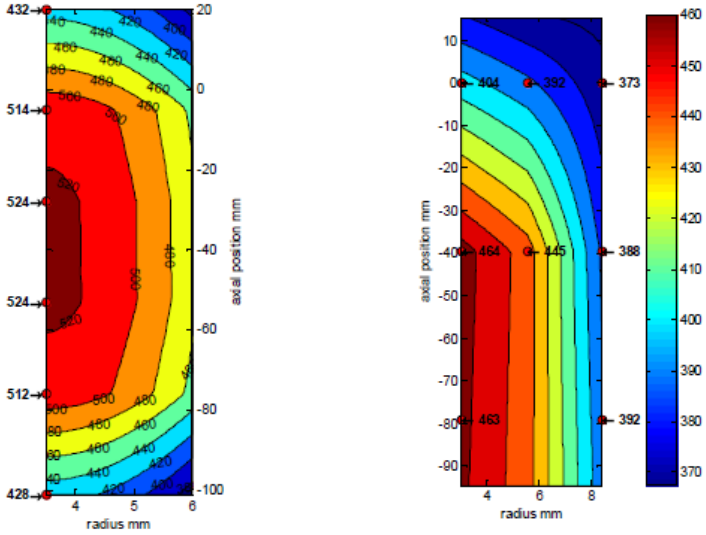

2D temperature distributions in the pebble beds for E8/4 (left) and E8/9 (right) experiments

21

Temperature reconstruction

Tritium inventory: $I \propto 10^{A+B\times 1000/T}$

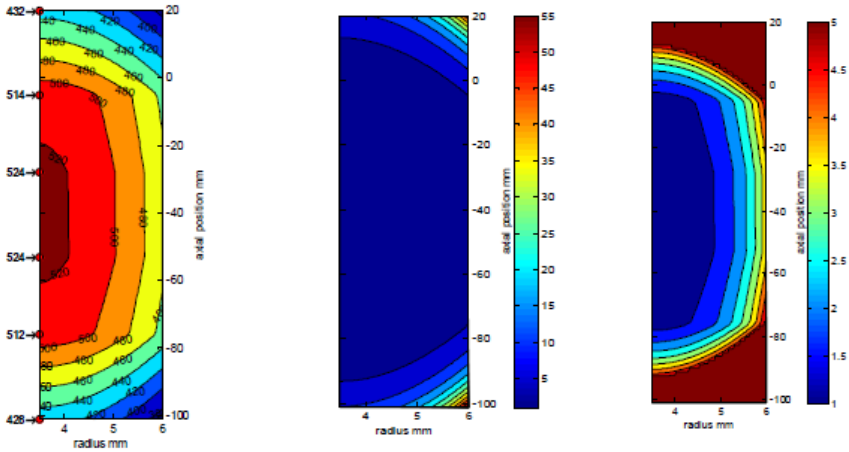

2D temperature distributions in the pebble beds for E8/4

2D map of relative tritium concentration in the bed of the experiment E8/4. Right figure presents a blowup of the central area

22

T_τ definition

$$10^{A+B\times\frac{1000}{\overline{T}_\tau}} = \frac{\int 10^{A+B\times\frac{1000}{T(r,z)}}\,dV}{V}$$

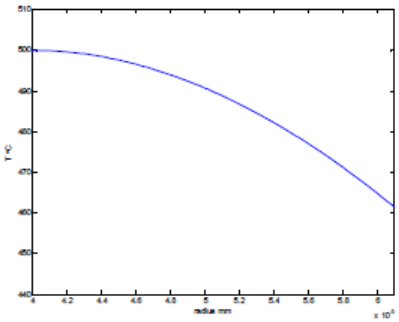

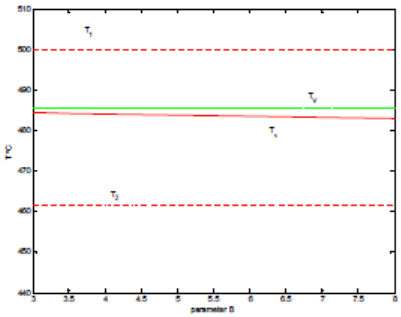

23

Tritium residence time τ and differential residence time $\Delta\tau$

$$\tau = 10^{A+B\times 1000/T}$$

$$\Delta\tau = |\tau_2 - \tau_1| = \frac{|\Delta I|}{G}$$

Red symbols present differential residence time $\Delta\ \tau$ measured in the in pile experiments.

Blue line presents the fit for the residence time.

Blue solid square symbol presents the tritium residence time measured in the PIE studies.

Blue open circle gives the *Ttau_24hr*, the characteristic temperature which corresponds to 24 hours of the residence time.

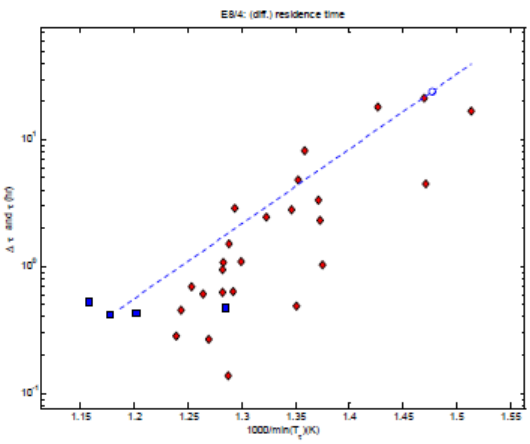

24

A 3D presentation of the differential residence time $\Delta\tau(T_{\tau,1},T_{\tau,2})$.

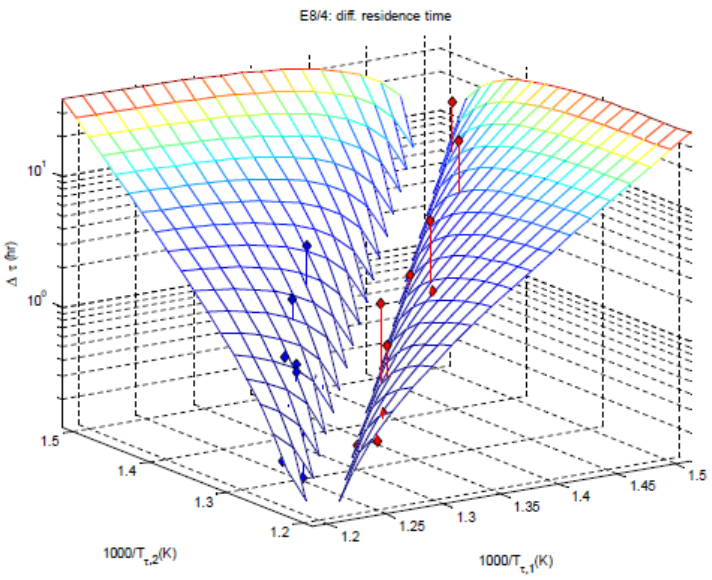

25

Differential residence time $\Delta\tau$

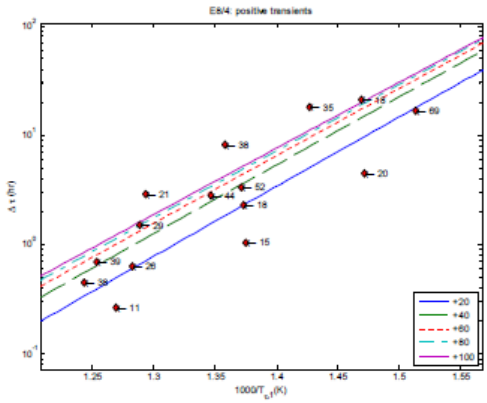

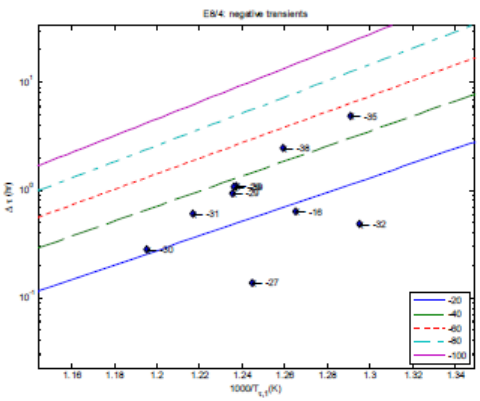

26

Fitting procedure

Collect data for every transient
$\{T_i\}_1, \{T_i\}_2, \Delta\tau$

↓

Reconstruct bed temperature distribution T(z,r) and calculate T_τ:

$\{T_i\}_1 \rightarrow T_1(z,r) \rightarrow T_{\tau,1}$
$\{T_i\}_2 \rightarrow T_2(z,r) \rightarrow T_{\tau,2}$

↓

Fit data

$$\left|10^{A+B\times1000/\overline{T}_{\tau,1}} - 10^{A+B\times1000/\overline{T}_{\tau,2}}\right| \rightarrow \Delta\tau$$

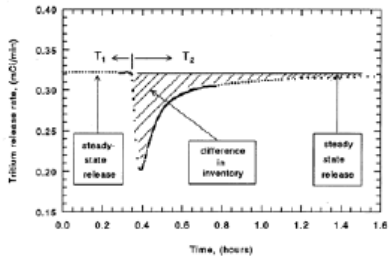

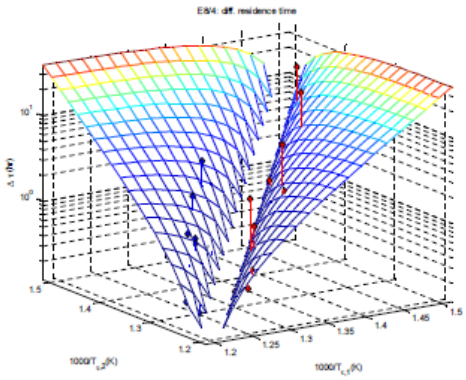

27

Tritium residence time measured in EXOTIC 8 experiments

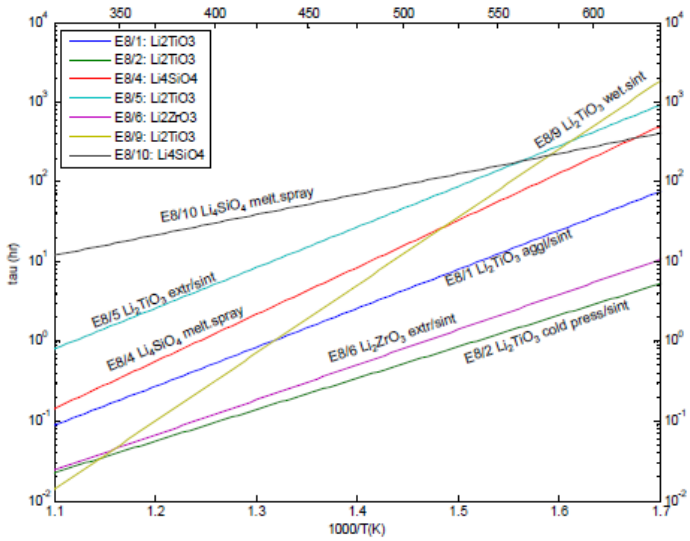

28

Tritium residence time measured in EXOTIC 9/1 experiments

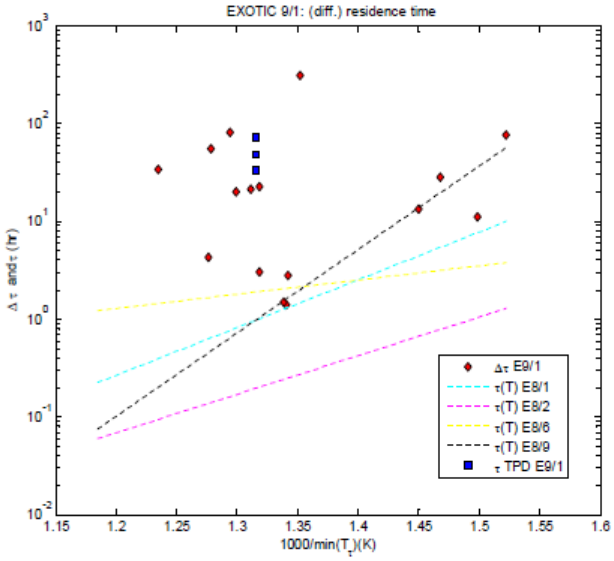

29

Exotic 9/1

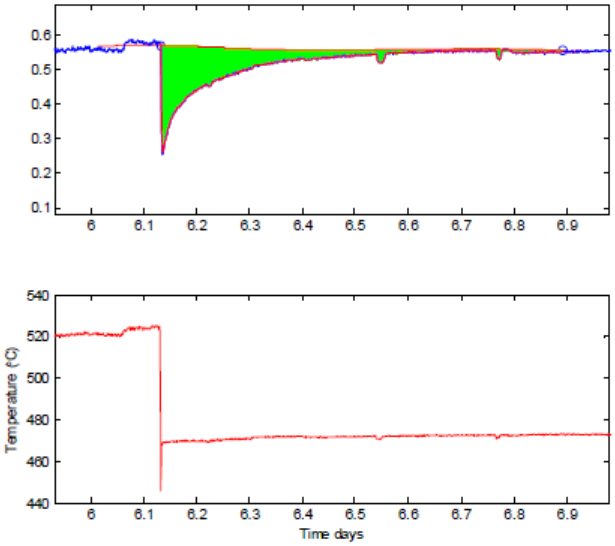

$$\Delta\tau = |\tau_2 - \tau_1| = \frac{|\Delta I|}{G}$$

Δτ = 1.31 h

30

Exotic 9/1

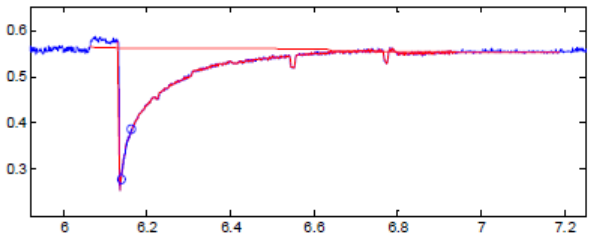

τ = 1.22 h

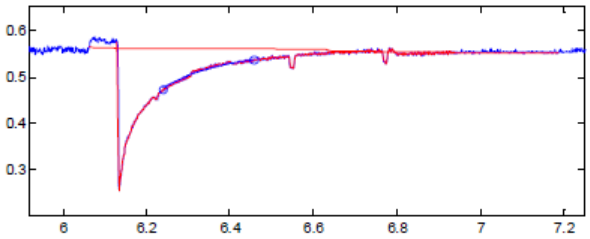

τ = 3.93 h

31

Exotic 9/1

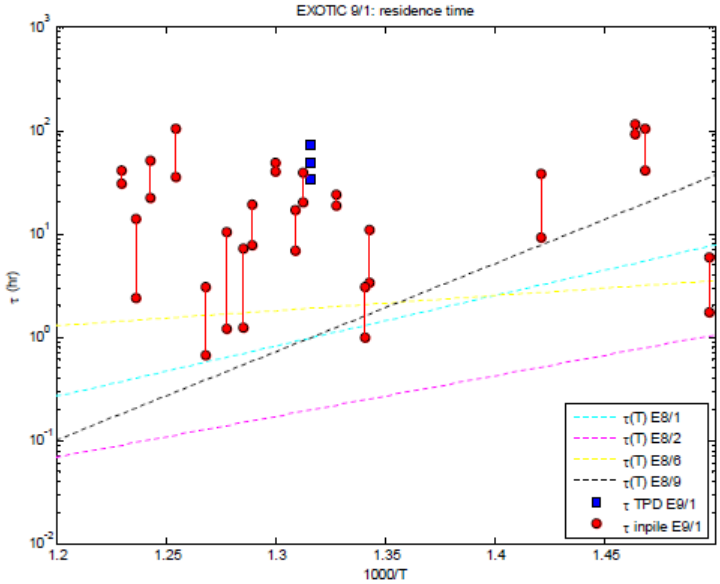

32

Mechanisms of tritium transport in Li-ceramics

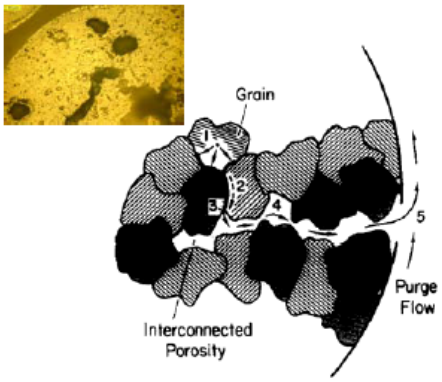

Mechanisms of Tritium Transport

1) Intragranular Diffusion
2) Grain Boundary Diffusion
3) Surface Adsorption / Desorption
4) Pore Diffusion
5) Purge Flow Convection

T-migration

HT,HTO -transport

Fig. 1. Mechanisms of tritium transport in solid breeders [37].

A.R. Raffray and M.A. Abdou, in: Advances in Ceramics,vol. 25 - Fabrication and Properties of Lithium Ceramics, eds. G.W. Hollenberg and I.J. Hastings (The American Ceramic Society, Ohio, 1989) p. 1

33

Conclusions

- EXOTIC experiments provided valuable data on tritium retention properties of lithium containing ceramics
- Various candidate breeder materials (composition, production route) were compared in terms of the tritium residence time
- Thermal mechanical properties of the ceramics under irradiation, elevated temperature and reducing atmosphere were studied

& Future developments

- Applying different (more sophisticated) theoretical model in the fitting procedure
- Improve experiment design to provide well defined and homogenous temperature profile in the bed

34

17. Hydrogen permeation through F82H tube under pressurized water

H. Tanigawa, A. Yoshikawa and M. Enoeda
Japan Atomic Energy Agency, Blanket Technology Group

In the design of a test blanket module (TBM) being developed by JAEA, cooling tubes made of F82H steel pass through pebble beds of Li2TiO3 and Be, and pressurized water of 15 MPa at a temperature of about 573 K is fed as coolant. In the breeder bed side, the partial pressure of tritium is controlled to be about 1 Pa using helium purge gas. The tritium diffusion coefficient in F82H steel is an important parameter for the permeation calculation. However, reported values are limited only for the samples with the clean surface. In the operating condition, the coolant side of the tube is subjected to the water of 15 MPa at about 573 K, and the surface will be oxidized. In the present study, deuterium gas behaviour passing through the F82H tube under the pressurized water is observed using an autoclave.

A F82H tube 2.5 mm thick is inserted into the autoclave, and heated to 573 K in the pressurized water. The tube is connected to a vacuum pumping system with a quadrupole mass spectrometer and a deuterium gas container. In the tube, 100 Pa of deuterium gas is filled and the partial pressure of deuterium is observed. For the sample with the polished surface, deuterium permeation was observed and hydrogen permeation in the different direction from the deuterium was simultaneously observed. The hydrogen is considered to be attributed to the oxidative reaction at the coolant side. In process of time, both deuterium and hydrogen permeation rates decreased. For the deuterium permeation, the rate decreasing results from the growth of the oxide layer that acts as a permeation barrier. For the hydrogen, the rate decreasing is considered to correspond with the decreasing of the oxidation rate.

The permeation behaviour of deuterium affected by the oxide layer was observed by the in-situ experiment. In addition, it was found that hydrogen caused by the oxidative reaction can permeate through the tube. Using the apparent diffusion coefficient obtained in the study, tritium permeation in the TBM is estimated.

CBBI-15

2009/09/4
Sapporo, JAPAN

Hydrogen permeation through F82H tube under pressurized water

Hisashi TANIGAWA, Akira YOSHIKAWA
and Mikio ENOEDA

Blanket Technology Group
Japan Atomic Energy Agency (JAEA)

1/15

Tritium behaviour in ceramic breeder blanket with water cooling

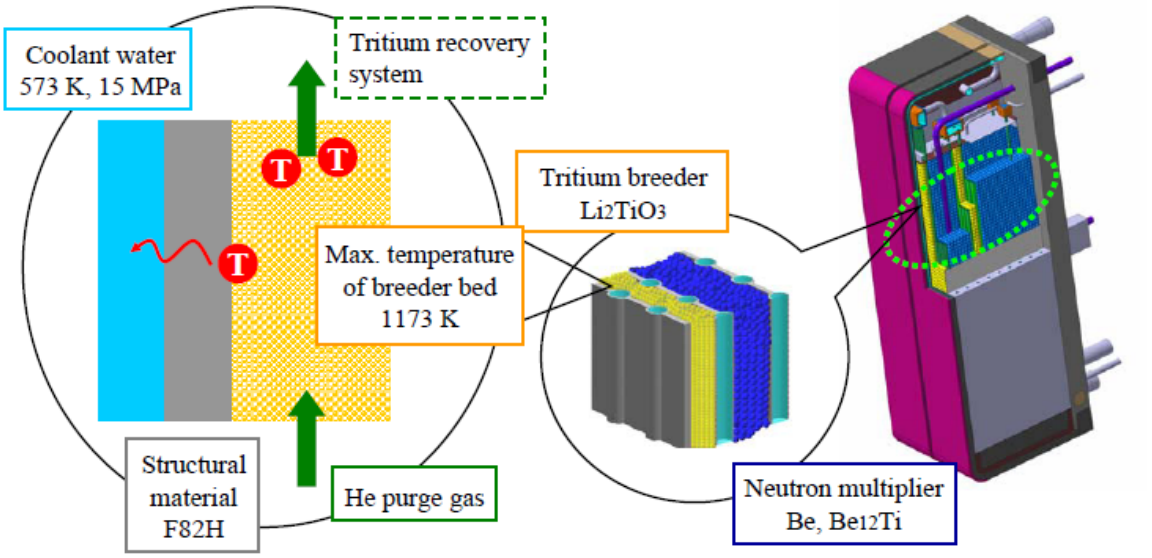

To estimate tritium permeation into the coolant water, and to decrease the permeation is necessary.

2/15

Purpose of this study

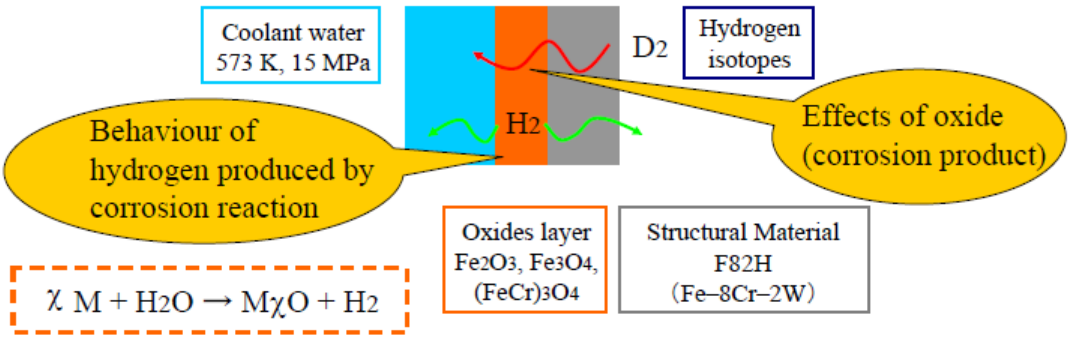

1. In-situ measurement of hydrogen permeation through F82H steel in service condition of TBM, in pressurized water of 15 MPa at 573K.

2. To elucidate the effects of corrosion oxides on the hydrogen permeation

3/15

Apparatus

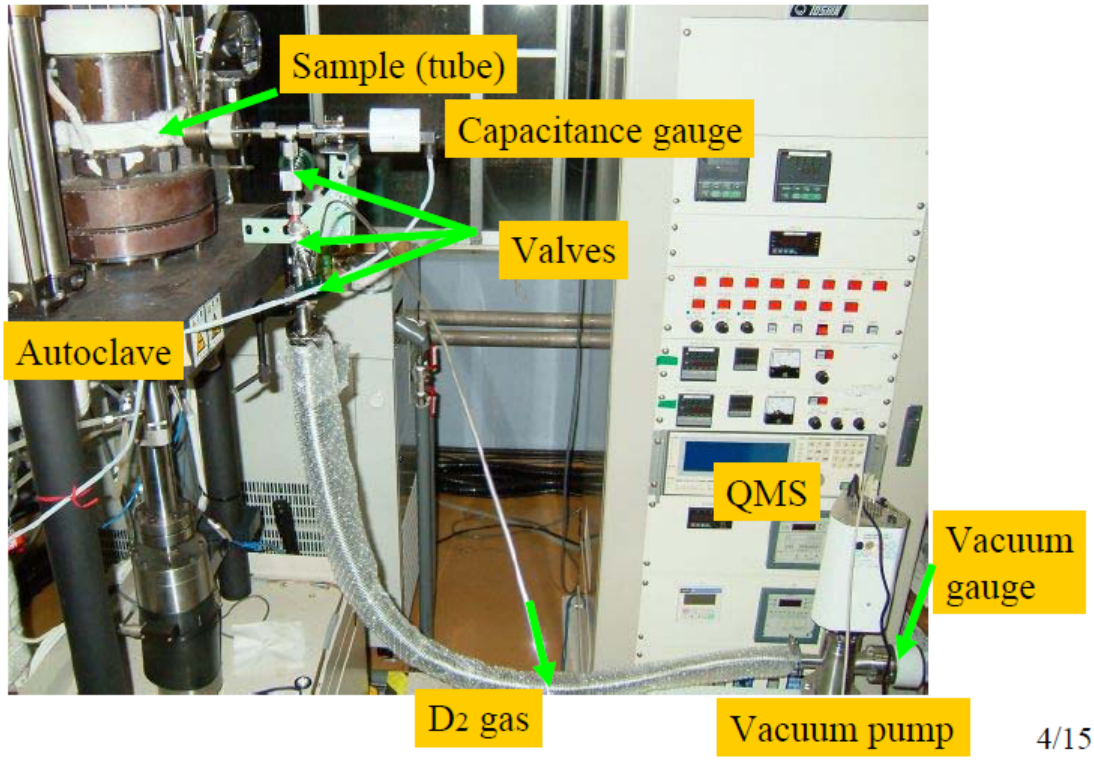

4/15

Configuration of in-situ measurement system

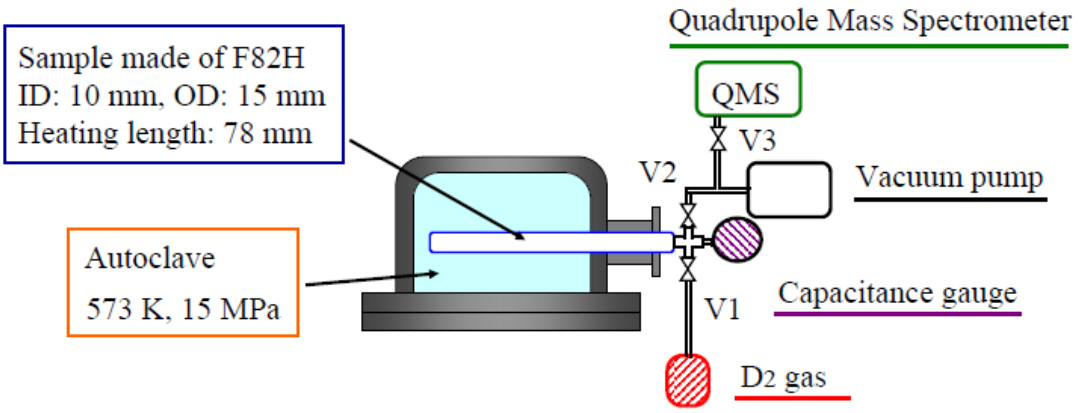

5/15

Experimental procedure

1. Degas treatment, heating at 773 K (25 MPa) for 35 hr
2. Measurement at 573 K (15 MPa)
3. Cool down to R.T.
4. Polishing outside sample
5. Measurement at 573 K (15 MPa)
6. Heating at 573 K (15 MPa) for 22 hr
7. Measurement at 573 K (15 MPa)

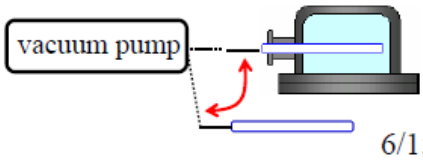

Always atmosphere inside the sample is controlled.

6/15

Scheme of background measurements

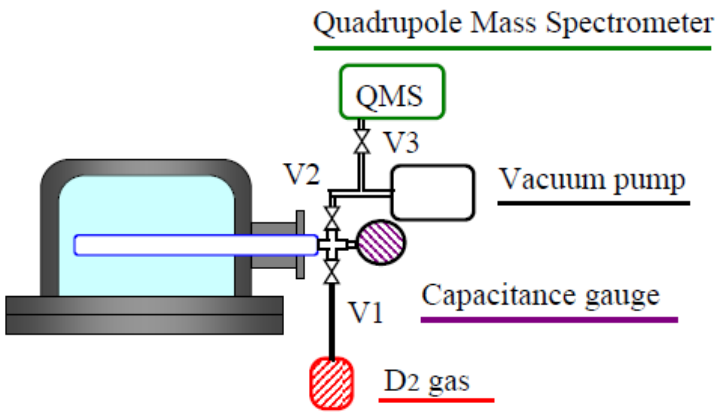

1. evacuate the inside sample less than 2×10^{-6} Pa through V2
2. close V2
3. measure the total pressure inside the sample
4. open V2 and QMS analysis

7/15

Increasing of internal pressure of the sample

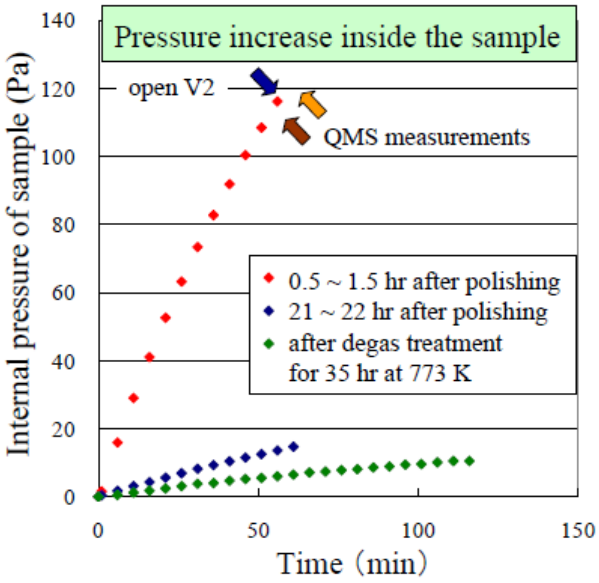

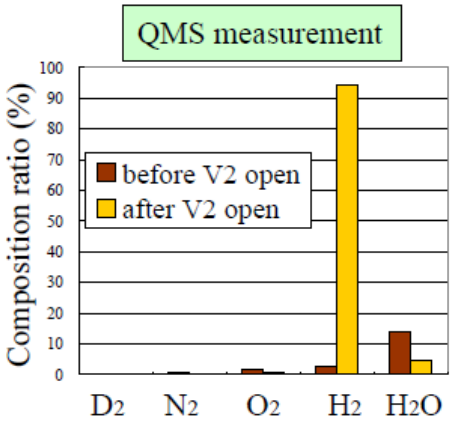

95% of the gas is H_2

- Polishing the outside sample leads to increase of internal pressure.
- Pressure rising rate decreased with time.

The increase of the pressure is attributed to the permeation of the hydrogen produced by oxidation reactions outside the sample.

8/15

Measurement scheme of D_2 permeation

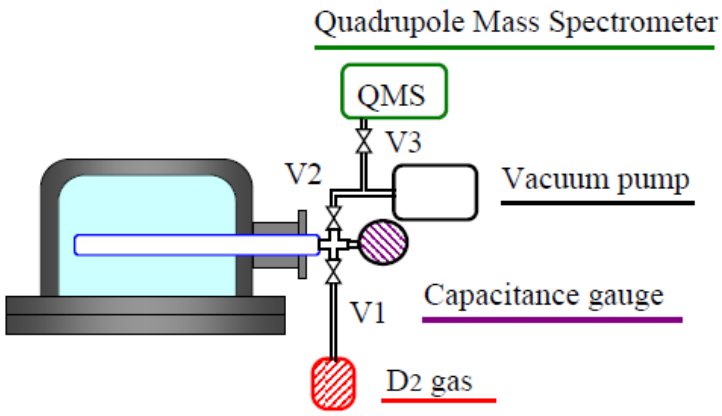

1. evacuate the inside sample less than 2×10^{-6} Pa through V2
2. charge D_2 gas of 100 Pa to the sample through V1, and to close V1 and V2
3. measure the total pressure inside the sample, and estimate permeation of D_2

9/15

Estimation of D_2 gas permeation

Internal pressure after charging D_2 gas of 100 Pa

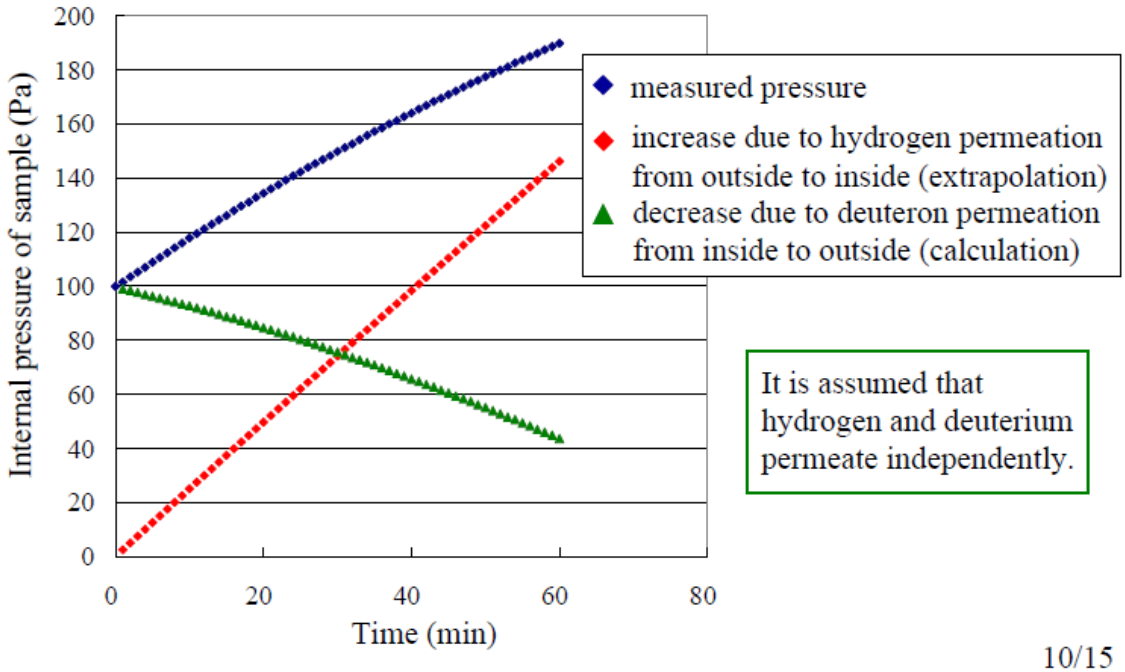

It is assumed that hydrogen and deuterium permeate independently.

10/15

In-situ measurement of D2 gas through F82H

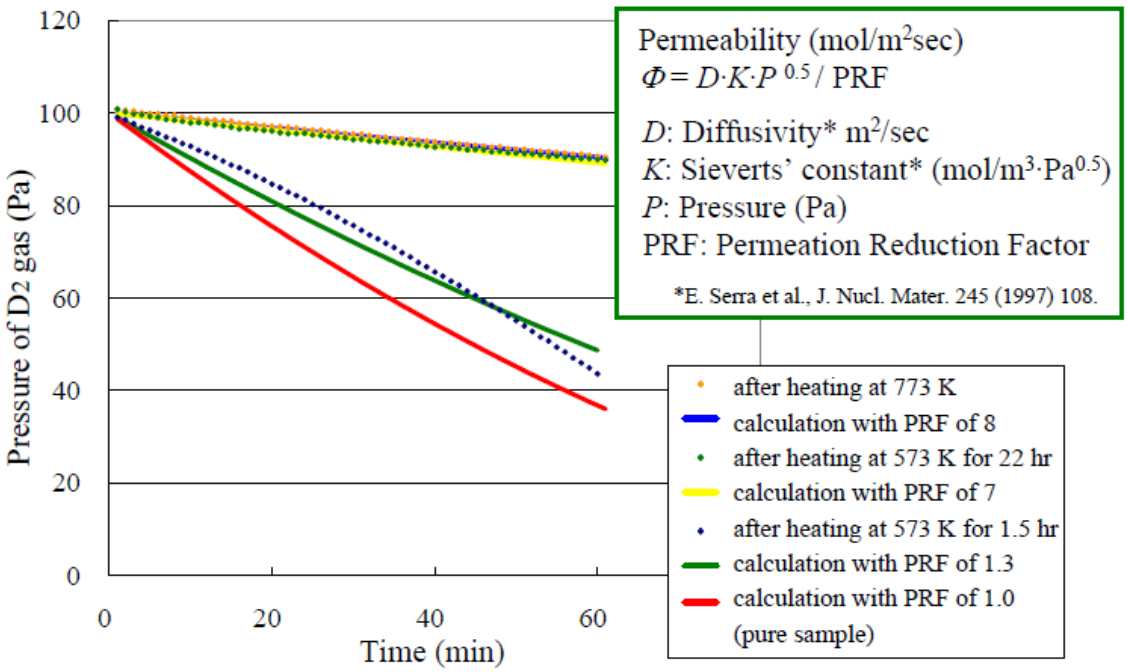

Permeability of deuterium decreases with corrosive oxidation.

11/15

H2 and D2 permeations are confirmed by QMS

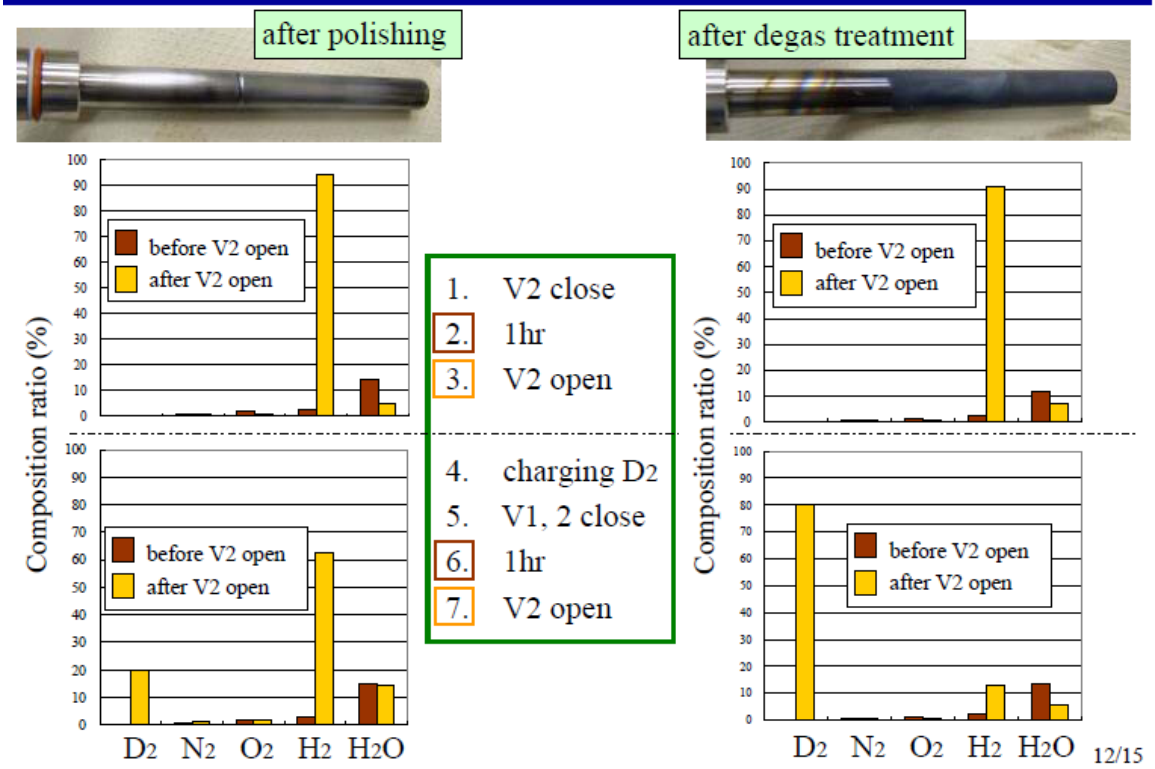

12/15

Tritium permeation into coolant water in TBM

- Temperature: 598K
- Sweep gas composition
  : He - 1,000ppmH_2
- Partial pressure of T: 1 Pa
- Diffusion coefficient at 598K
  : 6.5×10^{-9} m^2/s (F82H steel)
  : 1.1×10^{-16} m^2/s (Coating)

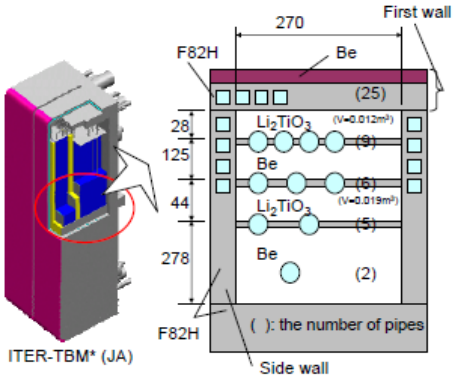

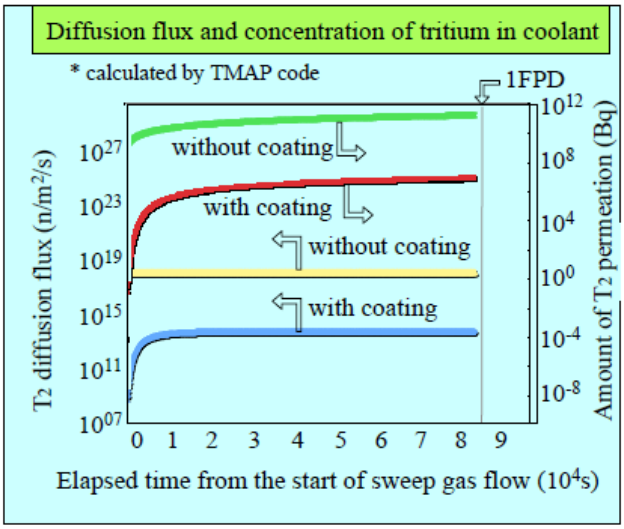

*Nakamichi et al., J. Nucl. Mater. 386-388 (2009) 692.

13/15

Ratio of permeated tritium to bred tritium

Bred tritium: ~ 1×10^{13} Bq

Permeated tritium for pure F82H: 9×10^{10} Bq
(with assumption that H_2 and T_2 follow Hickman's theory)

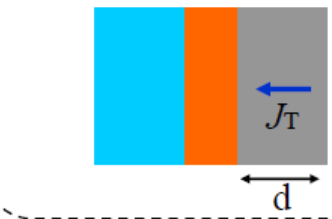

P_{H2}: ~ 100Pa
P_{T2}: ~ 1Pa

$$J_T = D_T \cdot C_T/d$$

$$C_T = \frac{P_{T2}}{P_{total}} \cdot K_{T2} \cdot \sqrt{P_{total}}$$

D: Diffusivity
K: Sieverts' constant

Ratio of permeated tritium to bred tritium

~1% for pure material
~0.1% for oxidized material with PRF of 10

14/15

Summary

- Experimental system for in-situ measurement of hydrogen permeation under pressurized water is developed.

- At 573 K in the pressurized water of 15 MPa, permeation of deuterium through F82H steel is measured. It is shown that permeability decreases with corrosive oxidation of the outer surface of F82H sample.

- Phenomena that hydrogen produced by corrosive oxidation at the outer surface permeates into the sample is observed.

15/15

18. Tritium Permeation Behavior in the Breeder part of Ceramic Breeder Blanket

[1]T. Hanada, [1]S. Fukada. [1]M. Nishikawa. [1]N. Yamashita, [1]T. Kanazawa, [1]H. Yamasaki, [2]M. Enoeda
[1]Interdisciplinary Graduate School of Engineering Sciences, Kyushu University,
6-10-1, Hakozaki, Higashiku, Fukuoka, 812-8581, Japan
[2]Division of Fusion Energy Technology, Japan Atomic Energy Agency,
801-1, Mukoyama, Naka-shi, Ibaraki-ken, 311-0193, Japan

Abstract

Tritium bred in the blanket must be effectively recovered to maintain the fuel cycle of a DT fusion reactor because the blanket is the only part that can produce tritium. The blanket system is divided into three parts, the breeding part packed with breeder pebbles, the recovery part adjusting tritium to the transferable form in the fuel cycle and the piping part connecting between breeder part and recovery part. Tritium permeation problem in the breeding part is discussed in this study. It is necessary to know the concentration profile of tritium and hydrogen in the breeding part and the chemical form of tritium released into the blanket purge gas for estimation of the permeation behavior. The present authors have already constructed the release model of bred tritium from ceramic breeder materials taking diffusion in grain, mass transfer resistance at interfacial layer of grain and surface reactions into count and it has been ascertained that release behavior estimated by this model shows good agreement with the out-of-pile or the in-pile tritium release data from various experiments [1, 2].

The permeation behavior of tritium to the coolant pipe in the Water Cooled Solid Breeder test blanket[3] packed with Li_2TiO_3 pebbles is estimated where concentration profile of the bred tritium and variation in the chemical form of tritium or hydrogen are estimated using the release model constructed by the present authors. Diffusivity and solubility reported by Serra et at.[4] for F82H-mod ferritic steel are used in the estimation.

The estimation in this study shows that the permeation loss of bred tritium into the coolant is small when the wall temperature is 593K, though it becomes near 1% when the wall temperature is around 773K.

References

[1] M. Nishikawa, T. Kinjyo, Y. Nishida, J. Nucl. Mater., **325**, 87-93(2007)
[2] T. Kinjyo, M. Nishikawa, N. Yamashita, T. Koyama, K. Suematsu, S. Fukada, M. Enoeda, Fusion Science and Technology., **54**, 557-560(2008)
[3] D.Tsuru, et al," Achievements of the Water Cooled Solid Breeder Test Blanket Module of Japan to the Milestones for Installation in ITER", 22nd IAEA Fusion Energy Conference (2008), Geneva, http://www-pub.iaea.org/MTCD/Meetings/FEC2008/ft_p2-6.pdf
[4] E. Serra, A. Perujo, G. Benamati, J. Nucl. Mater., **245**(1997)108

Tritium Permeation Behavior in the Breeder part of Ceramic Breeder Blanket.

[1]**T. Hanada**, [1]S. Fukada. [1]M. Nishikawa.
[1]N. Yamashita, [1]T. Kanazawa, [1]H. Yamasaki,
[2]M. Enoeda

[1]Graduate School of Engineering Sciences, Kyushu University

[2]Division of Fusion Energy Technology, Japan Atomic Energy Agency

---

Tritium release model

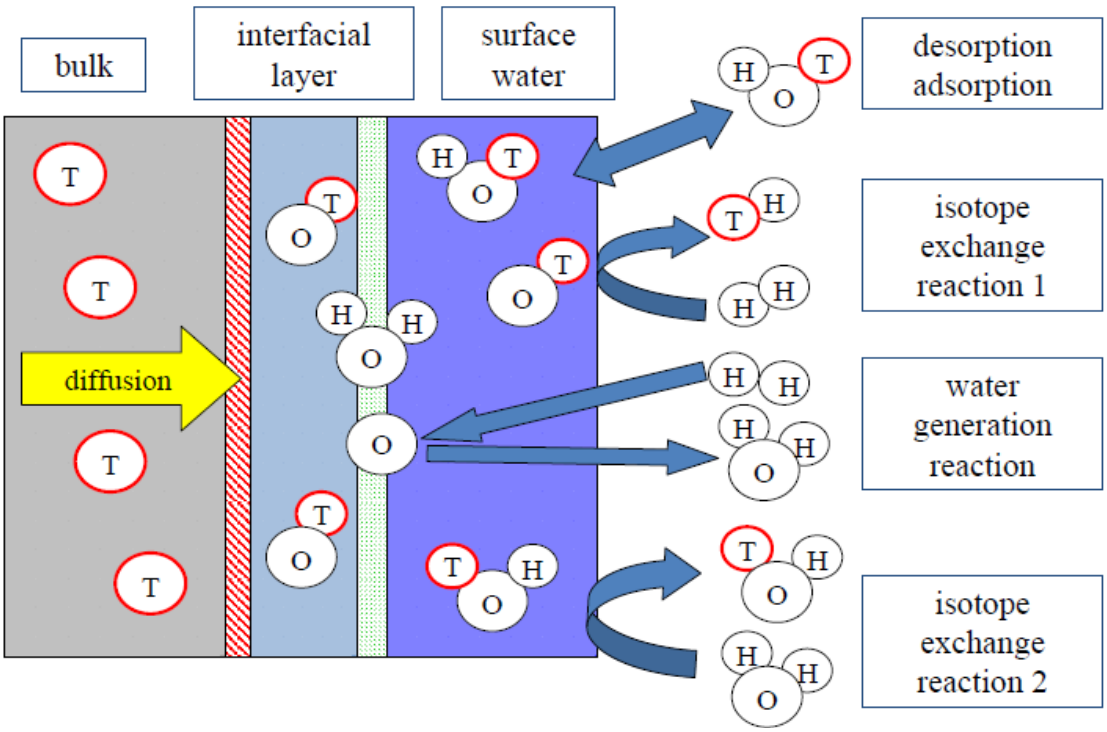

Fitting curves for data of out-pile experiment

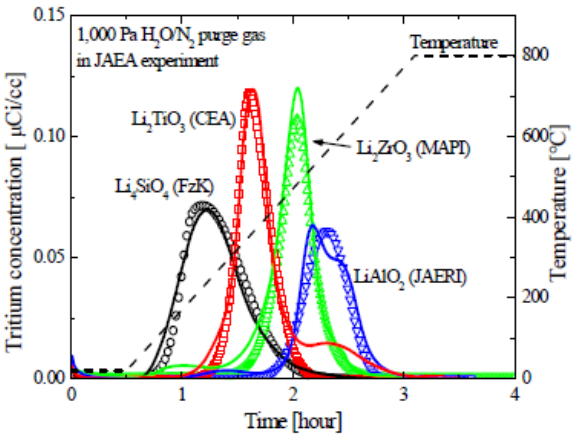

1,000Pa H_2O/N_2 purge gas

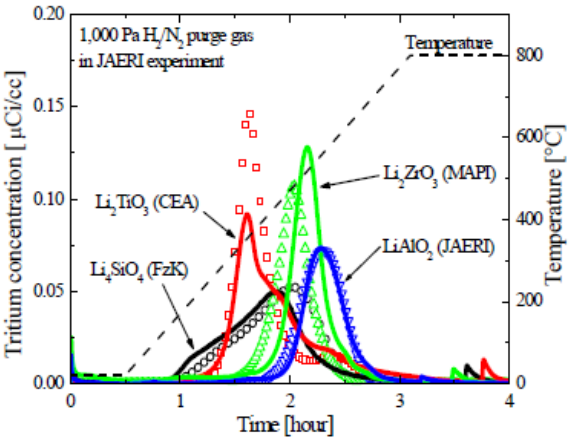

1,000Pa H_2/N_2 purge gas

Tritium release curves estimated using our model agree well with the tritium release curves obtained from our previous out-pile tritium release experiments.

Fitting curves for data of in-pile experiment

Middle temp.experiment *JMTR-123 Li_2TiO_3 (NFI)*

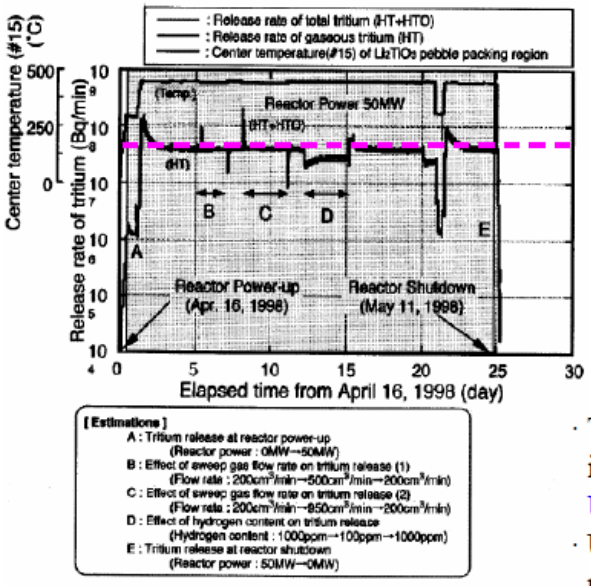

Fig.4-34 Result of the third irradiation test in the 123rd cycle.

temperature : 300°C ~ 450°C

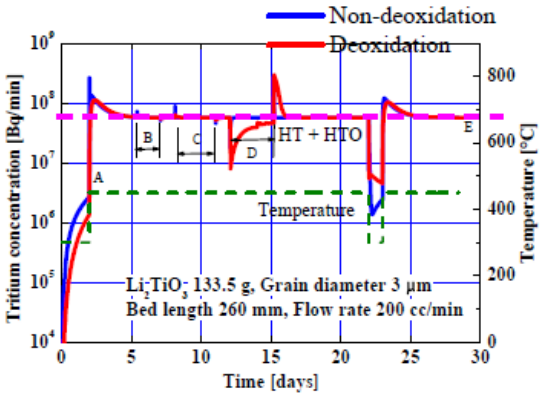

- The degree of surface deoxidation is controlled by '**Temperature** and **Using time**'.
- Understanding of using record is necessary for estimate of tritium release behavior.
- The understanding of surface water condition is important.

Fitting curves for data of in-pile experiment

----EXOTIC-8 (Li_2TiO_3)----

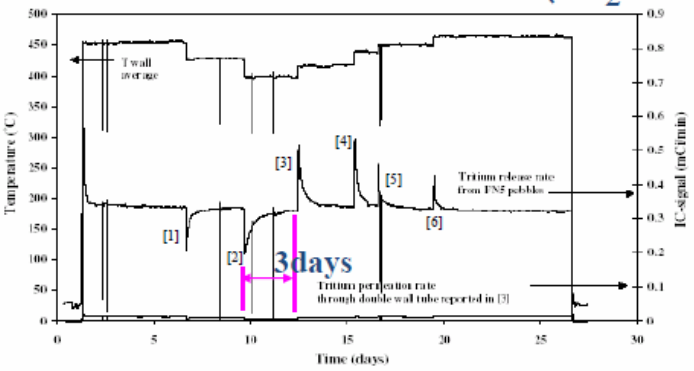

・応答時間は**3日**という、日単位→Li_2ZrO_3と比べ、トリチウム離れのよいとされるLi_2TiO_3としては矛盾。

・**還元による表面抵抗**を考慮する事により実験値とのよい一致を得た。

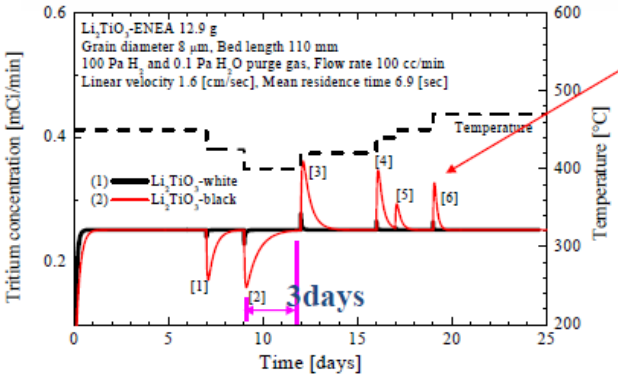

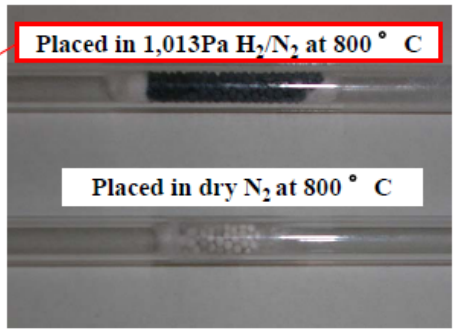

Schematic diagram of experimental apparatus for water release

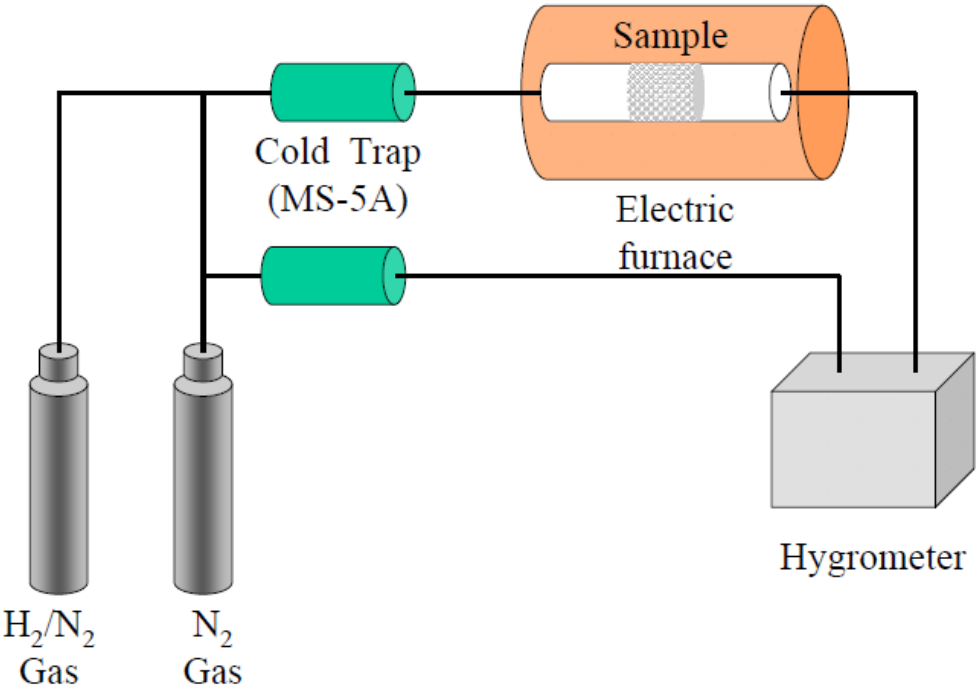

Experiment result of water release from Li_4SiO_4

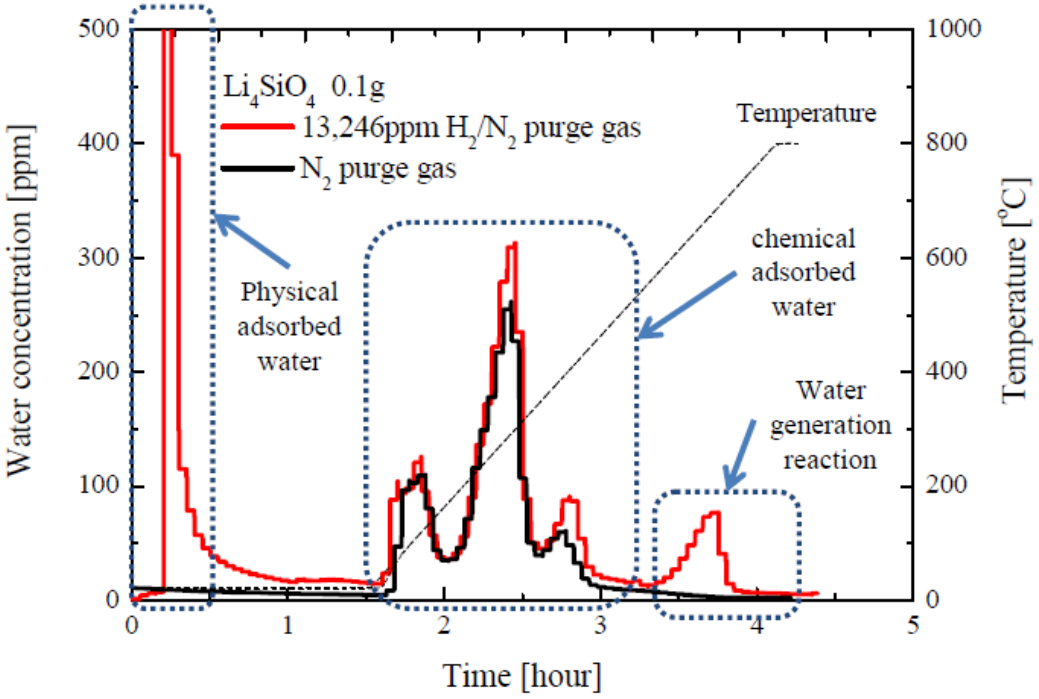

ITER-TBM type model

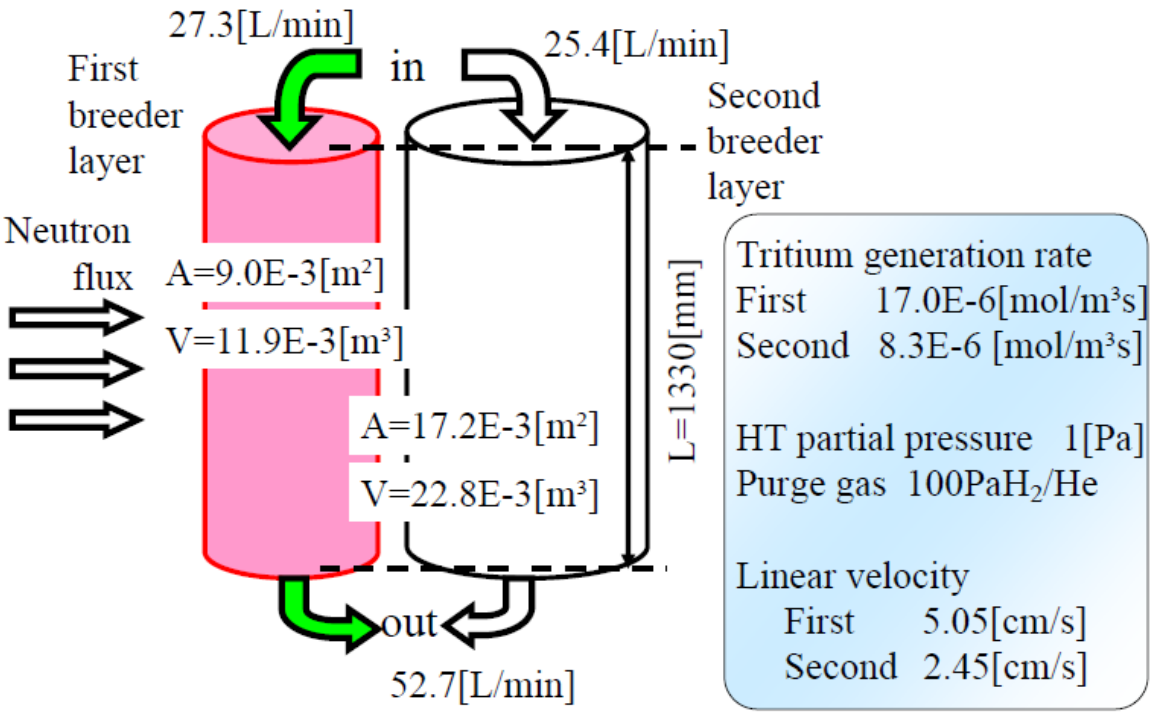

The simulation of water release from ITER-TBM

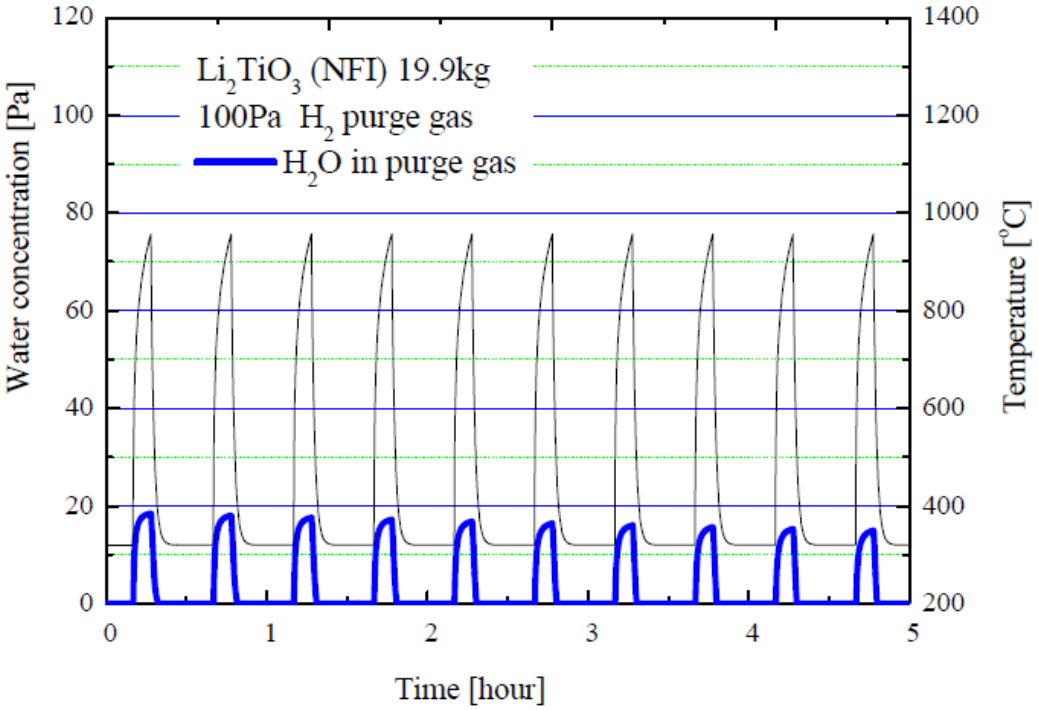

The simulation of water release from ITER-TBM

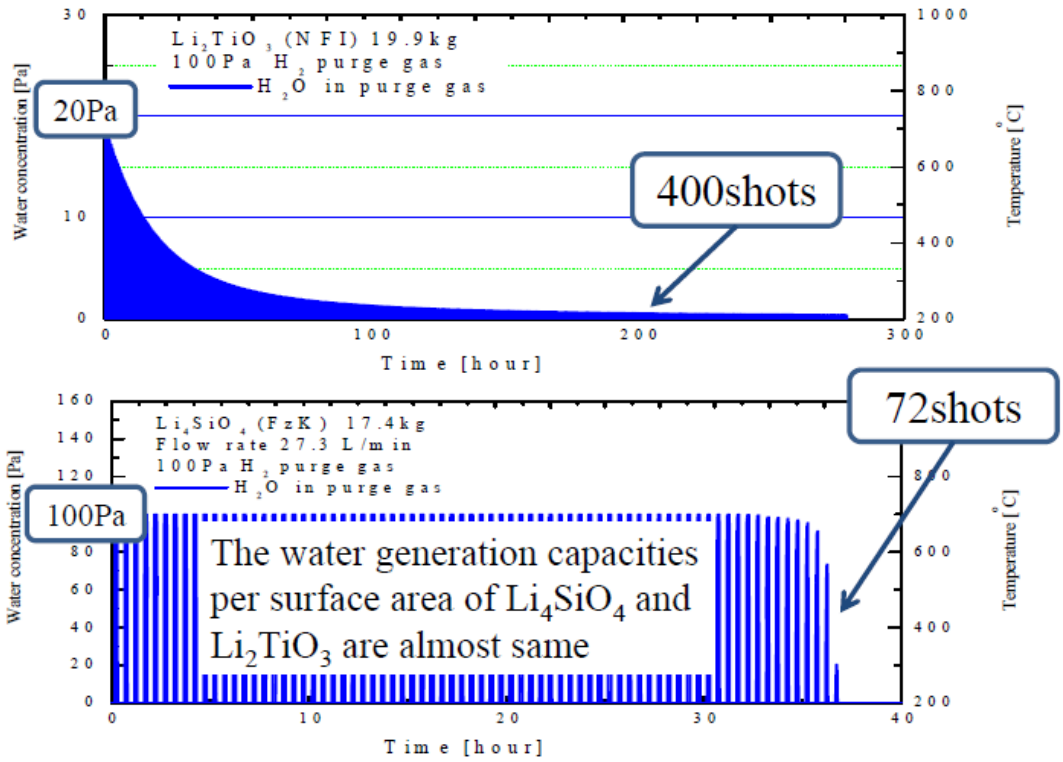

The simulation of tritium release

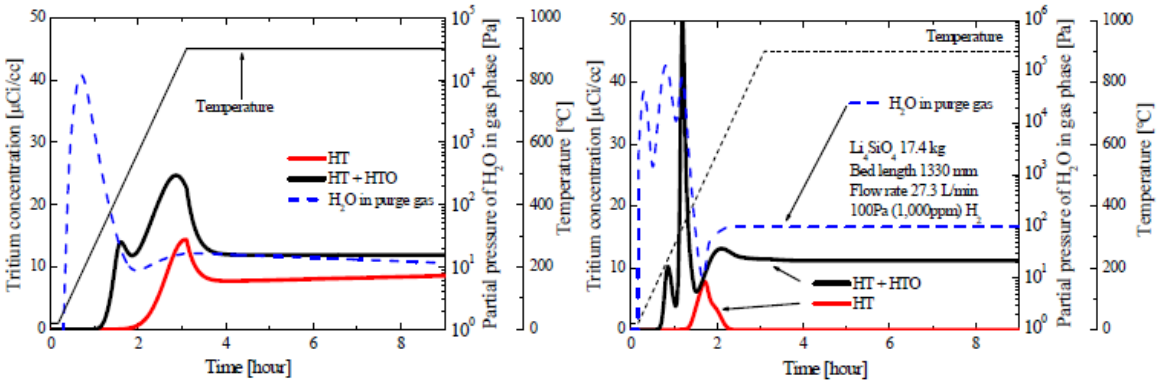

Li_2TiO_3 (grain size: 5.0 μ m)

Li_4SiO_4 (grain size: 1.0 μ m)

	The water release time from ITER-TBM	The amount of chemical adsorbed water(t)	The amount of water generation reaction(t)
Li_2TiO_3(NFI) 550t	400shots(25days)	6.42	0.82
Li_4SiO_4(FzK) 300t	72shots(4.5days)	10.3	0.69

The change of Li_4SiO_4 after the heating

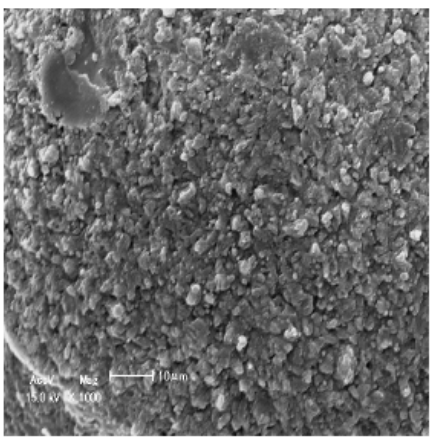

As-received

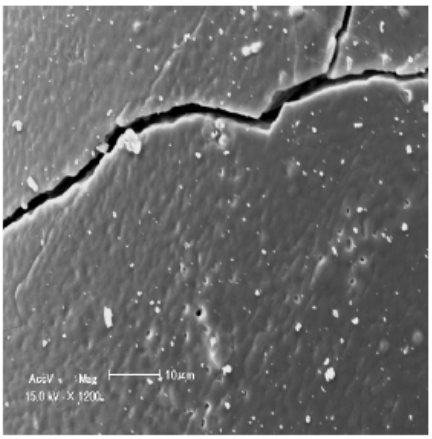

Placed in dry N_2 gas (800°C)

sintering

Such change of the surface in this study has not been observed for other solid breeder materials (Li_2TiO_3, $LiAlO_2$, and Li_2ZrO_3)

Those results imply that control of the surface water is important for operation of the Li_4SiO_4 blanket.

Permeation problems in recovery of bred tritium

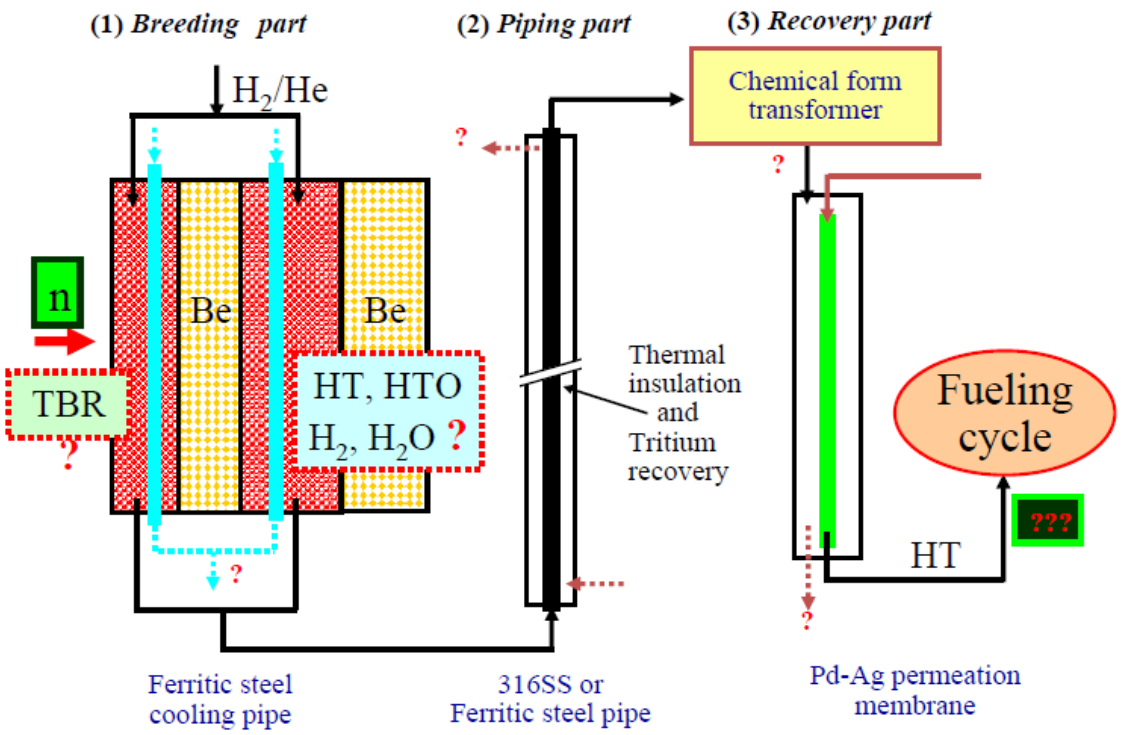

Schematic diagram of experimental apparatus for permeation

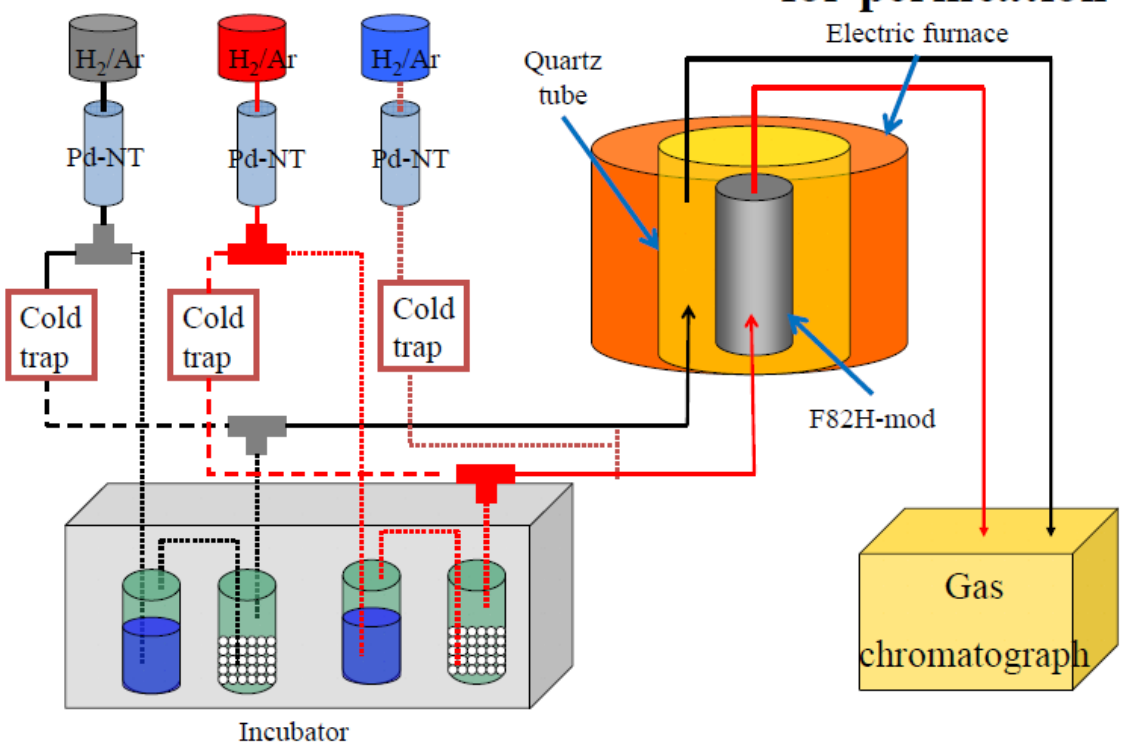

Permeation of hydrogen through F82H-mod

- Outer 10,000ppmH_2/Ar, Inner 500ppm%H_2/Ar

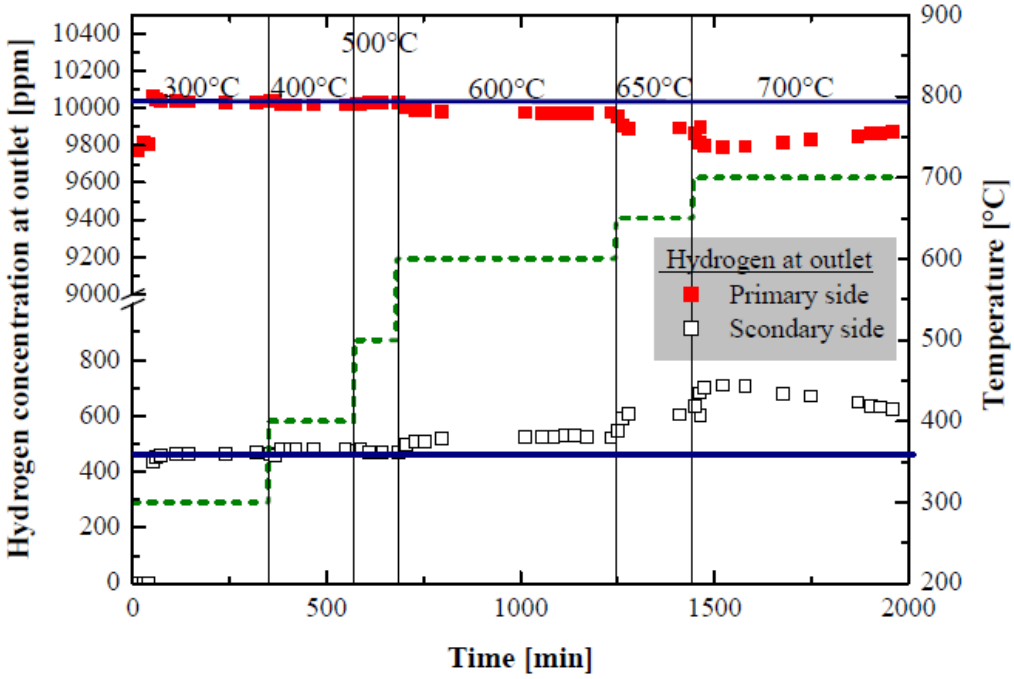

Permeability of hydrogen through F82H-mod

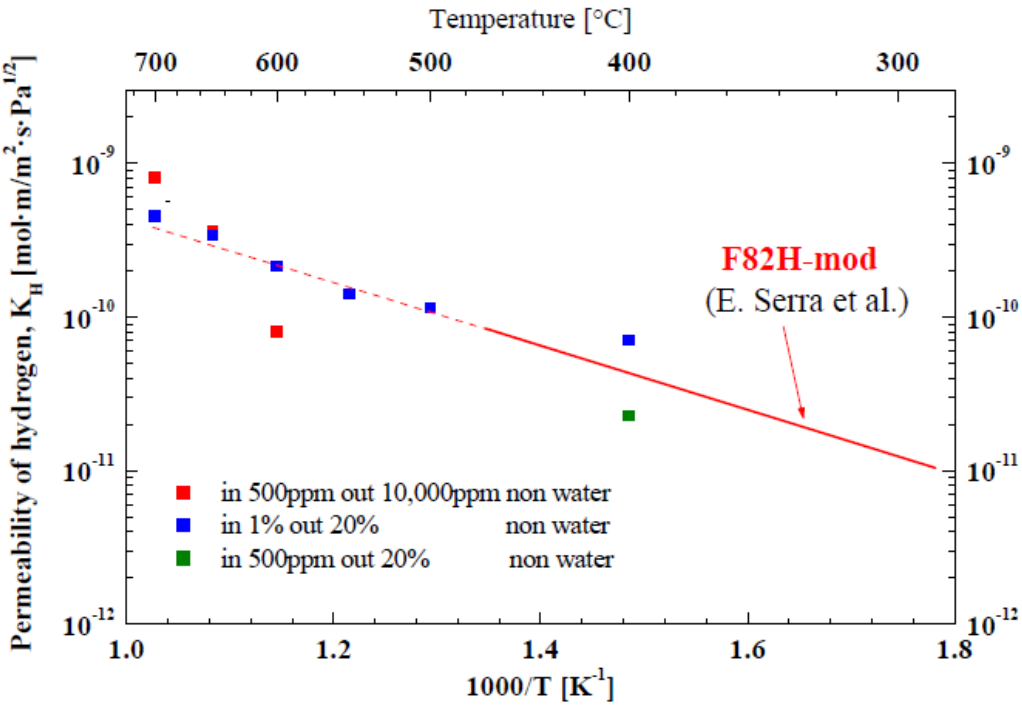

The diffusivity in F82H-mod

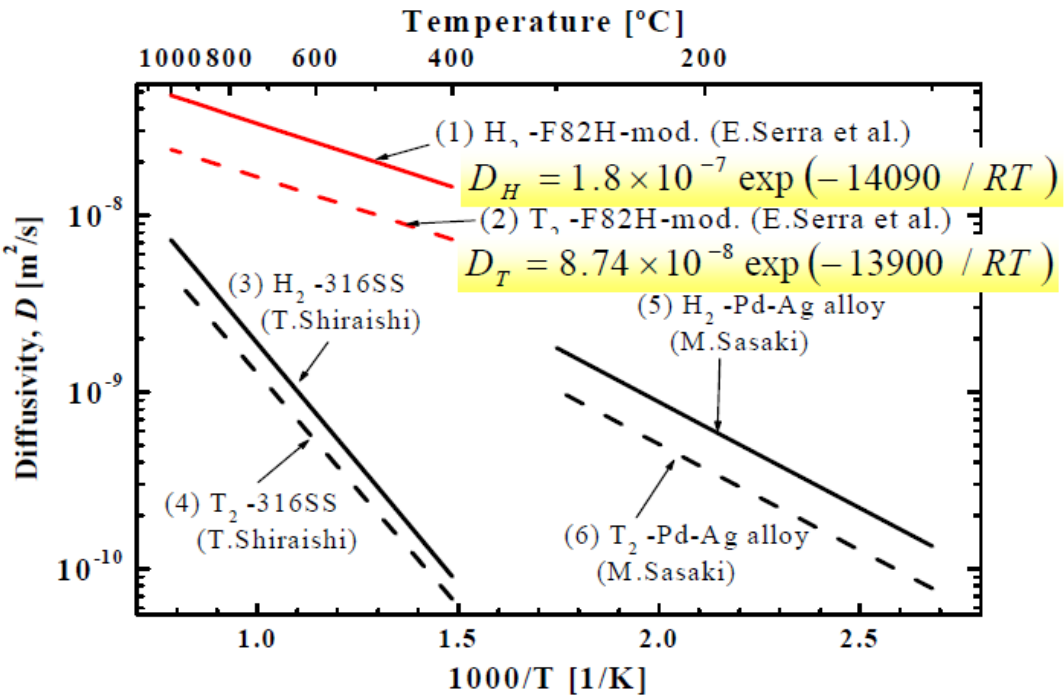

The solubility in F82H-mod

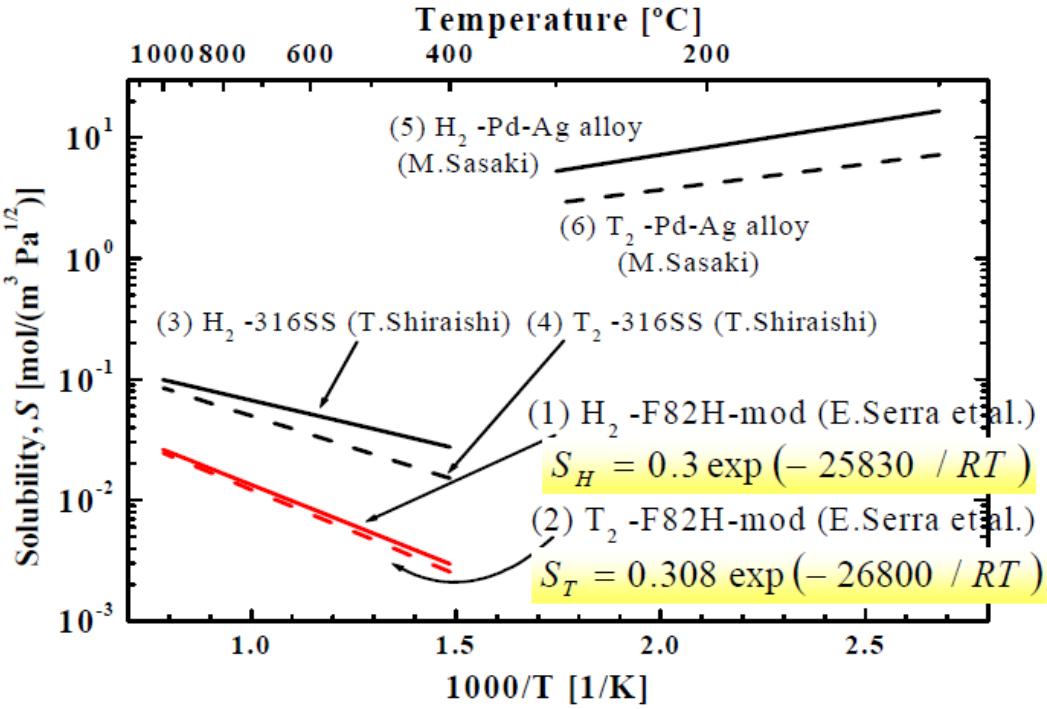

Tritium release model with cooling pipe

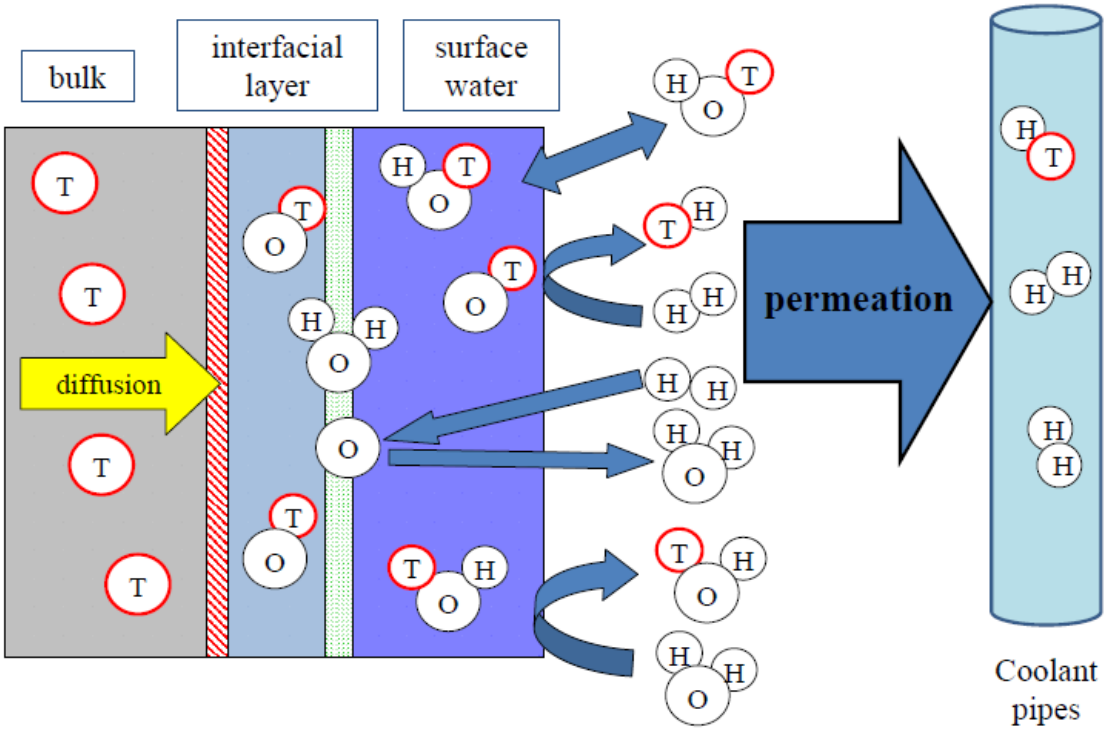

The simulation model of permeation

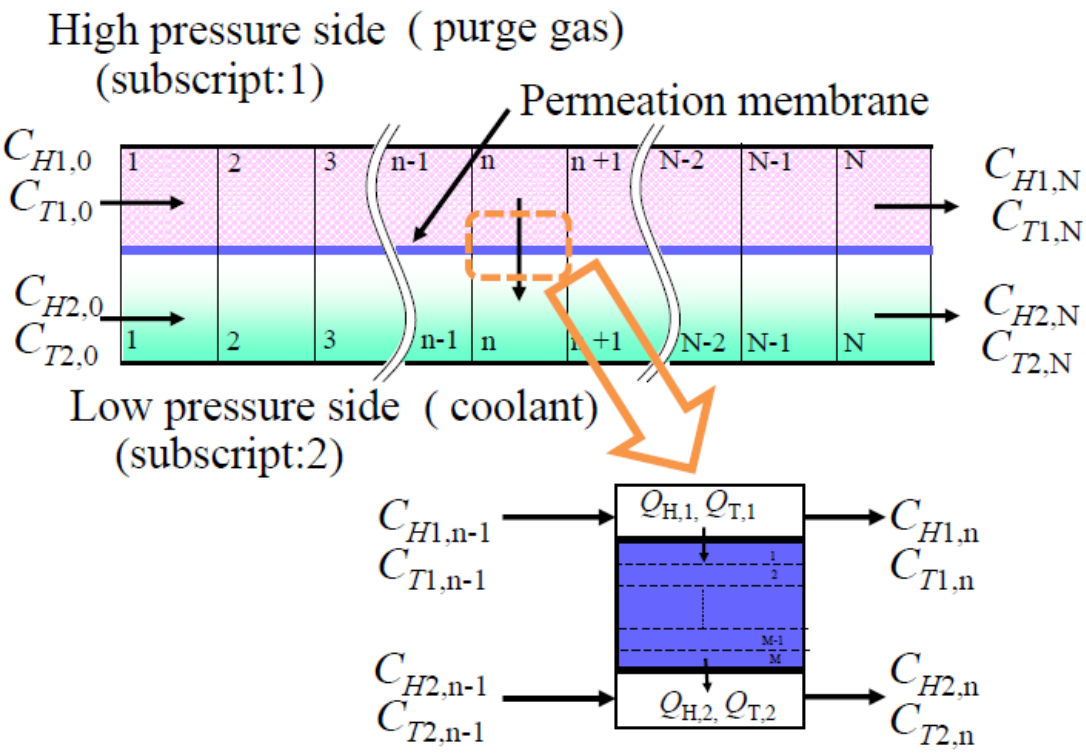

Blanket model with cooling pipes

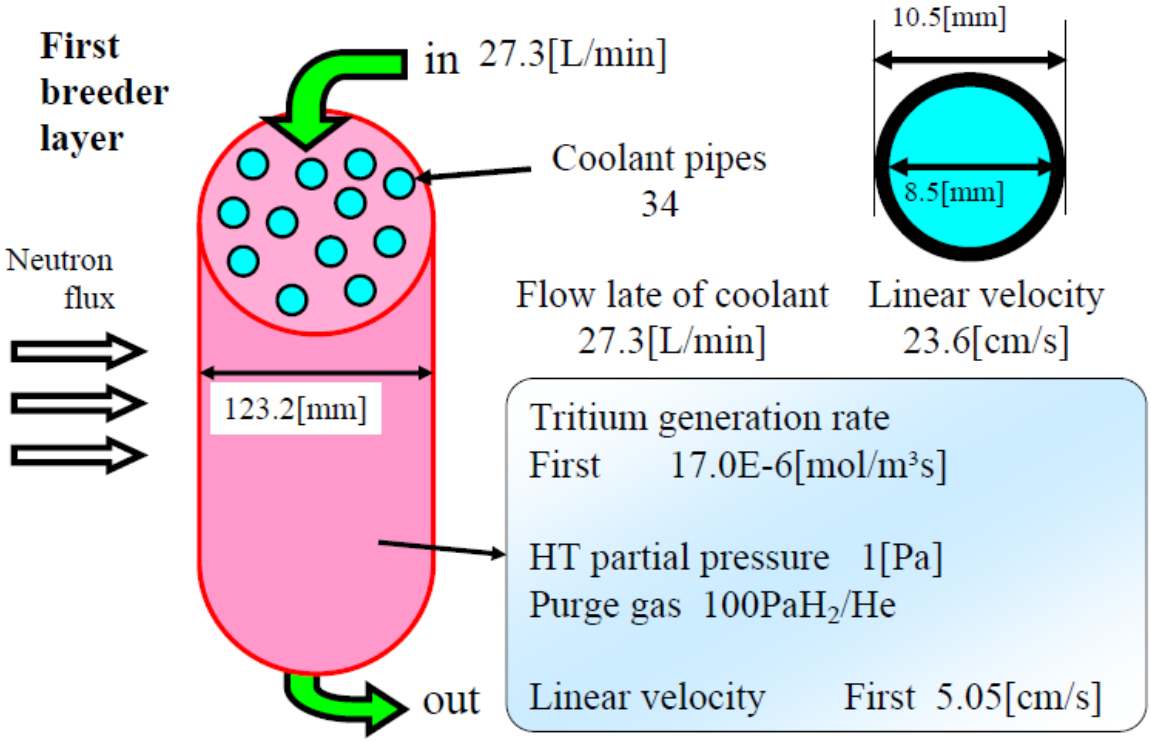

The simulation of tritium behavior in the Li_2TiO_3 blanket

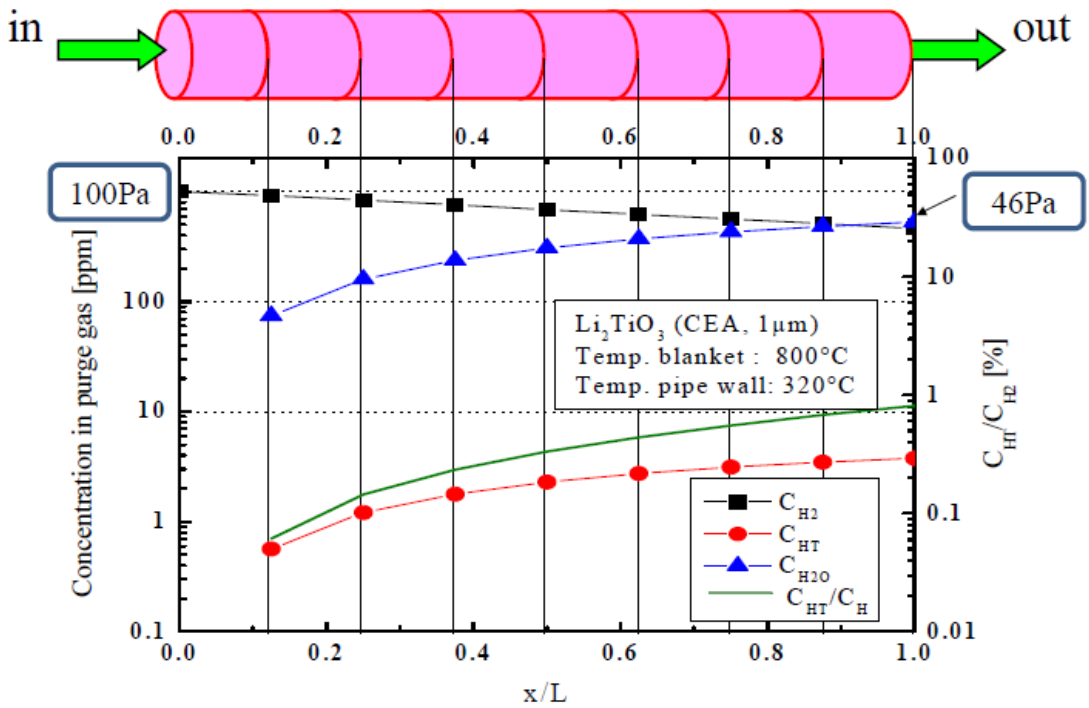

The simulation of tritium behavior in the Li_2TiO_3 blanket

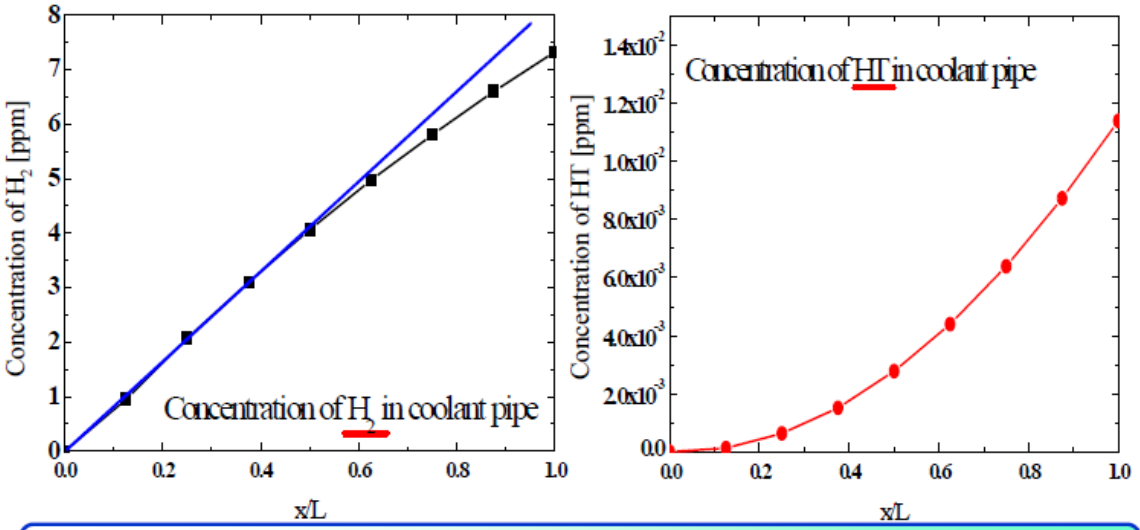

With the increase of HT in the blanket purge gas, permeation of tritium to the coolant pipes increase.

The simulation of tritium permeation to F82H-mod pipes in the Li_2TiO_3 blanket

Blanket temperature 800°C, **Coolant pipes temperature 320°C**

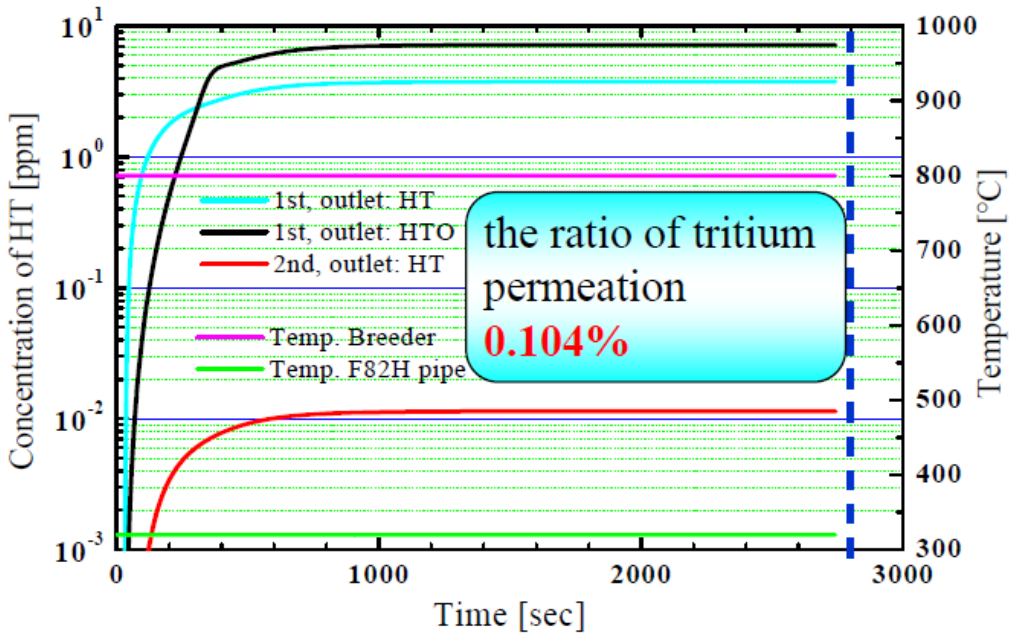

The simulation of hydrogen permeation to F82H-mod pipes in the Li_2TiO_3 blanket

Blanket temperature 800°C, Coolant pipes temperature 320°C

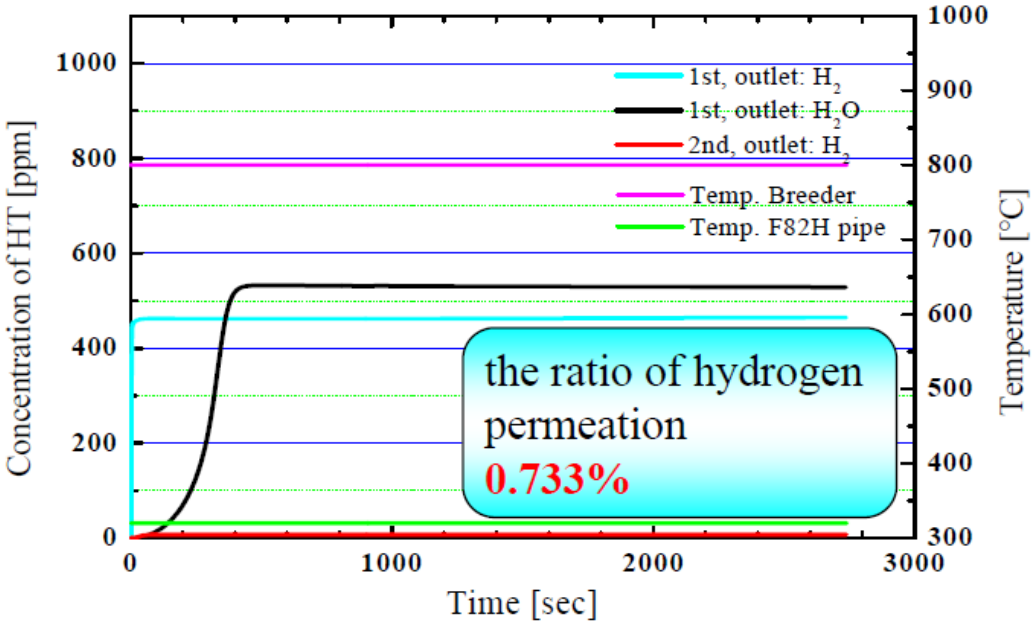

The simulation of tritium permeation to F82H-mod pipes in the Li_2TiO_3 blanket

Li_2TiO_3 (the water generation reaction has finished)

Blanket temperature 800°C, Coolant pipes temperature 320°C

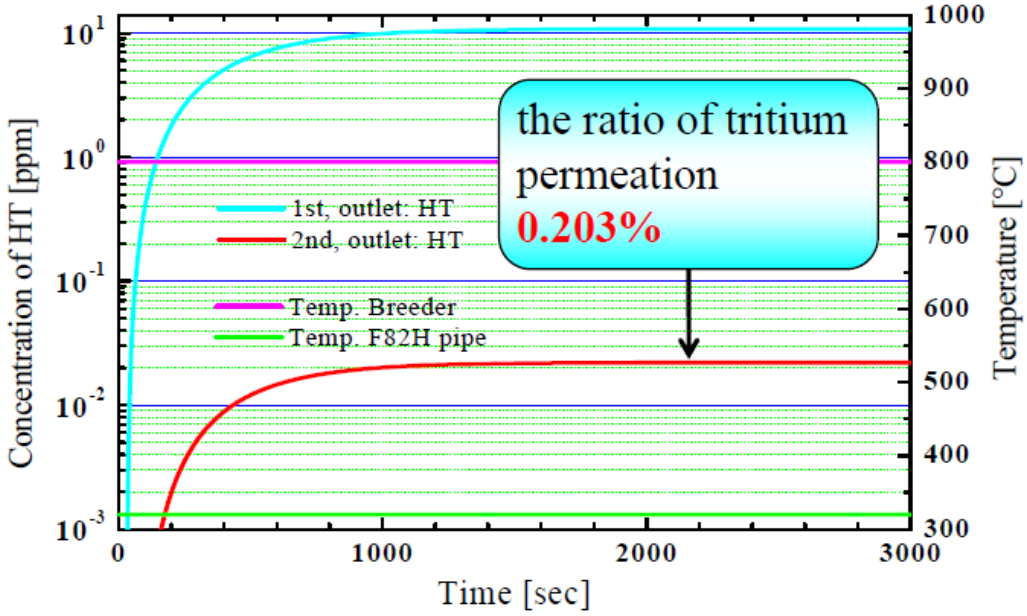

comparison of permeation
(Coolant pipes temperature 320°C)

	inlet concentration of H_2 [Pa]	100Pa
water generation reaction	outlet concentration of H_2 [Pa]	46Pa
	the ratio of HT permeation[%]	0.104%
	the ratio of H_2 permeation[%]	0.780%
Non-water generation reaction	outlet concentration of H_2 [Pa]	98Pa
	the ratio of HT permeation[%]	0.203%
	the ratio of H_2 permeation[%]	0.880%

The simulation of tritium permeation to F82H-mod pipes in the Li_2TiO_3 blanket

Blanket temperature 800°C, Coolant pipes temperature 500°C

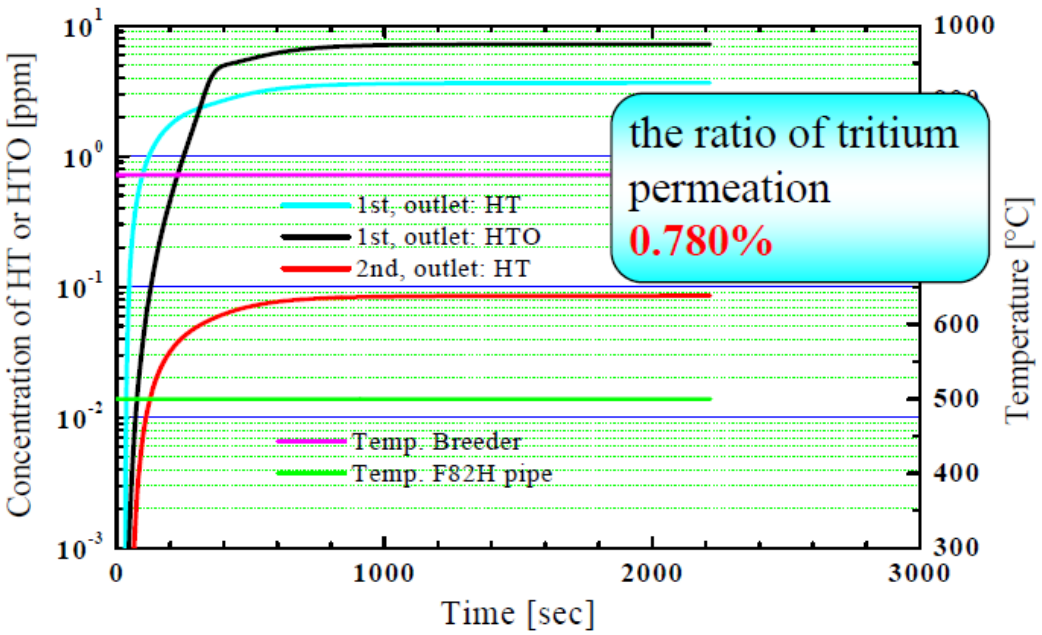

The simulation of hydrogen permeation to F82H-mod pipes in the Li_2TiO_3 blanket

Blanket temperature 800°C, Coolant pipes temperature 500°C

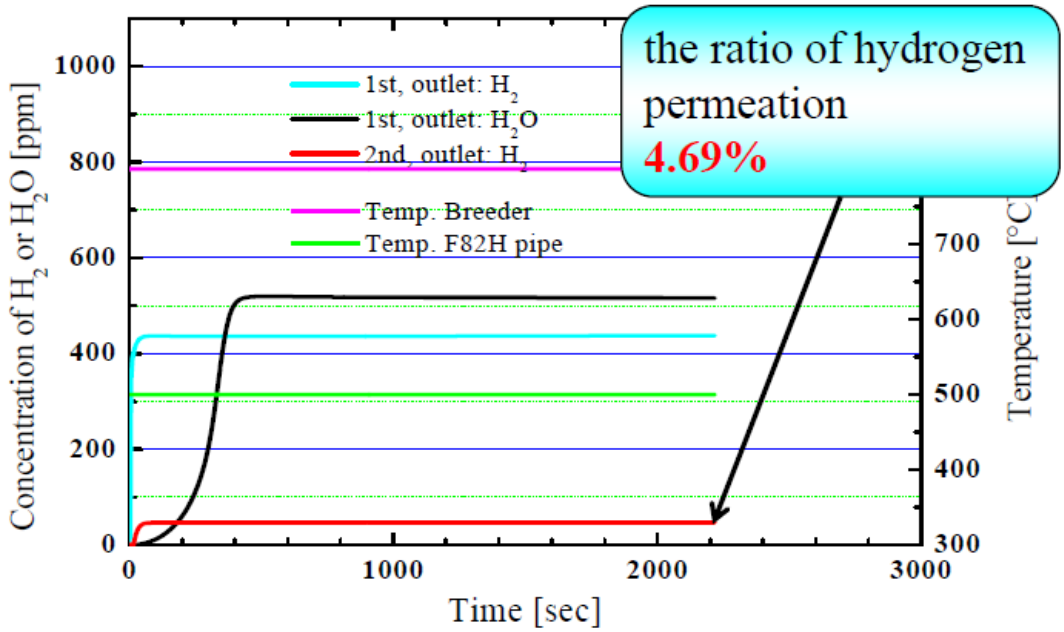

comparison of permeation

	Temp. coolant pipes	320°C	500°C	800°C
water generation reaction	the ratio of HT permeation[%]	0.104%	0.780%	4.66%
	the ratio of H_2 permeation[%]	0.733%	4.69%	20.0%
Non-water generation reaction	the ratio of HT permeation[%]	0.203%	1.57%	10.0%
	the ratio of H_2 permeation[%]	0.880%	5.94%	34.6%

Conclusion

- The water generation capacities per surface area of Li_4SiO_4 and Li_2TiO_3 are almost same. However, the water generation rate from Li_4SiO_4 is much faster than that observed for Li_2TiO_3.

- Li_4SiO_4 pebbles have the nature to react rapidly with water vapor and melt in water. Therefore, control of the surface water is important for operation of the Li_4SiO_4 blanket.

- When coolant pipes temperature is 320ºC, the ratio of HT permeation is 0.104%. When coolant pipes temperature is 500ºC, the ratio of HT permeation increases to about 7times. And the ratio of H_2 permeation is about 7times ratio of HT permeation.

- When the water generation reaction has finished, the ratio of HT permeation increases to about twice ratio, and the ratio of H_2 permeation increases to about 1.2 times ratio.

19. Tritium Balance in Blanket System of Fusion Reactor

Masabumi Nishikawa
Graduate School of Engineering Science, Kyushu University
6-10-1 Hakozaki Higashi-ku, Fukuoka 812-8681, Japan

Abstract

The amount of tritium bred in the breeding part of blanket system of a fusion reactor must exceeds the amount of tritium consumed in the reactor and the remainder is stored for the initial inventory of the next reactor to be constructed. It is found recently that not a little amount of tritium is trapped to the re-deposition layer of the first wall material of the plasma vessel. It is also anticipated that some amount of tritium is lost from the plasma driven permeation through the first wall material of the plasma vessel when the wall temperature becomes higher.

The tritium mass balance in a fusion reactor is discussed in this presentation considering tritium burning efficiency in plasma, tritium loss ratio in the fueling system, tritium loss due to β decay of tritium inventory and recovery efficiency in tritium production in the blanket system. The allowable range of tritium recovery efficiency in the blanket system obtained from this estimation is compared with the estimated permeation loss at the breeding part of the JAEA type test blanket module for ITER where the tritium concentration profile is calculated using the tritium release model from ceramic breeder materials composed by the present authors.

0CBBI－15, 2009

International Workshop on Ceramic Breeder Blanket Interaction-15
September 3-5,2009, Sapporo, Japan

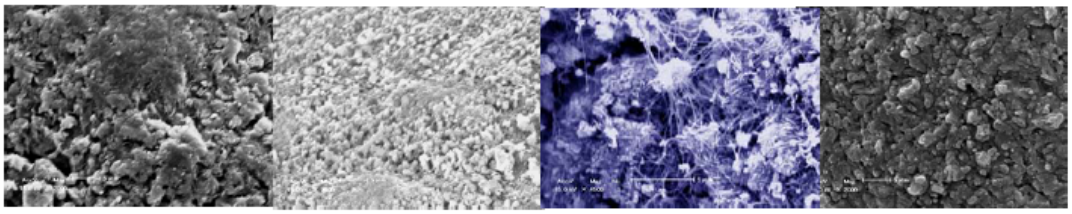

Tritium Balance in Blanket System of a DT Fusion Reactor

Masabumi Nishikawa
Graduate School of Engineering Science
Kyushu University, Japan

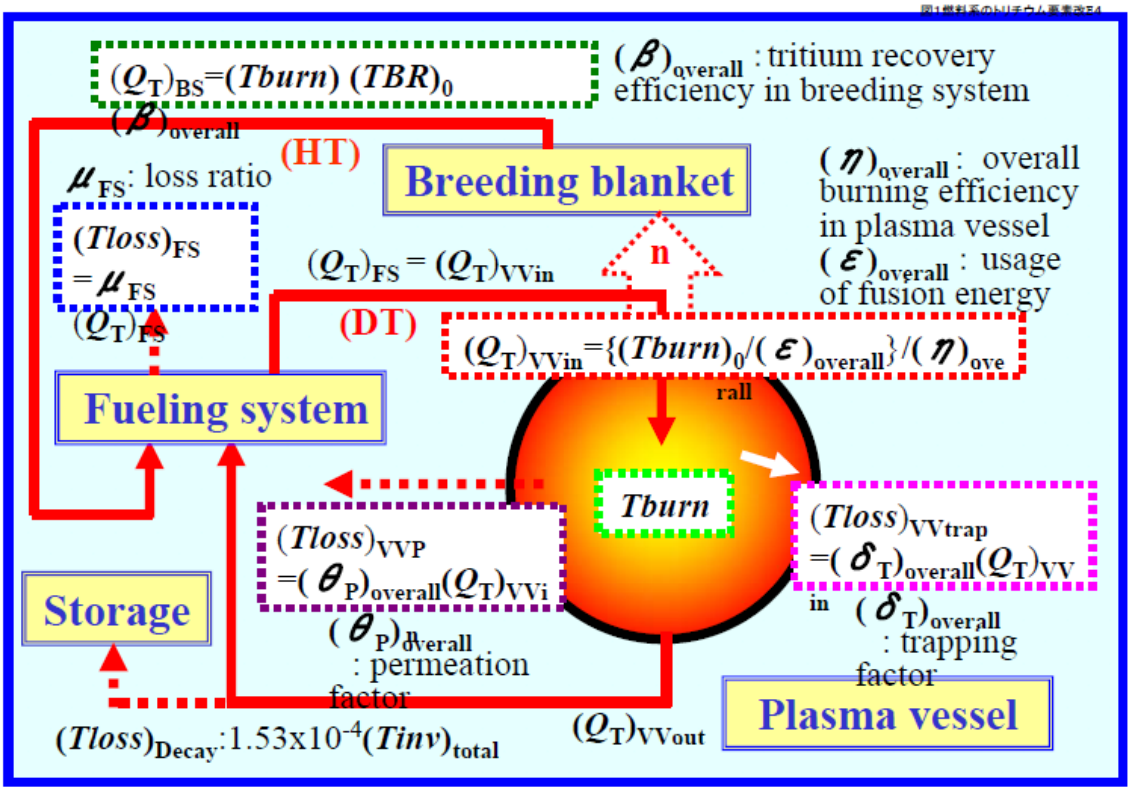

Tritium balance in a DT fusion reactor

Conditions necessary to achieve DT fuel self sufficiency was discussed by Prof. Abdou et al. in 1986. They stated that the uncertainties due to nuclear data and calculation methods were found to be significant.

By Abdou

Tritium inventory on vessel surface

Sum of both processes:

by Roth et al.

comparison of materials options

EU assessment

Review for PPCF, submitted March 2008

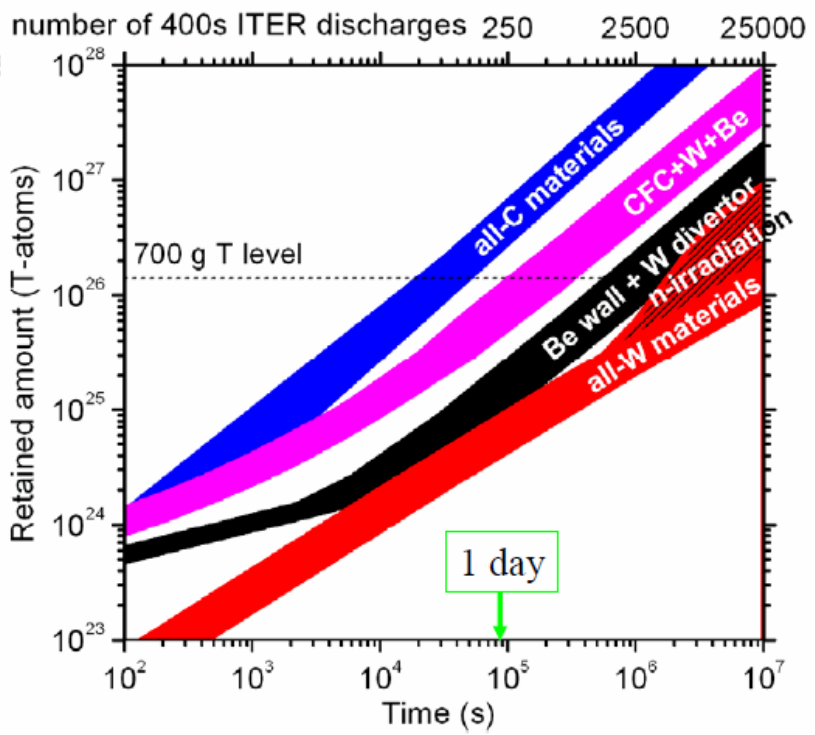

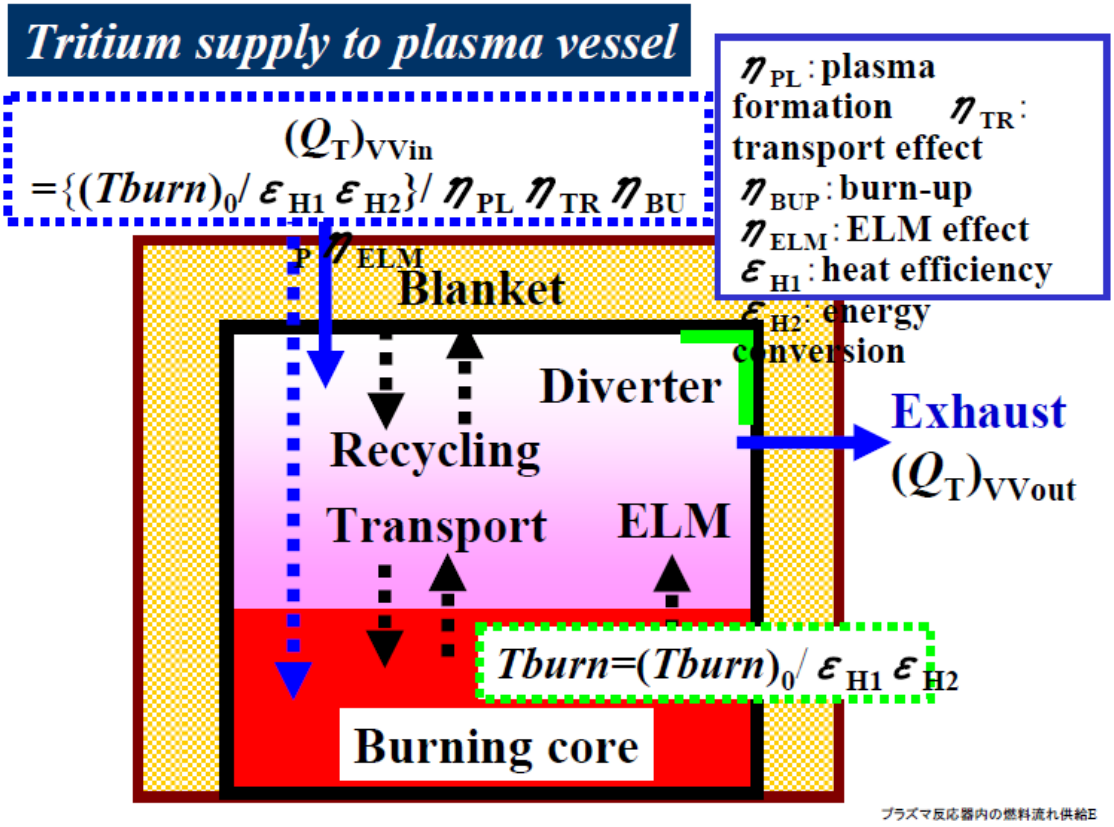
Tritium supply to plasma vessel
$(Q_T)_{VVin}$
$=\{(Tburn)_0/\varepsilon_{H1}\varepsilon_{H2}\}/\eta_{PL}\eta_{TR}\eta_{BU}$
η_{PL} : plasma formation
η_{TR} : transport effect
η_{BUP} : burn-up
η_{ELM} : ELM effect
ε_{H1} : heat efficiency
ε_{H2} : energy conversion
η_{ELM}
Blanket
Diverter
Recycling
Transport
ELM
Exhaust
$(Q_T)_{VVout}$
$Tburn=(Tburn)_0/\varepsilon_{H1}\varepsilon_{H2}$
Burning core
プラズマ反応器内の燃料流れ供給E

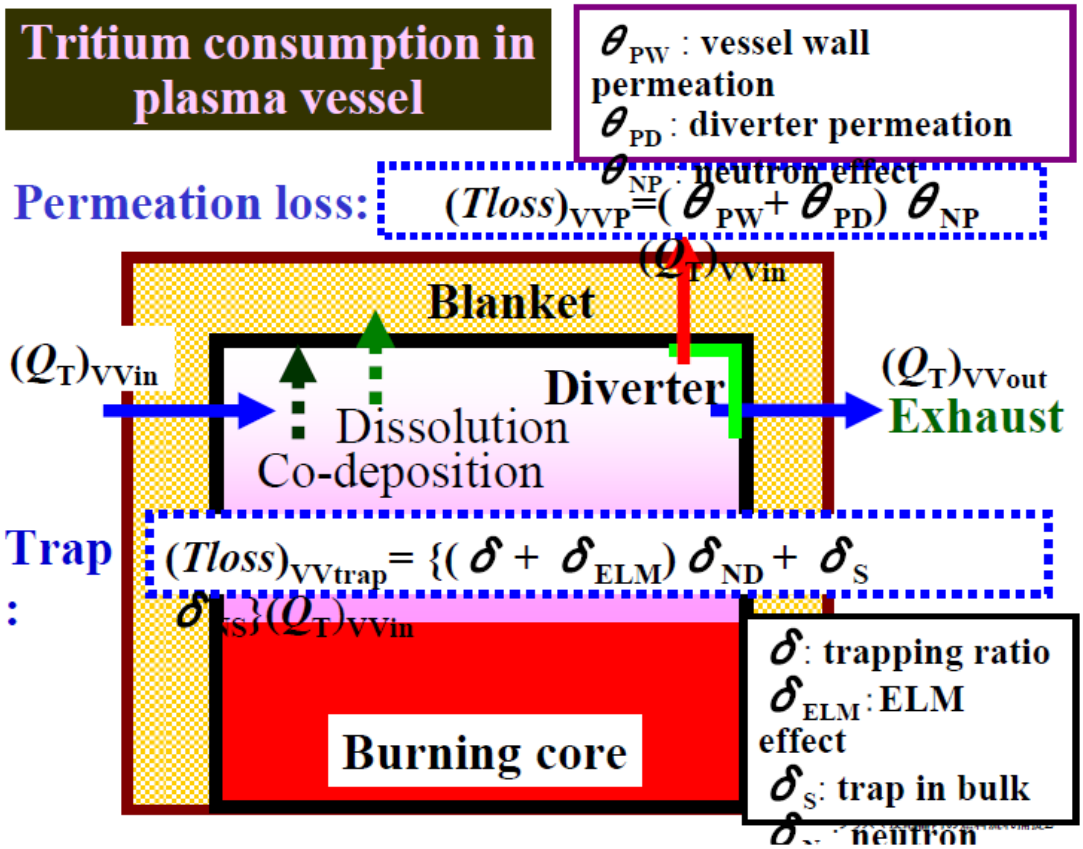
Tritium consumption in plasma vessel
θ_{PW} : vessel wall permeation
θ_{PD} : diverter permeation
θ_{NP} : neutron effect
Permeation loss:
$(Tloss)_{VVP}=(\theta_{PW}+\theta_{PD})\theta_{NP}(Q_T)_{VVin}$
Blanket
$(Q_T)_{VVin}$
Diverter
$(Q_T)_{VVout}$
Exhaust
Dissolution
Co-deposition
Trap :
$(Tloss)_{VVtrap}=\{(\delta+\delta_{ELM})\delta_{ND}+\delta_S\delta_{NS}\}(Q_T)_{VVin}$
δ: trapping ratio
δ_{ELM} : ELM effect
δ_S: trap in bulk
Burning core

Tritium production at blanket system

Tritium from blanket system:

$$(Q_T)_{BS}=(Tburn)(TBR)_0\,\beta_{VV}\,\beta_{MD}\,\beta_{BT}$$

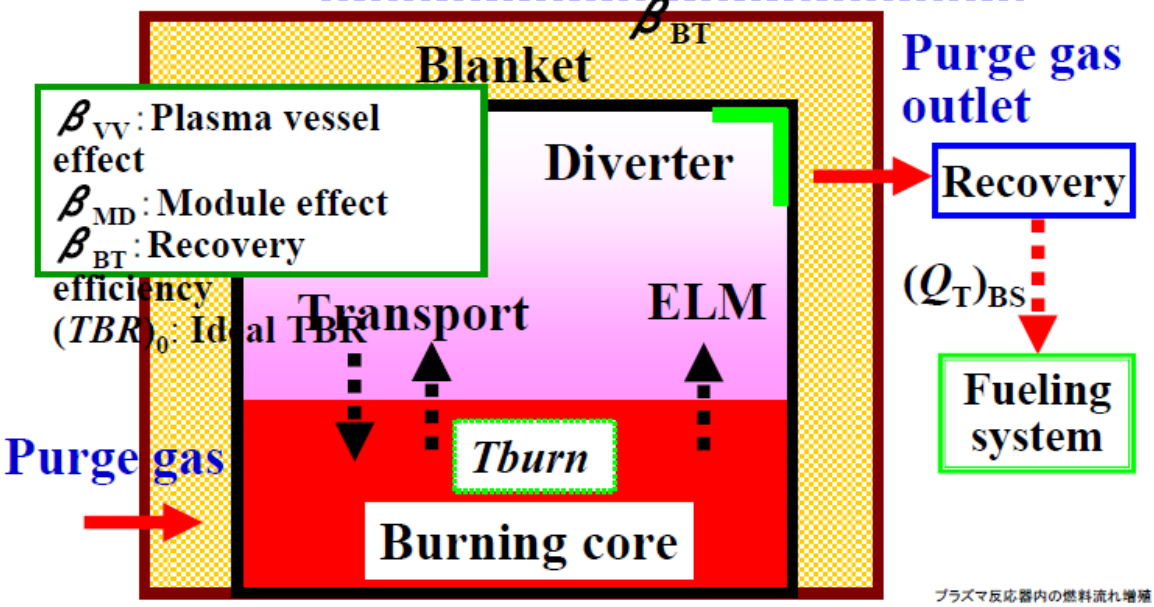

プラズマ反応器内の燃料流れ増殖
E

トリチウムバランス式1

Tritium gain from a fusion reactor

$$(Q_T)_{gain}=(Q_T)_{BS}-(Tburn)-(Tloss)_{VVtrap}-(Tloss)_{VVP}-(Tloss)_{FS}-(Tloss)_{Decay}$$

$(Q_T)_{BS}$: Tritium output from blanket system, gT/day
$Tburn$: Tritium burning rate in plasma vessel, gT/day
$(Tloss)_{VVtrap}$: Tritium loss due to trap in plasma vessel, gT/day
$(Tloss)_{VVP}$: Tritium loss due to permeation at plasma vessel, gT/day
$(Tloss)_{FS}$: Tritium loss in main fueling system, gT/day
$(Tloss)_{Decay}$: Tritium loss due to decay of active inventory, gT/day

$$= (Tburn)[(TBR)_0(\beta)_{overall}-1-\{(\delta_T)_{overall}+(\theta_P)_{overall}+\mu_{FS}\}/(\eta)_{overall} - 1.53\times10^{-4}(Tinv)_{total}/(Tburn)]$$

$$= (Tburn)\{(TBR)_{BS}-1-(\Delta_T)_{overall}/(\eta)_{overall}-1.53\times10^{-4}(Tinv)_{total}/(Tburn)\}$$

Reactor base tritium breeding ratio: $\{(Q_T)_{gain}+(Tburn)\}/(Tburn)$

$$(TBR)_R = (TBR)_{BS} - \{(\delta_T)_{overall}+(\theta_P)_{overall}+\mu_{FS}\}/(\eta)_{overall} - 1.53\times10^{-4}(Tinv)_{total}/(Tburn)$$

$$= (TBR)_R - (\Delta_T)_{overall}/(\eta)_{overall} - 1.53\times10^{-4}(Tinv)_{total}/(Tburn)]/(TBR)_0$$

Allowable range of overall recovery efficiency in tritium breeding which is decided from tritium balance in a fusion reactor.

$$1 \geqq (\beta)_{overall} \geqq \{(TBR)_R + (\Delta_T)_{overall}/(\eta)_{overall} + 1.53\times10^{-4}(Tinv)_{total}/(Tburn)\}/(TBR)_0$$

Tritium balancing factor in a DT fusion reactor

$$\Gamma_T = \frac{(\beta)_{overall}\,(TBR)_0}{(TBR)_R + (\Delta_T)_{overall}/(\eta)_{overall} + 1.53\times10^{-4}(Tinv)_{total}/(Tburn)}$$

Tritium balancing factor in plasma vessel

$$(\Gamma_T)_{VV} = (\text{Overall tritium loss ratio})/(\text{Overall burning efficiency}) = \{(\delta_T)_{overall}+(\theta_P)_{overall}+\mu_{FS}\}/(\eta)_{overall}$$

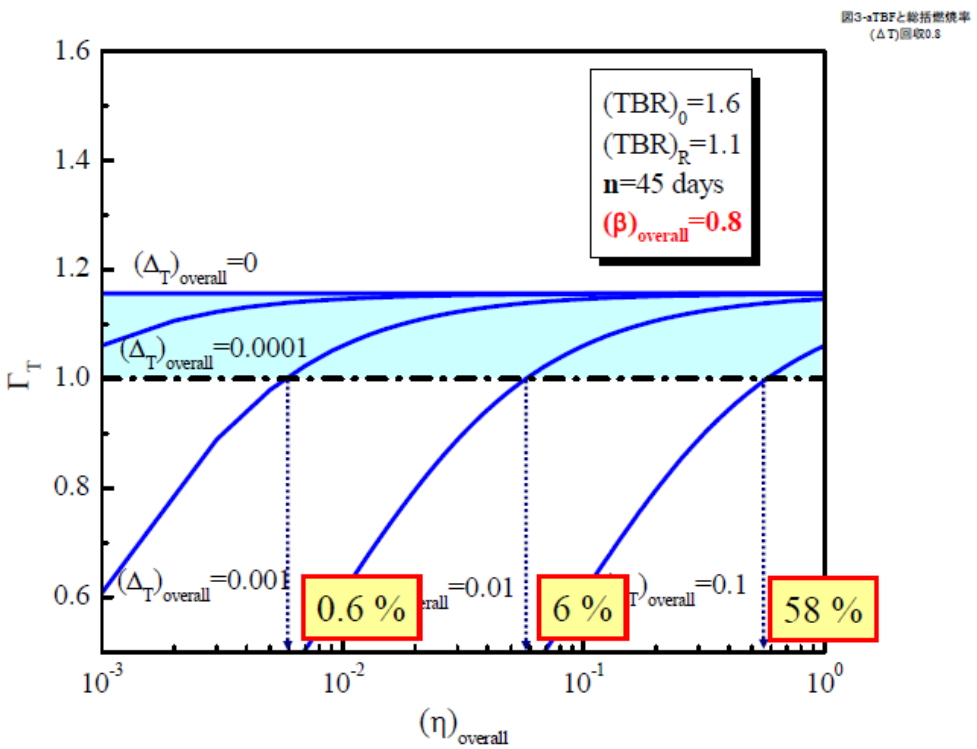

Fig. 3-a Effect of $(\eta)_{overall}$ and $(\Delta_T)_{overall}$ on tritium balancing factor when $(\beta)_{overall}$ is 0.8.

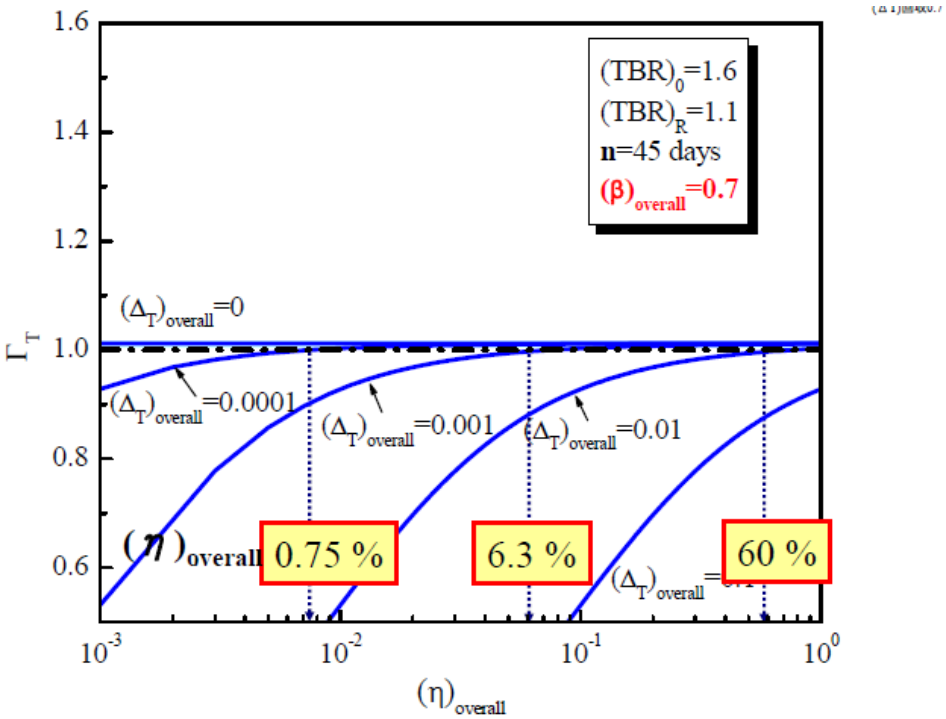

Fig. 3-b Effect of $(\eta)_{overall}$ and $(\Delta_T)_{overall}$ on tritium balancing factor when $(\beta)_{overall}$ is 0.7.

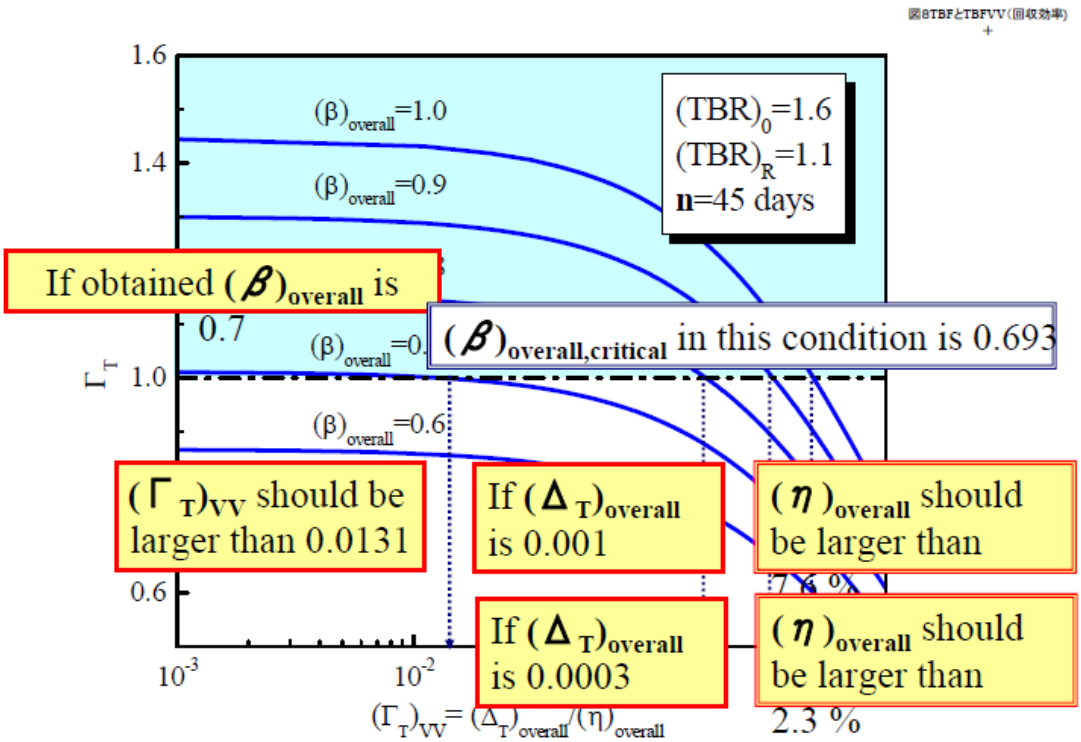

Fig. 8 Tritium balancing factor in plasma vessel and tritium balancing factor (parameter:$(\beta)_{overall}$).

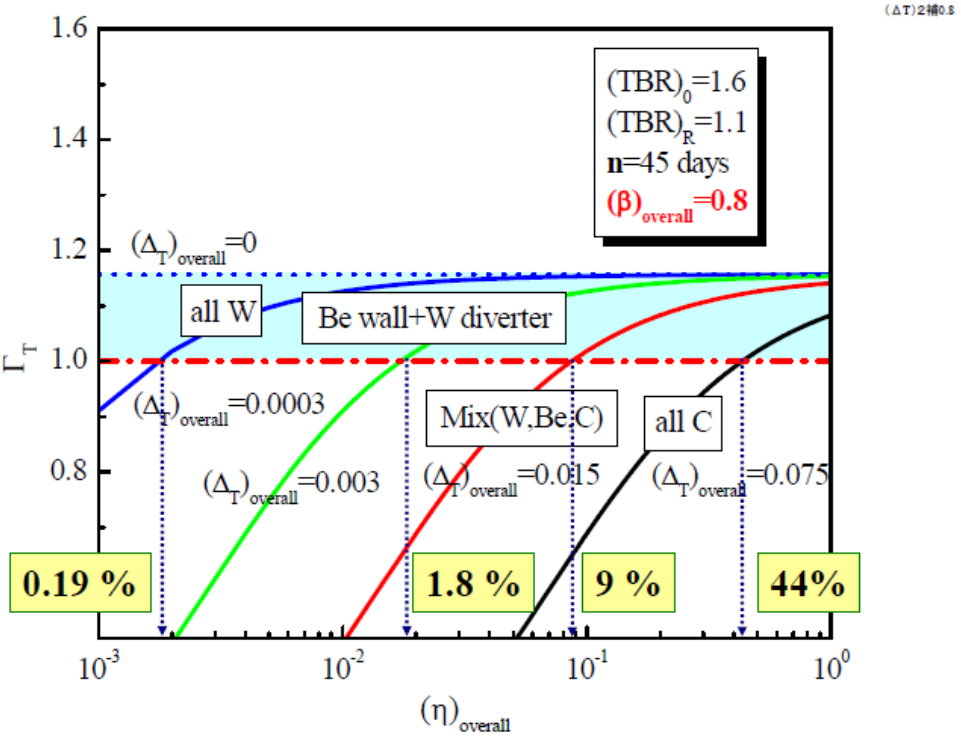

Fig. 4 Comparison of Tritium balancing factor estimated for various first wall materials.

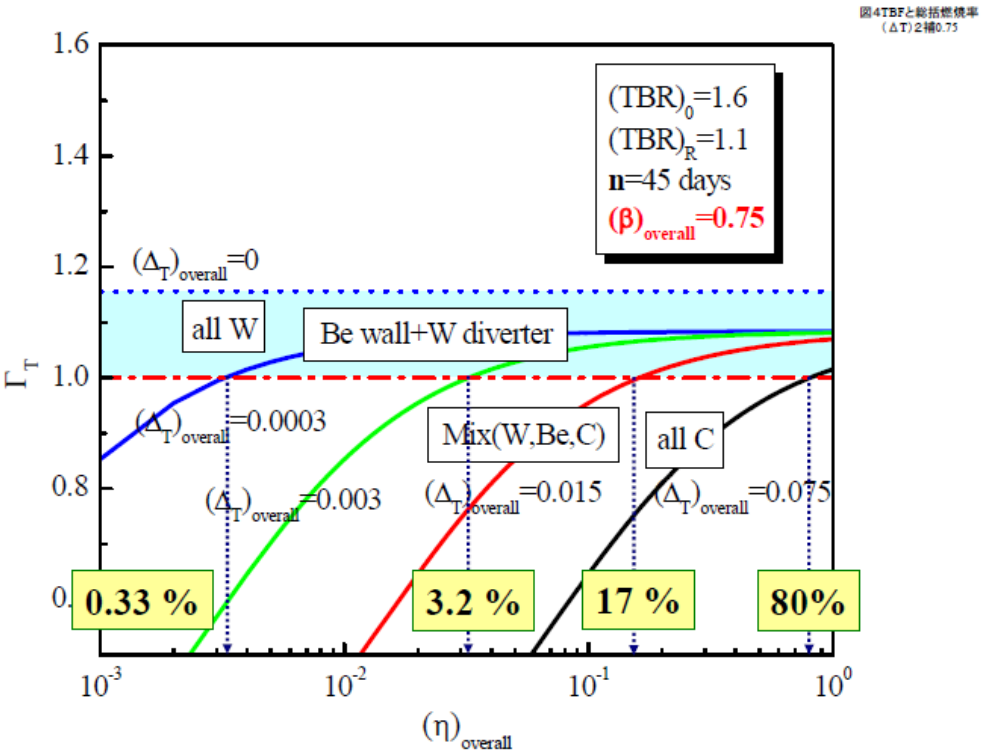

Fig. 4 Comparison of Tritium balancing factor estimated for various first wall materials.

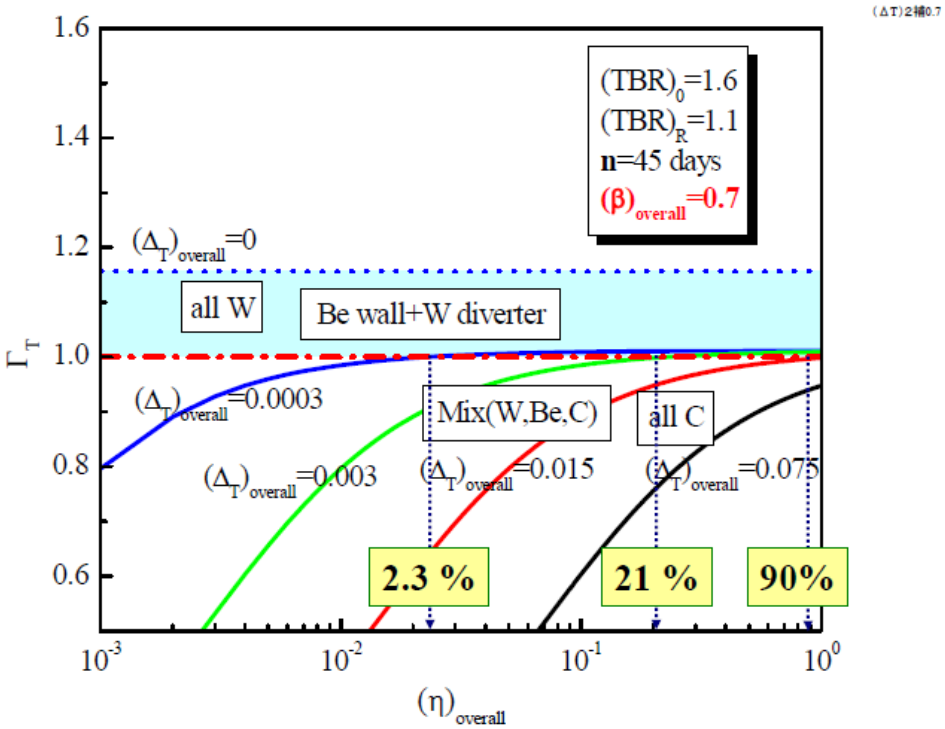

Fig. 4 Comparison of Tritium balancing factor estimated for various first wall materials.

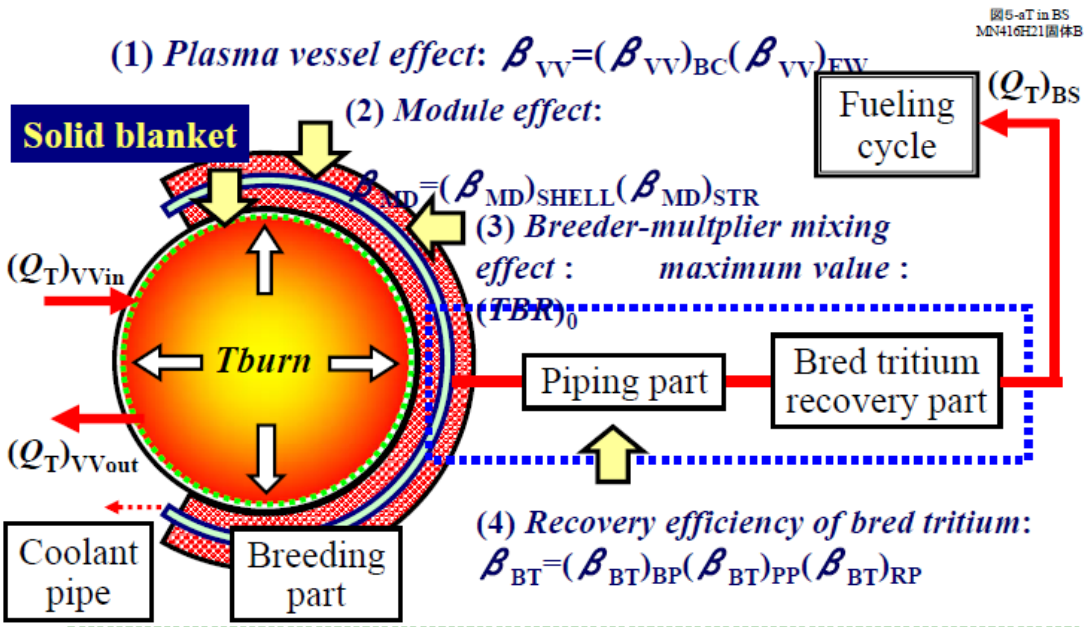

Fig. Maximum overall recovery efficiency $(\beta)_{overall,\ Max}$ ·

Table 2. Results of TBR calculation with candidate options of materials and structures. (Enoeda et al. Nucl. Fusion (2003))

Materials	Li2O/Be		Li2TiO3/Be		
6Li enrichment (%)	30	90	30	90	90
Packing structure	Breeder/multiplier separate				
Temperature limit	breeder		900		900
	multiplier		600		900
Local TBR	1.53	1.56	1.41	1.52	1.37
Coverage requirement (%)	69	67	74	69	77

Required coverage fraction of plasma-facing surface of the breeding region of the blanket in the total area of the plasma facing surface to achieve a net TBR of 1.05 .

$(\beta)_{overall} = \beta_{VV} \{(\beta_{MD})_{SHELL} (\beta_{MD})_{STR}\} \beta_{BT}$

Coverage requirement may include a part of $(\beta_{MD})_{SHELL}$.

トリチウムバランス式3

***Tritium breeding rate*: $(Q_T)_{BS}$ [gT/day]**

$$(Q_T)_{BS} = (Tburn)(TBR)_0 \beta_{VV} \beta_{MD} \beta_{BT}$$
$$= (Tburn)(TBR)_0 (\beta)_{overall}$$

Tritium bred in breeding part of blanket

$$(Q_T)_{bred} = (Tburn)(TBR)_0 \beta_{VV} \beta_{MD} \quad \text{,gT/day}$$

Overall recovery efficiency in tritium breeding system

$$(\beta)_{overall} = \beta_{VV} \beta_{MD} \beta_{BT}$$

β_{VV}: plasma vessel effect

β_{MD}: module effect

β_{BT}: recovery efficiency of bred tritium

***Blanket base tritium breeding ratio*: $(Q_T)_{BS}/(Tburn)$**

$$(TBR)_{BS} = (TBR)_0 (\beta)_{overall}$$

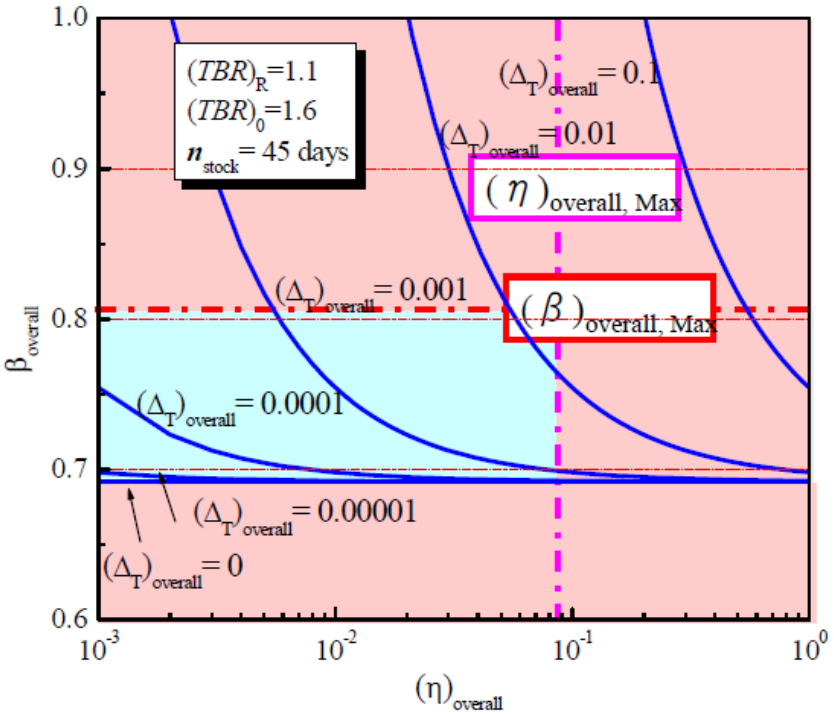

Fig. 3 Effect of tritium loss and burning efficiency in plasma vessel on recovery efficiency in tritium breeding system

---

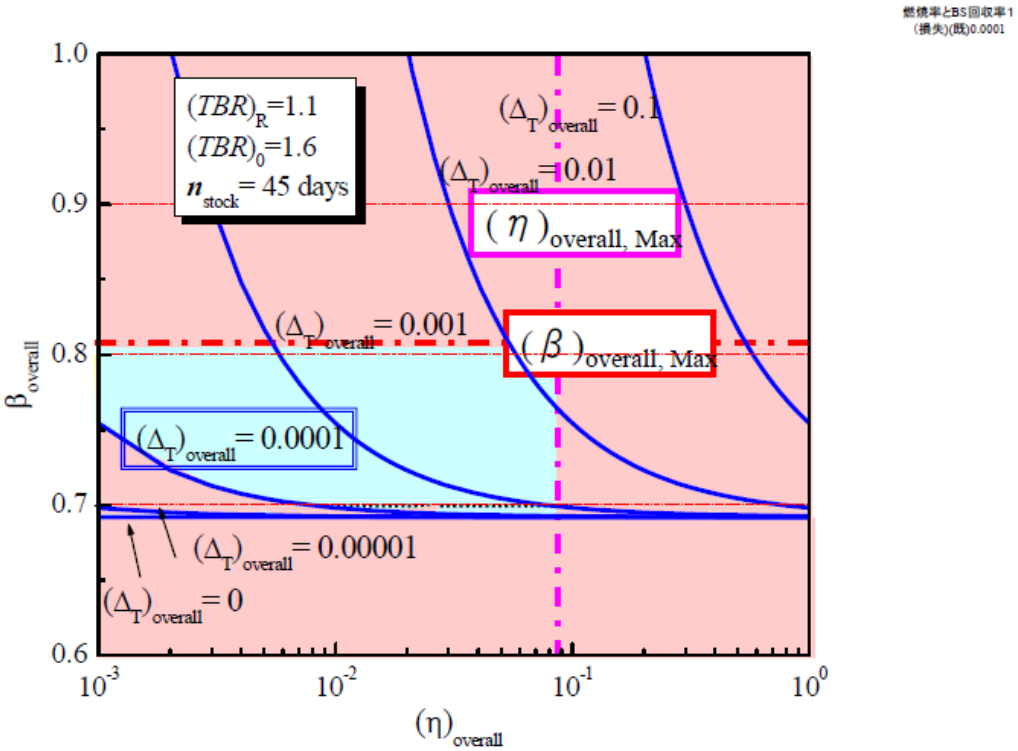

Fig. 3 Effect of tritium loss and burning efficiency in plasma vessel on recovery efficiency in tritium breeding system

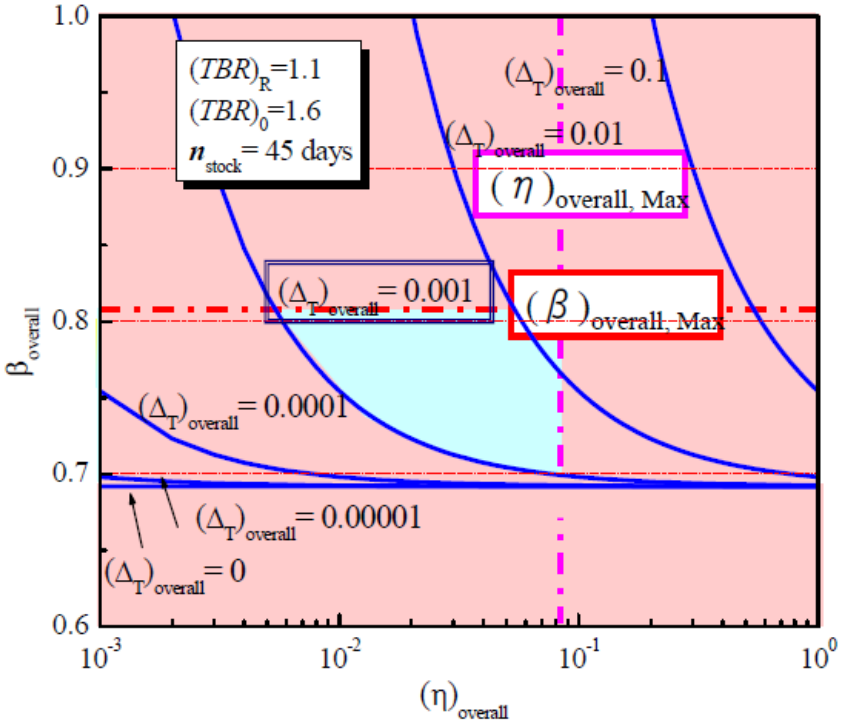

Fig. 3 Effect of tritium loss and burning efficiency in plasma vessel on recovery efficiency in tritium breeding system

---

表1 増殖T回収の要因

Conclusion :Ways to improve tritium balancing factor of reactor

(1) Increase of tritium production rate in blanket system

1. Development of effective breeder-multiplier system $(TBR)_0$
2. Effective usage of fusion neutron (β_{VV}), (β_{MD})
   - i. Increase of blanket coverage $(\beta_{MD})_{BC}$
   - ii. Reduction of neutron absorption $(\beta_{VV})_{FW}$, $(\beta_{MD})_{SHELL}$, $(\beta_{MD})_{ST}$

(2) Reduction of tritium loss in breeding blanket system (β_{BT})

1. Reduction of tritium loss at breeding part $(\beta_{BT})_{BP}$
2. Reduction of tritium loss at piping part $(\beta_{BT})_{PP}$, $(\beta_{BT})_{HP}$
3. Reduction of tritium loss at recovery part $(\beta_{BT})_{RP}$
4. Recovery system of permeated tritium $(\beta_{BT})_{BP}$, $(\beta_{BT})_{PP}$

(3) Reduction of tritium loss in plasma vessel $(\Gamma_T)_{VV}$

1. Increase of overall tritium burning ratio $(\eta)_{overall}$
2. Reduction of tritium loss at plasma facing material $(\Delta_T)_{overall}$

20. In-situ observation of hydrogen isotopes interacting with radiation defects in $LiTaO_3$

Kenichiro Ikuno [1], Takuji Oda[1], Kisaburo Azuma[1], Satoru Tanaka[1]

[1]*Department of Nuclear Engineering and Management: The University of Tokyo, Tokyo, Japan*

Understanding the mechanism of tritium desorption from breeding materials (ternary lithium oxide such as Li_2TiO_3) is an important research subject for enhancing the reliability of fuel cycle in nuclear fusion reactors. Previous studies have frequently indicated that radiation defects affect tritium diffusion and desorption behaviors. However, there are few studies observing behaviors of hydrogen isotopes and radiation defects at the same time. In the present study, therefore, we simultaneously performed thermal desorption spectroscopy (TDS), UV-VIS spectroscopy and IR spectroscopy (FT-IR), with the aim of identifying factors that determine behavior of hydrogen isotopes interacting with radiation defects in ternary lithium oxides. As a ternary lithium oxide, $LiTaO_3$ was chosen, because single crystals of $LiTaO_3$ can be used and thus precise spectroscopy experiments are feasible.

Specimens of $LiTaO_3$ <001> single crystals ($10\times10\times1$ mm^3) were irradiated by deuterium ion (D^+) of 300 keV in order to load hydrogen isotopes and radiation defects closely. Then, irradiated specimens were heated in a vacuum. In heating, we analyzed desorbed gases by TDS, amounts of defects by UV-VIS, and chemical forms of hydrogen isotopes by FT-IR

In TDS, deuterium was mainly released as hydrogen molecules (HD, D_2) in the temperature range of 350 to 500 °C.

In UV-VIS, a broad peak in wavelength range of 300 to 800 nm appeared and increased in proportion to the irradiation fluence during D^+ irradiation. This peak decreased in the temperature range of 300 to 400 °C during heating after the irradiation. These phenomena are considered to be derived from generation of radiation defects by D^+ irradiation and recovery of radiation defects by heating.

In FT-IR, two sharp O-D vibration peaks were observed at 2560 cm^{-1} and 2620 cm^{-1}. The peak at 2620 cm^{-1} has not been observed by experiments in that deuterium was thermally loaded into $LiTaO_3$. By heating, the intensity of this peak increased in the temperature range of 350 ºC to 430 ºC together with increase of D_2 desorption in TDS, and then decreased. These results indicate correlation between release behavior of hydrogen isotopes and their chemical forms in the material. The factors that determine behavior of hydrogen isotopes interacting with radiation defects were discussed.

In-situ observation of hydrogen isotopes interacting with radiation defects in $LiTaO_3$

Kenichiro Ikuno, Takuji Oda, Satoru Tanaka
The University of Tokyo

Background & Objective:
Behavior of hydrogen isotopes in ternary Li oxides

<Behavior of hydrogen isotopes>

Hydrogen isotopes, injected into materials by an irradiation or created by nuclear reaction, interact with radiation defects .

<**O defects (F centers)** ,
Li vacancy, **metal defects**>

Diffusion coefficients of hydrogen isotopes are reduced by the interaction.

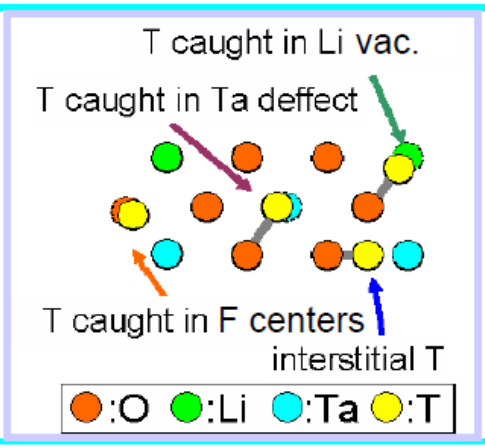

In order to understand diffusion and release behavior of hydrogen isotopes, it is required to observe **behavior of defects and hydrogen isotopes** simultaneously.

Approach (1/2): $LiTaO_3$ and D^+ ion irradiation

We use
- Lithium Tantalate ($LiTaO_3$) as sample.
- D^+ ion irradiation as method of injecting D into material.

$LiTaO_3$

- ✓ < 001 > Single crystal (10x10x1 mm)
- ✓ Single crystals are available
- ✓ To observe behaviors of –OD^- and radiation defects in material accurately.

D^+ ion irradiation

- ✓ Irradiation defects are generated in materials
- ✓ So, it is able to simulate a condition of fusion rector material

---

Approach (2/2): in-situ/simultaneous spectroscopy

In order to observe behaviors of defects and hydrogen isotopes **simultaneously**, we perform **three types of in-situ spectroscopies** during D^+ irradiation and during heating after the ion irradiation.

① F centers	⇒UV-VIS spectroscopy
② -OD^- (interacting with defects)	⇒FT-IR spectroscopy
③ Component of desorption gas	⇒Thermal Desorption spectroscopy

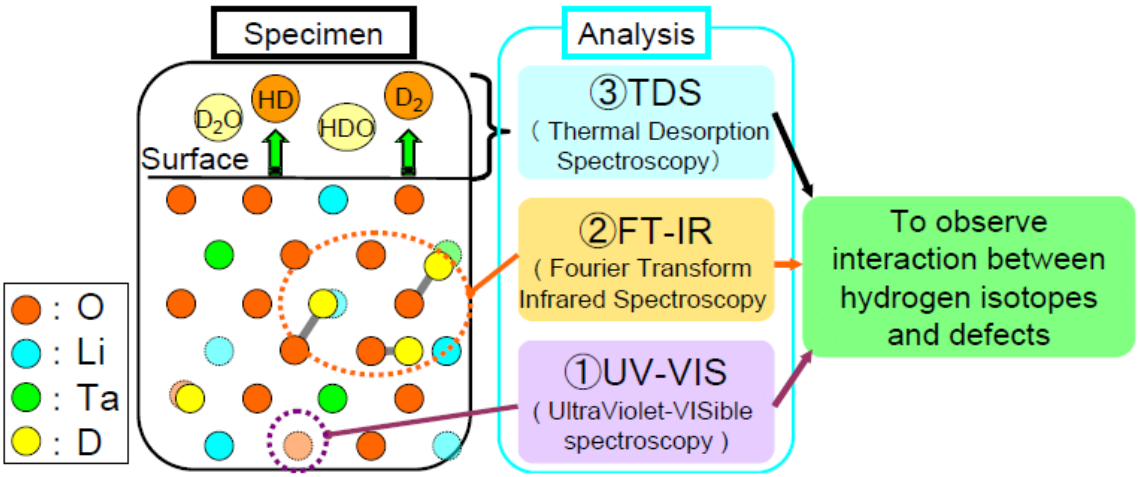

Experimental

Irradiation

- ✓ To inject D and defects.
- ✓ **300 keV D^+ ion irradiation**
- ✓ Irradiation time : 12 [hour]
- ✓ Flux : 1.25×10^{16} [D^+ $m^{-2}s^{-1}$]
- ✓ Ion fluence : 5.0×10^{20} [D^+ m^{-2}]

Heating

Constant rate heating to 750 ° C
Heating rate was 3K/min

Experimental apparatus

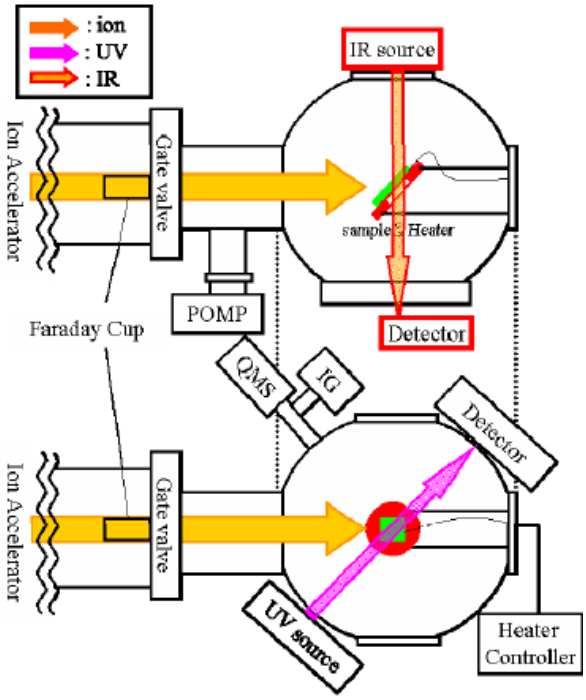

Result & Discussion

Result 1 : During irradiation
- 1-1 : UVVIS spectroscopy
- 1-2 : FT-IR spectroscopy

Result 2 : During constant rate heating after the irradiation
- 2-1 : UVVIS spectroscopy
- 2-2 : FT-IR spectroscopy
- 2-3 : TD spectroscopy

Discussion 1 : Behaviors of D and defects

Result 1 : During irradiation

Result 1 : During irradiation
- 1-1 : UVVIS spectroscopy
- 1-2 : FT-IR spectroscopy

Result 2 : During constant rate heating after the irradiation
- 2-1 : UVVIS spectroscopy
- 2-2 : FT-IR spectroscopy
- 2-3 : TD spectroscopy

Discussion 1 : Behaviors of D and defects

Result 1-1 : UVVIS spectroscopy
(observation during 300 keV D^+ irradiation)

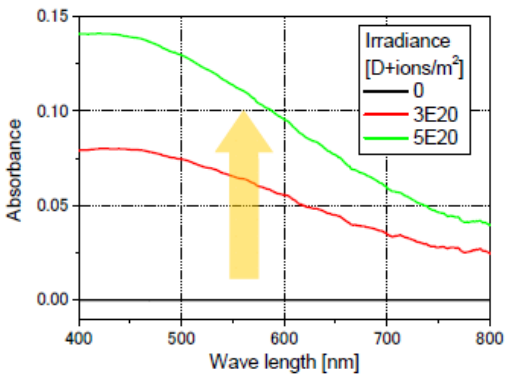

UVVIS spectra

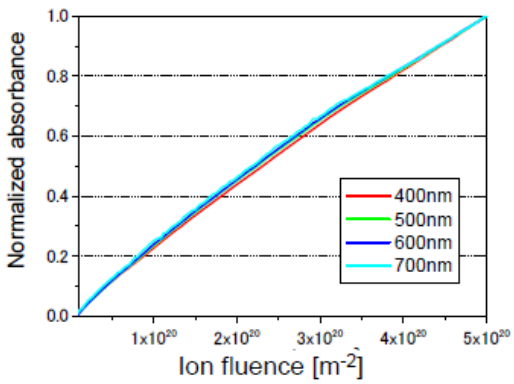

Normalized absorbance

- ✓ In irradiation, absorbance of UVVIS between 400 ~ 800 nm was increased.
- ✓ In normalized absorbance spectra, increasing rate at each wave length have the same dependency for ion irradiance fluence.

⇒By ion irradiation, **O vacancies were generated**.

Result 1-2 : FT-IR spectroscopy
(observation during 300 keV D^+ irradiation)

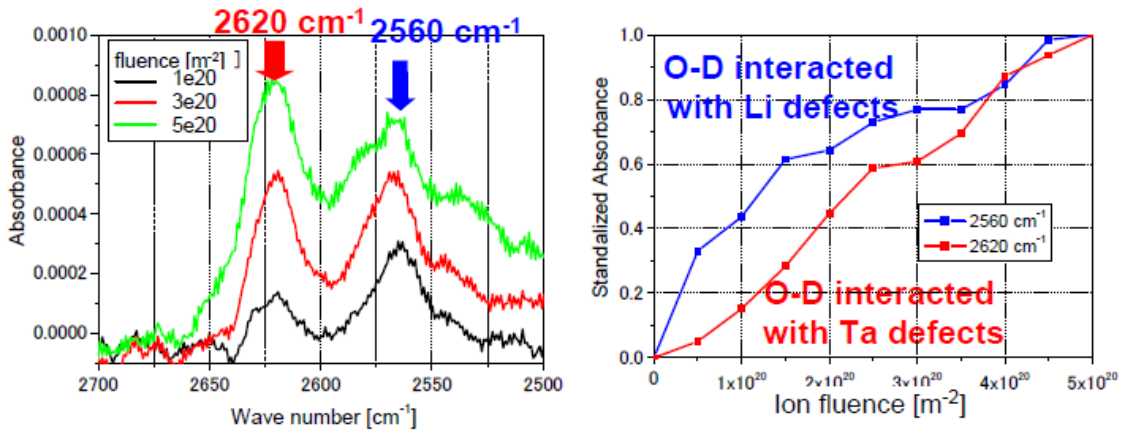

In-situ FT-IR spectra during D^+ irradiation Normalized absorbance

- ✓ During irradiation, two sharp peaks appeared at **2560 cm^{-1}** and **2620 cm^{-1}**.
- ✓ It was reported [X. Feng et al., J Phys. Condens. Matter 3 (1991) 4145.] that
  - peak at **2560 cm^{-1}** correspond to O-D interacting with a **Li** defect.
  - peak at **2620 cm^{-1}** correspond to O-D interacting with a **Ta** defect.
- ✓ Our FT-IR data agree with this report. The 2560 cm^{-1} peak grew prior to the 2620 cm^{-1} peak, because there are few Ta defects at the beginning.

Result 2 : During heating

Result 1 : During irradiation
- 1-1 : UVVIS spectroscopy
- 1-2 : FT-IR spectroscopy

Result 2 : During constant rate heating after the irradiation
- 2-1 : UVVIS spectroscopy
- 2-2 : FT-IR spectroscopy
- 2-3 : TD spectroscopy

Discussion 1 : Behavior D and defects

Result 2-1 : UVVIS spectroscopy
(During constant rate heating)

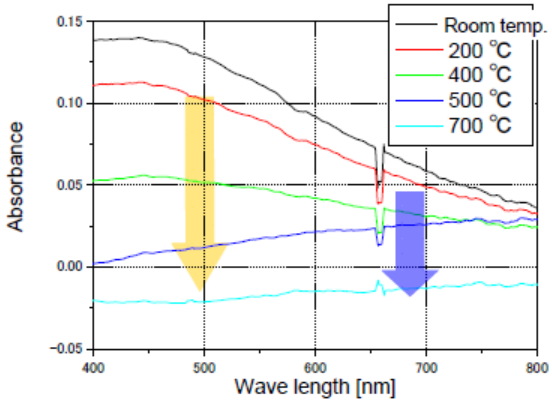

UV-VIS spectra

Plot of integral values of UV-VIS absorbance at 400~800 nm

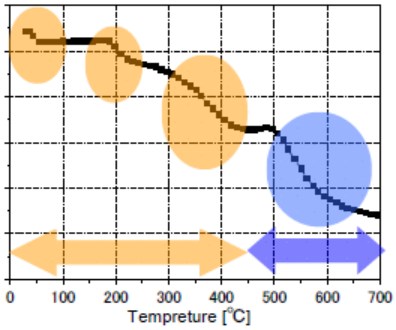

Temperature alteration of UV-VIS absorbance

- ✓ During heating, absorbance of UVVIS between 400 ~ 800 nm was decreased **stepwise with four typical decrease stages**.
- ✓ At first, absorbance at lower wavelength region was decreased
- ✓ Then, absorbance at higher wavelength region was decreased from 500 ° C

Result 2-2 : FT-IR spectra

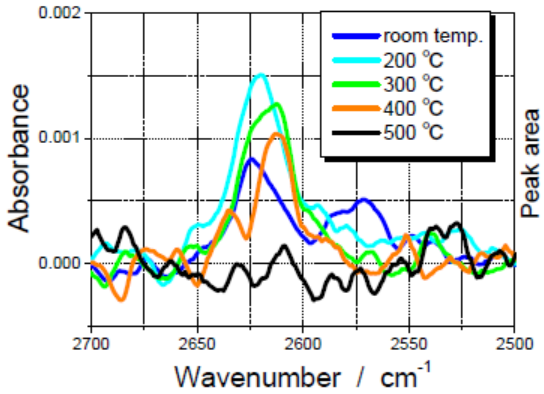

FT-IR spectra

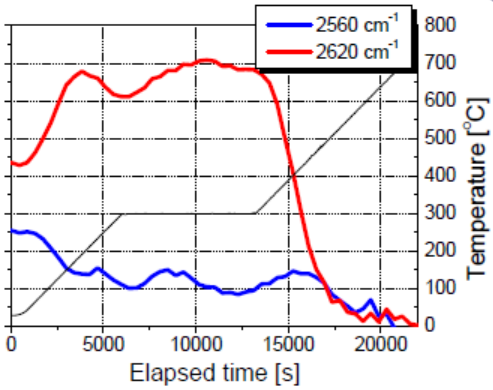

Temperature alternation of each peak area

- ✓ Peak at **2620 cm^{-1}** moved to low wave number area with temperature rising, increased until 200 ° C and decreased after 300 ° C.
- ✓ Peak at **2560 cm^{-1}** decreased until 200 ° C.
- ✓ Increase of **2620 cm^{-1}** peak and decrease of **2560 cm^{-1}** peak were observed simultaneously.

Result 2-3 : TDS spectra

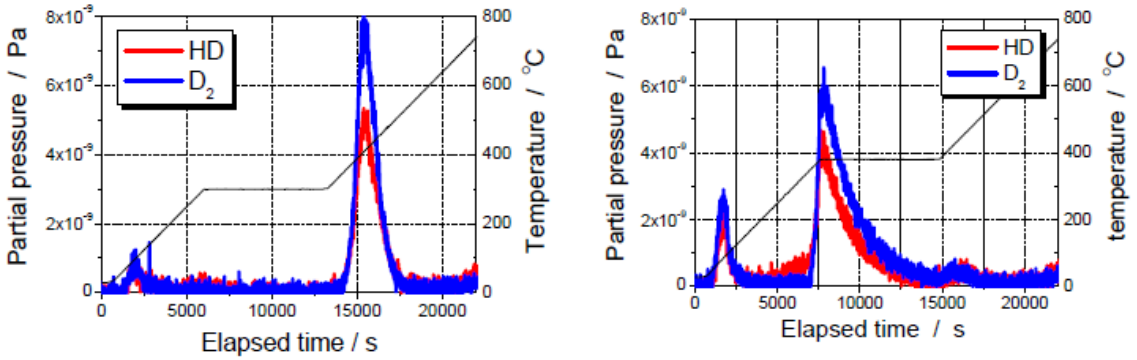

(Keeping at 300 ° C) (Keeping at 380 ° C)

Partial pressure of desorption gas (by QMS)

- ✓ Most of deuterium loaded into the sample was released as HD & D_2 gasses at 300~500℃.
- ✓ The D_2 and HD release around 100℃ is from the sample holder.

Discussion :

Result 1 : During irradiation

1-1 : UVVIS spectroscopy

1-2 : FT-IR spectroscopy

Result 2 : During constant rate heating after the irradiation

2-1 : UVVIS spectroscopy

2-2 : FT-IR spectroscopy

2-3 : QMS spectroscopy

Discussion 1 : Behaviors of D and defects

Discussion : Behaviors of D and defects

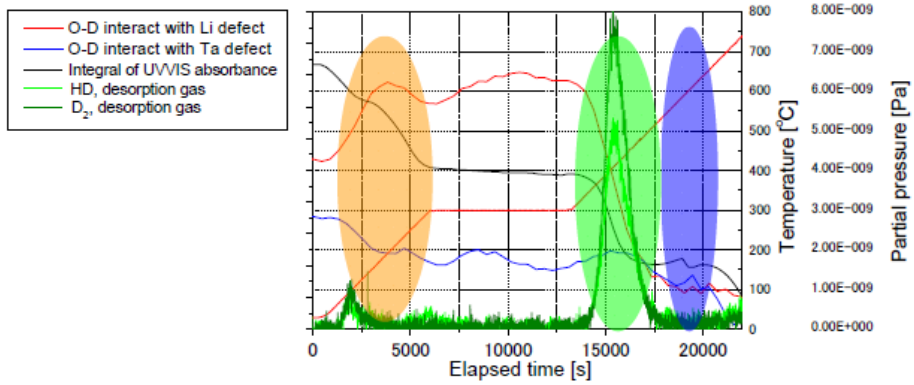

Behavior of D and defects

	1st step	2nd step	3rd step
O vacancies	decreasing	decreasing	decreasing
O-D with Li defect	decreasing	no change	no change
O-D with Ta defect	increasing	decreasing	no change
HD &D2 gas release		O	

Discussion : Behavior of D and defects (1st step)

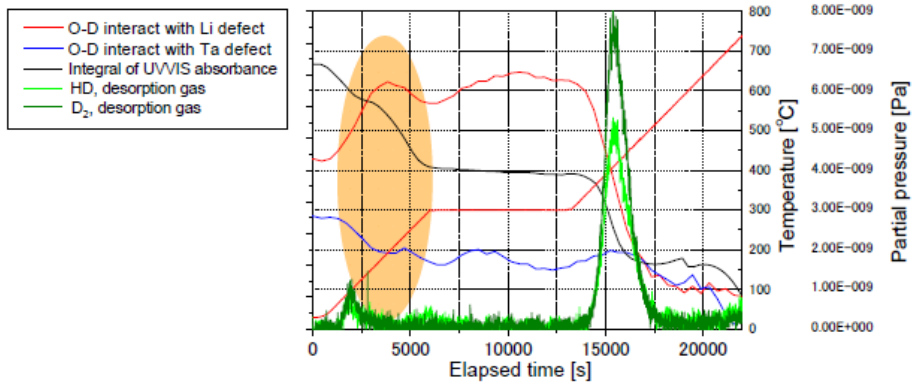

Behavior of D and defects

✓ UVVIS absorbance stepwise decreasing cause two behavior of O vacancies.

1. O vacancies decrease stepwise.
2. O vacancies decrease constantly, and D trapped in O vacancies released (O vacancies that caught D was not observed by UVVIS spectroscopy.)

In 1st step, O vacancies behave as 2nd case. D trapped in O vacancies release and form $-OD^-$ interacting with Ta defects

Discussion : Behavior of D and defects (2nd step)

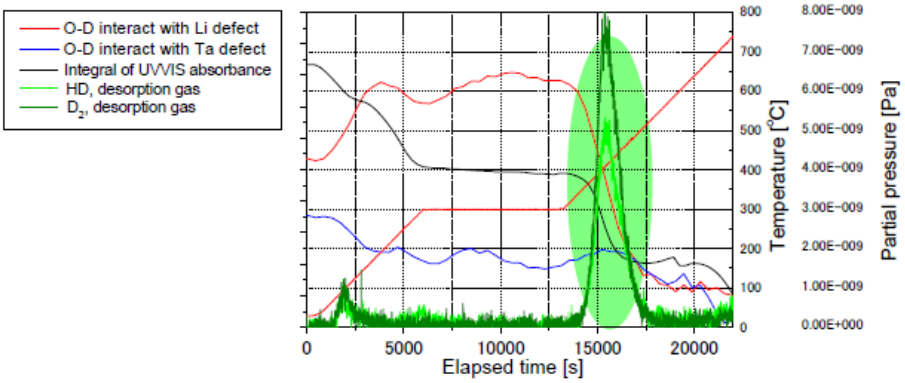

Behavior of D and defects

In 2nd step, -OD⁻ interacting with Ta defects and O vacancies decreased similarly and desorption of HD & D_2 gasses was observed.

>> O-Ta complex defects (O vacancy + Ta defect) are formed.

In this step, O-Ta complex defects are recovered. Finally, D that form –OD⁻ interacting with Ta defect is detrapped, then diffuse and desorb from the surface.

Discussion : Behaviors of D and defects (3rd step)

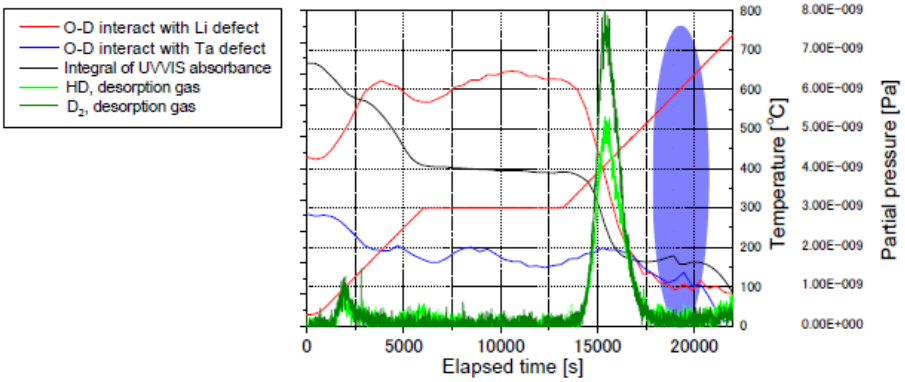

Behavior of D and defects

In 3rd step, O vacancies that was observed in deferent area from that in 1st and 2nd step was decreased.

This O vacancy would the one capturing two electrons.

(the one decreased at 1st and 2nd stage may capture one electron)

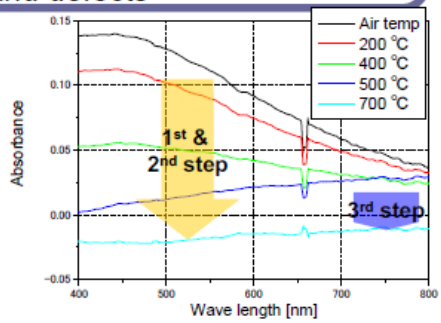

Summary : Interaction between D and defects

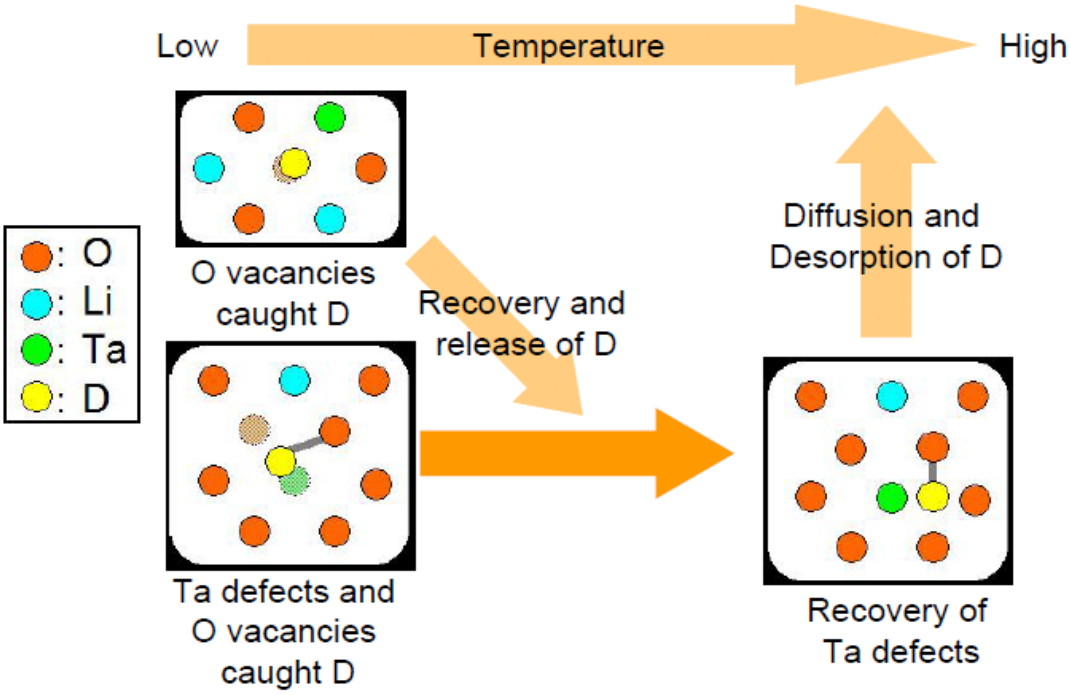

Summary : Interaction between D and defects

- ✓ By 300keV D^+ irradiation, O vacancies and Ta defects generated in $LiTaO_3$. O vacancies was able to be observed with UVVIS spectroscopy.
- ✓ Some of irradiated deuterium forms $-OD^-$ and the other are captured by F centers.
- ✓ At low temperatures (～ 200 ° C), oxygen vacancies recover and trapped D is release. Some of released D are caught by Ta defects.
- ✓ At high temperatures (350 ° C ～), O-Ta complex defects are recovered. Then, trapped D are release released from the sample as D_2 or HD.

21. Fabrication Routes of Sub-Components for Water Cooled Solid Breeder Blanket Module

T. Hirose[1], H. Tanigawa[1], H. Serizawa[2], Y. Kawahito[2], S. Katayama[2] and M. Enoeda[1]

[1] Japan Atomic Energy Agency, 801-1 Mukoyama, Naka, Ibaraki, 311-0193 Japan
hirose.takanori@jaea.go.jp
[2] Osaka University, 1-1 Yamadaoka, Suita, Osaka, 565-0871 Japan

This paper describes recent achievements in R&D on the fabrication routes of sub-components for Water Cooled Solid Breeder (WCSB) ITER-Test Blanket Module (TBM). Mock-ups of sub-components have been successfully developed in industrial scale using a reduced activation ferritic/martensitic steel, F82H. The structural for the sub-components must be thin and gas-tight from an tritium management point of view. Moreover the structure is required to have the capability of cooling for heat injection from plasma and volume heat generation.

Full scale container for breeder pebbles were successfully developed with the fiber laser welding technique for its high focusing capability. Butt welding between 1.5 x 4 x 990 mm^3 plates and ϕ11 x 1 x 990 mm^3 tubes were successfully bonded without penetration of weld bead through the tubes. It means the cooling channels are free from heat-affected-zone, which degrades mechanical strength and compatibility with the coolant. A couple of membrane panels, tube plates and side walls were also joined by the techniques to form the container, and its dimensions are 74 x 112 x 990 mm^3. It was confirmed to be gastight under pressurized helium up to 0.5 MPa.

As for fabrication method for the side wall structures, gun-drill method was applied to form the built-in cooling channels. The cooling channels with 10 mm of diameter and 1450 mm of depth were successfully formed in F82H side wall with 30 mm thickness. Veer in the channel was measured to be within 0.5 mm over the 1450 mm, and this is small enough for the components. The side wall was to be fabricated with hot isostatic pressing in the conventional fabrication route. However, the drilling method could be the attractive alternative from the view point of quality assurance. The manifold structures for these sub-components are to be discussed.

15th International Workshop on Ceramic Breeder Blanket Interactions
Sept. 3-4, 2009 at Sapporo Industries Cultivation Center
811 : Experiments and Modeling of Thermo-hydraulics in a Solid Breeder Blanket

Fabrication Routes of Sub-Components for Water Cooled Ceramic Breeder Blanket Module

-Fabrication of wall with built in channels-

T. Hirose, H. Tanigawa, M. Enoeda
Japan Atomic Energy Agency

H. Serizawa, Y. Kawahito, S. Katayama
Joining and Welding Research Institute,
Osaka University

Background

- Reduced Activation Ferritic/Martensitic steel, RAF/M is the structural material of ITER-test blanket module. Mechanical properties of RAF/M strongly depend on thermal history.
- Blanket component is to be regulated as a nuclear device. The quality of the component must be strictly controlled.
- On selecting fabrication route, thermal history on RAF/M and inspection method of the component must be carefully considered.

Common technologies for TBM fabrication

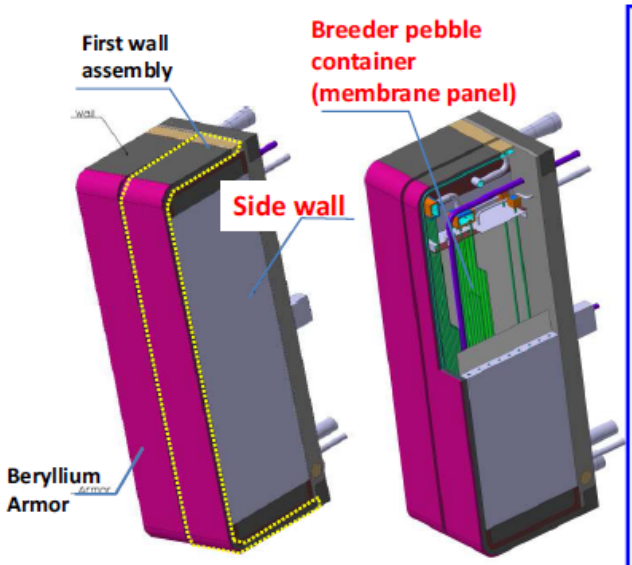

Japanese WCCB-TBM

- RAF/Ms as structural (plates, tubes and slabs)
- U-shaped FW
- Beryllium armor
- Box structure

- Wall and partition w/ built-in cooling channels
  - Side wall (poloidal flow FW)
  - Top plates, bottom plates (toroidal flow FW)
  - Partition between breeder and multiplier

Collaborating with JFE and Toyo engineering

FABRICATION OF
SIDE WALL W/ BUILT IN COOLING CHANNELS

Side walls for WCCB TBM

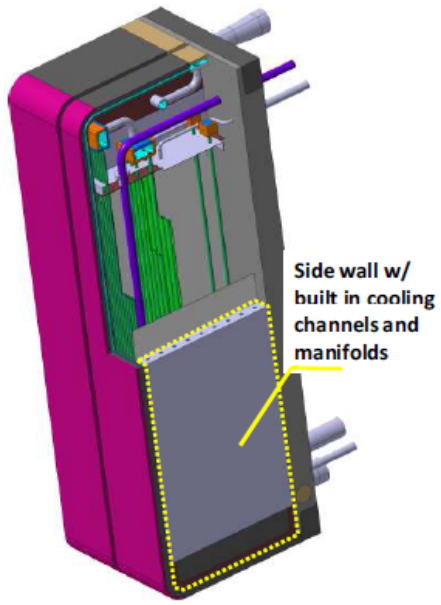

Japanese WCCB-TBM

Outline of side wall

- RAF/M as the structural material, F82H
- The wall has built-in channels and manifolds for coolant

  COOLING
- Welded to the first-wall and the back-wall. And the box structure must withstand 15 MPa of internal pressure (leakage to breeding layer)

  STRUCTURAL DURABILITY

Fabrication routes of wall w/ built-in cooling channel

	Cross sectional view	Fabrication route	Parts	Merits	Issues
A	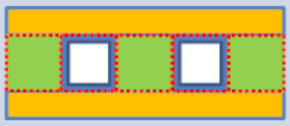	HIPping	Plates Tubes Spacer	No interface on pressure boundary First wall like	Cost, Thermal history Gap at triple point
B	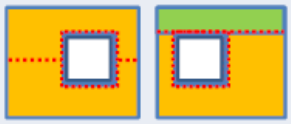	HIPping	Grooved Plates Tubes Plates	No interface on pressure boundary	Cost, Thermal history Accurate groove
C	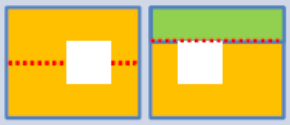	Hot pressing	Grooved plates Plates	No canning Joint in the vacuum	Cost, Thermal history Accurate groove Interface on pressure boundary
D		Gun drilling	Plate	Cost	Accuracy (deflection and misalignment of drill) Cooling capacity

..... : interface

In case of HIP and HP, tolerance induces assembly gap.
As for SW, Gun Drilling is applicable because of moderate heat generation.

SW fabrication by drilling

- Two 30^{T} x 400^{W} x 1550^{L} mm plates were prepared from 800 kg charge of F82H
- ϕ10 x 1450^{Depth} mm holes were drilled from an end
- No thermal history during the drilling
- Straightness of the hole should be evaluated

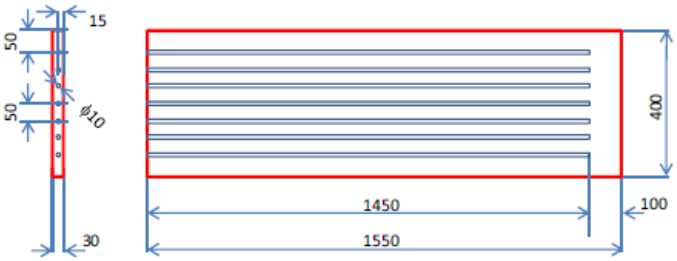

Fig. Drawing for drilled SW

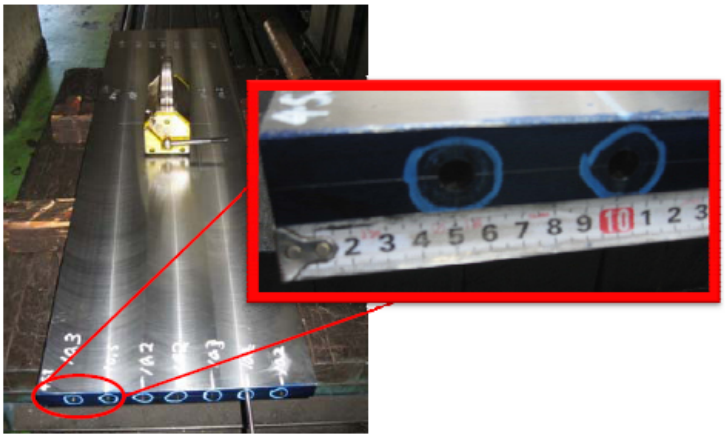

Straightness of drilled hole

Deflection

- Since the drill is thin and long, the drill may be deflect.

Misalignment

- Misalignment of insert angle may cause difference in position.

- These error could reduce wall thickness
- The holes were inspected by ultrasonic thickness meter and X-ray

Straightness of drilled hole, UT inspection

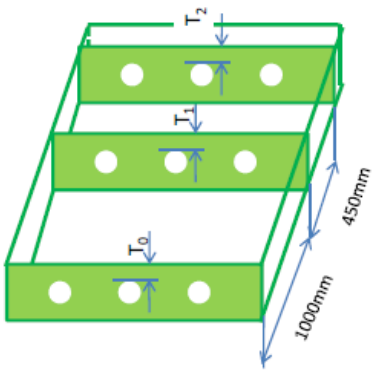

Change in the minimum thickness, Dt
$Dt = T_i - T_0$, i=1, 2

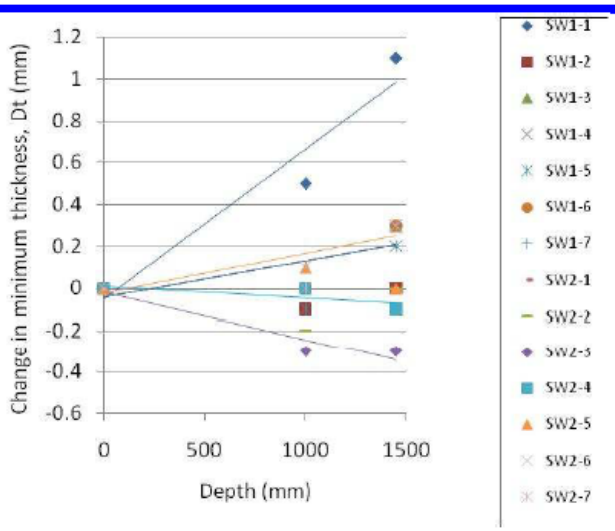

- No significant deflection was observed
- Difference in the position was caused by insert angle
- Thickness of channel wall was not significantly reduced

Straightness of drilled hole, X-ray inspection

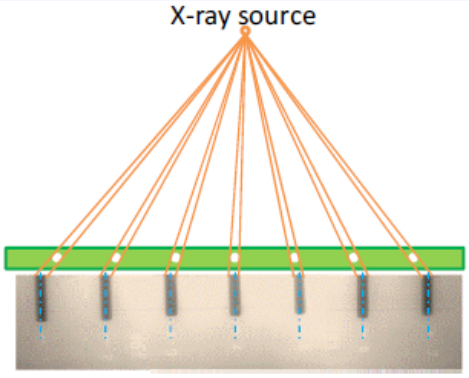

X-ray inspection was conducted on the end of the channels

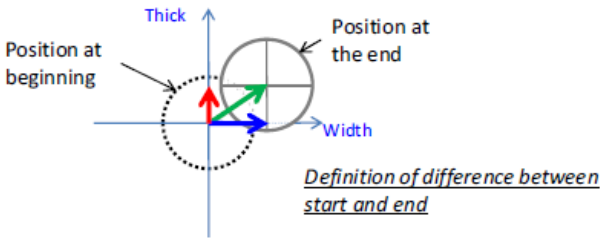

Definition of difference between start and end

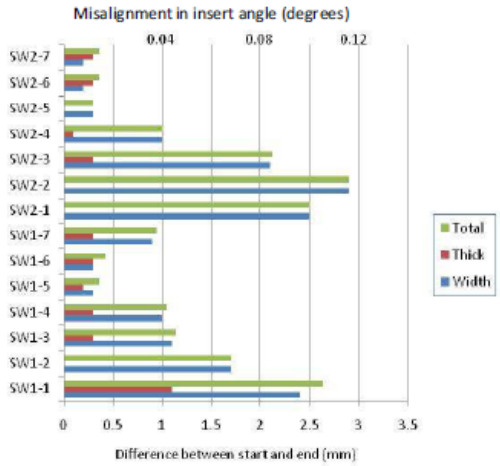

- 7 of 14 holes demonstrated positional difference less than 1 mm
- Channel quality was inspected by NDI
- ϕ23 manifolds are to be gun-drilled to penetrate these 7 holes, and the SWs are welded to FW mock up

Manifolds for the SW

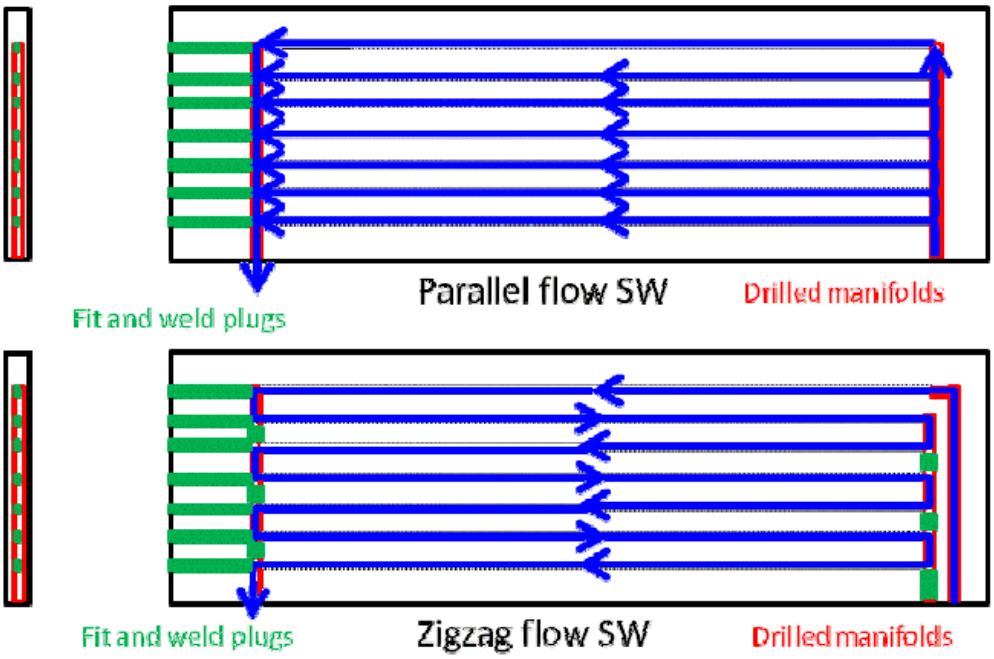

These SWs are to be cut to fit the FW and welded to the FW fabricated by HIP

Collaborating with IHI and JWRI, Osaka Univ.

FABRICATION OF BREEDER PEBBLE CONTAINER W/ MEMBRANE PANELS

Breeder Pebble Container for WCCB TBM

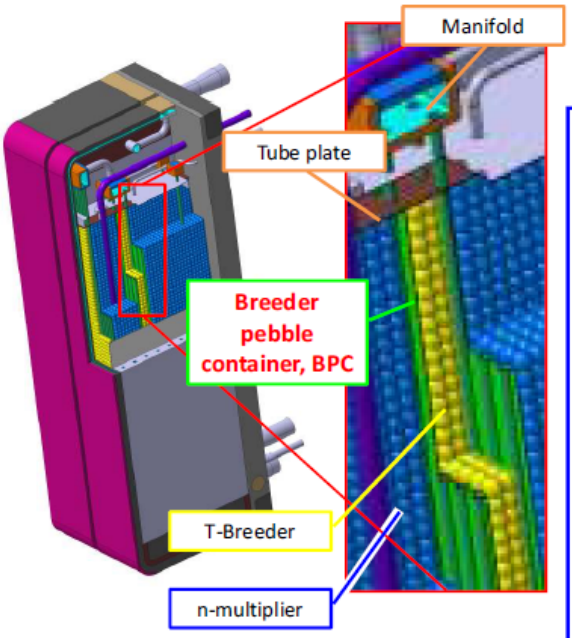

WCCB-TBM cut model

Requirements for Breeder Pebble Container, BPC

- Minimize the structural material to maximize TBR (Thin wall)
- Breeder must be separated from multiplier for inventory (Gastight partition)
- Cooling of nuclear heating (Cooling)

Fabrication routes of partition for BPC

	Cross sectional view	Fabrication route	Fraction of structural	Merits	Issues
A	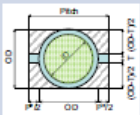	Gun drilling and EDM (Plate)	1.0	Min. structural material No interface	Large scale EDM Costs
B	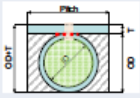	Brazing (FSW) (Grooved plate /Tubes)	1.44	No interface on pressure boundary	Fabrication of thin plates Accurate groove
C	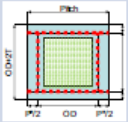	HIPping (Plate/Tubes)	3.90	First wall like	Too much structural material
D	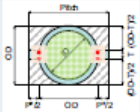	Welding (Ribs/Tubes) Membrane panel	1.0	Min. structural material No interface on pressure boundary	Fabrication of thin plates Softening at HAZ Interface on gas boundary

Structural material | Vacancy | Coolant | HAZ | ····· : interface

High power density Fiber Laser Welding (FLW) was applied to fabricate the partition w/ cooling channels.

Fabrication Process of BPC

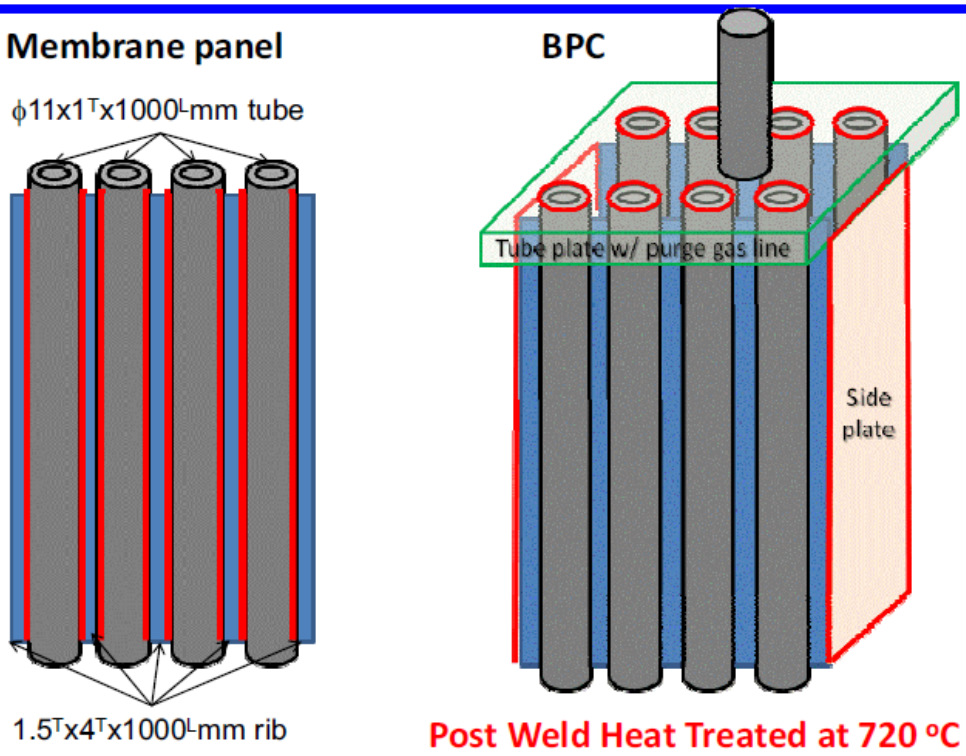

BPC fabrication by FLW

- ϕ11x1^{T}x1000^{L} tubes were cold milled from F82H forged cylinder.
- 1.5^{T}x4^{W}x1000^{L} mm ribs were cold rolled.
- The tubes and ribs were FLWed to form membrane panel.
- The panels were welded with tube plates and side walls to form BPC.

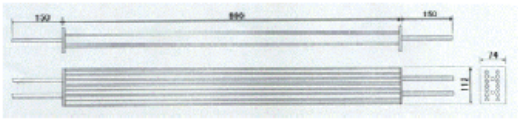

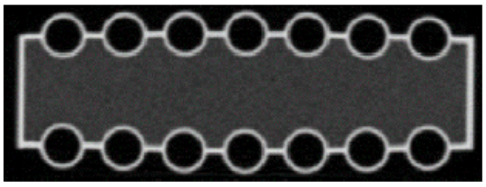

Cross sectional view by X-ray CT

Inspection on PBC

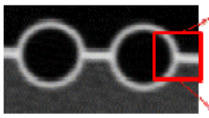

Cross sectional view of the membrane

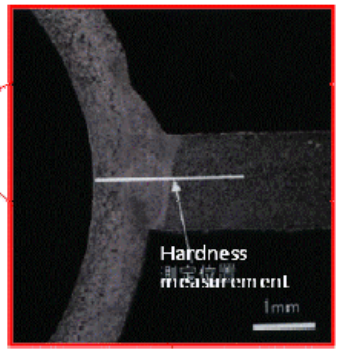

- Gastight structure was confirmed by He leak check.
- No softening was observed in the tubes.
- FLW enabled gastight structure without softened HAZ.

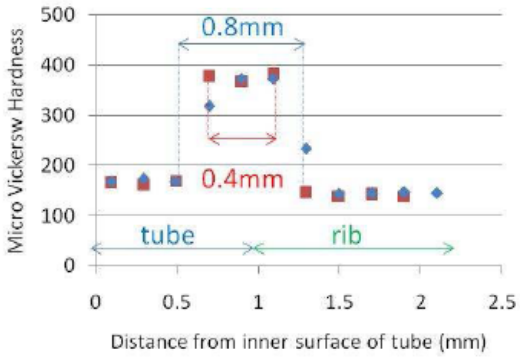

Conclusions

Wall and partition w/ built-in cooling channels have been successfully developed by drilling and welding

- Side Wall Structure
  - successfully developed by gun-drilling method
  - channel depth of 1450 mm with 1 mm of positional error
  - internal structure can be inspected by UT and X-ray
- Breeder Pebble Container
  - successfully developed with fiber laser welding
  - no weld metal nor no softening in the tube wall
  - gastight structure with thin tubes and plates are achieved
  - can be inspected by X-ray and endoscope

22.

UCLA

Development of a robust Be/F82H diffusion bond for ITER TBM

R.M. Hunt, S.H. Goods, A. Ying, C.K. Dorn, M. Abdou

University of California, Los Angeles

CBBI-15

September 4, 2009

Acknowledgements

Collaborators include:

- UCLA: Alice Ying, Mohamed Abdou
- Sandia National Laboratories: Steve Goods, Michael Ulrickson
- JAEA/UCSB: Takuya Yamamoto
- Brush Wellman: Chris Dorn
- Axsys Technologies
- Bodycote
- Electrofusion Products
- Thin Film Technology

Outline

- Objectives
- Current Knowledge
- Bonding Layering Scheme
- Characterization of Cu//F82H bond
- Analysis of Ti//Cu Diffusion Zone
- Conclusions
- Ongoing Work

3

Introduction

- *Application*: ITER requires a 2mm coating of Beryllium on plasma facing surfaces of TBMs
  - Be used as armor layer
  - RAFM steel used as structural material (F82H, Eurofer, etc.)
- *Research objective*: create a robust diffusion bond between two dissimilar metals strong enough to survive in ITER:
  - Beryllium & RAFM steel (F82H)

4

Current Knowledge

- Be reacts with just about everything
  - Exceptions: Ge, Si, Ag, Al
  - Forms brittle intermetallic compounds
  - Need a ***diffusion barrier*** material

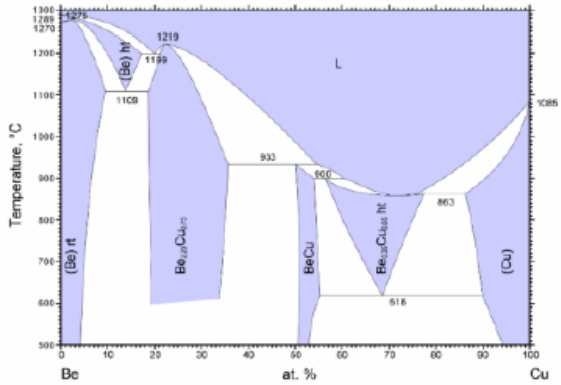

Fig. 1: Beryllium-Copper binary phase diagram [16]

- Much research in last 15 years to solve this problem in relation to FW beryllium bonds
  - Be to CuCrZr, Be to SS, Cu to SS
  - Arrived at Ti/Cu interlayer scheme [ref. 4,6,9,12,13,14,15]

5

Layering Scheme

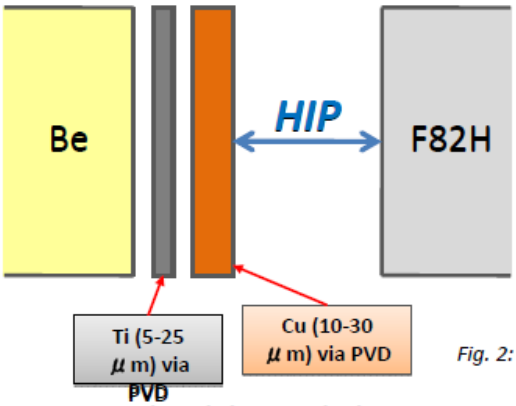

Fig. 2: Proposed layering scheme

- Piggyback on FW shield module research:
  - Titanium diffusion barrier
    - Must be as thin as possible
      - Costly to fabricate thick layer; too thick Ti may fail from brittle fracture
  - Copper compliant layer
    - Stress from thermal expansion difference is absorbed by ductile Cu

6

Limitations on Joint

- Fabrication
  - HIP temp bounds:
    - ≤ 850 C recrystallization temperature of Beryllium
      - Want lowest temp possible to avoid excessive heat treatment of TBM structural joints
    - ≥ 650 C insufficient bonding below this temp (expected from FW research)
  - i.e. FW Be/CuCrZr bond uses 2 µm Ti, 25 µm Cu @ 560 C HIP, for 2 hrs
- Implementation
  - Strength of interface need exceed stress in region
    - σ =57 MPa predicted from thermal stress by Lee et. al [17]
    - Will perform detailed stress analysis of interface region under ITER relevant conditions.

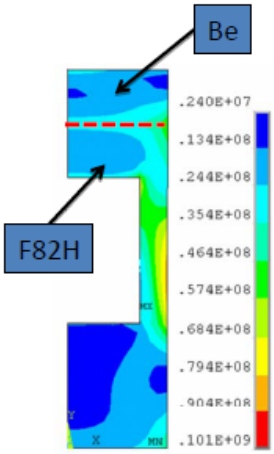

Fig. 3: 2D stress analysis showing max. Von Mises stress in first wall of TBM with 2mm Be armor [ref. 17].

Initial progress

(Prior to inclusion of Beryllium)

1. Measure strength of Cu direct bond to RAFM steel
   - Previously, Cu to SS easy to bond. SS had nickel to aid diffusion. RAFM has much less Ni. Cu may not bond as well.
   - *Experiment 1*: Measure Cu to F82H bond strength
     - Tensile, shear, and toughness at interface
2. Determine min. thickness of Ti that still blocks diffusion at HIP temperatures
   - *Experiment 2*: For each possible HIP temp., measure depth of diffusion of Cu into Ti

Experimental Procedure

- Cu/F82H HIP experiment
  1. Fabricate 5 HIP SS cans with Cu & F82H substrates inside
  2. HIP for 2 hours, 103 MPa @ 650, 700, 750, 800, 850 ° C
  3. Measure strength in tensile, shear & toughness

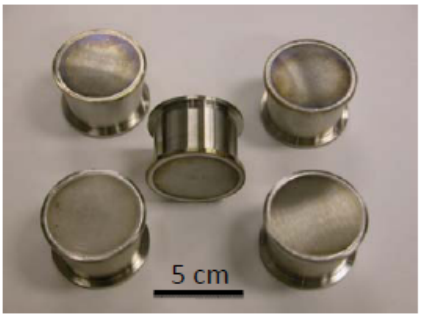

Fig. 4: Stainless steel cans containing Cu and F82H substrates prior to HIP .

- Ti/Cu interdiffusion experiment
  1. Fabricate samples
  2. Anneal in vacuum furnace to simulate HIP bond
  3. Measure diffusion depth via EMP line scans

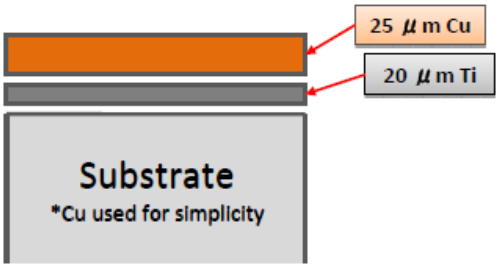

Fig. 5: Layering scheme for Ti/Cu diffusion experiment.

Characterization of Cu//F82H bond

Composition:

- AES shows very narrow (~1 μm) diffusion zone after 850 ° C HIP
  - *(Analysis of lower temps underway)*

Strength:

- @ 850 C and **@ 750 C** → Failure in Cu bulk material
  - achieves **211 MPa** min. tensile strength
- @ 650 C → Failure at material interface
  - creates insufficient bond

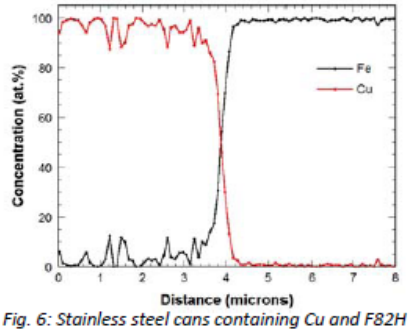

Fig. 6: Stainless steel cans containing Cu and F82H substrates prior to HIP .

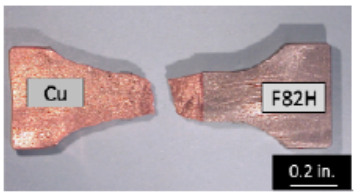

Fig. 7: Tensile sample HIP'ed at 650 ° C, showing fracture at interface (left). Tensile sample HIP'ed at 850 ° C, showing ductile failure in copper (right).

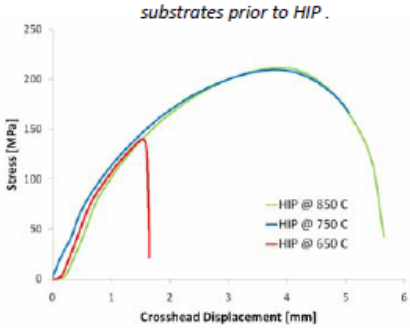

Fig. 8: Plot of tensile tests of samples HIP'ed at 650 ° C, 750 ° C, and 850 ° C.

Analysis of Ti//Cu Diffusion Zone

- Samples annealed 30 min.
  - Use data to predict depth for 2 hour HIP cycle →

Note: Oxygen levels in Ti higher than expected. PVD chamber potentially problematic. May Cause slightly different diffusion behavior.

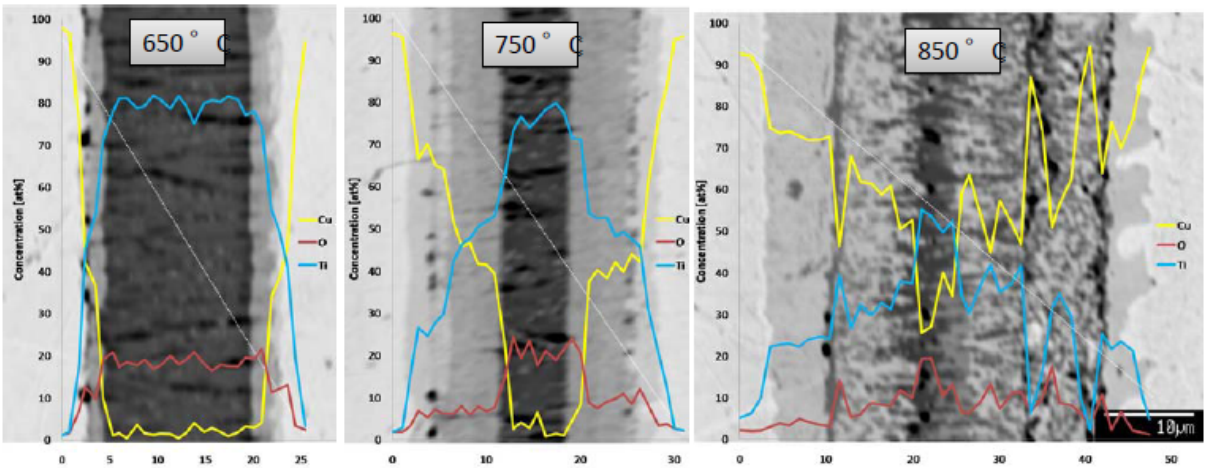

Fig. 9: Backscattered secondary electron images of Cu/Ti diffusion zone, with EMP elemental line scan overlay at 650 ° C (left), 750 ° C (middle), 850 ° C (right). Diagonal line corresponds to scan path.

Initial Conclusions

- Ti/Cu interlayers, HIP at 750 ° C for 2 hrs, 103 MPa, appear to be viable recipe for bonding.
  - 750 ° C is promising result, close to PWHT of TBM, (as desired by JAEA research)
  - 800, 700 ° C Cu/F82H HIP cycle results underway

- Higher temp HIP cycles may require unreasonable amount of Ti to *completely* block diffusion of Cu into Be
  - 750 ° C requires approx. 20 μm (reasonable amount)

12

Future Work

Full Joint

- Manufacture coupons to include Beryllium, utilizing analysis from current experiments
  - 10 sample matrix:
    - Expect failure in Ti/Cu intermetallics
    - For comparison - direct bond, only Ti, only Cr, Cr/Cu

Design Analysis

- Show that bond will survive in ITER
- Perform FEM stress analysis of TBM. Include:
  - Primary (pressure) and Secondary (thermal) loading in region
  - Detailed stress analysis of interfacial zone
    - Effects of irradiation will not be studied. Suggested as future work for qualification.

13

References

1. T. Hirose, M. Ando, H. Ogiwara, H. Tanigawa, M. Enoeda, and M. Akiba, Interfacial properties of HIP joints betwen Beryllium and RAF/M Steel, International Conference of Fusion Related Materials – 13, Nice, France, 2007.
2. J.-S. Lee, J.-Y. Park, B.-K. Choi, D.-W. Lee, B.-G. Hong, & Y.-H. Jeong, Beryllium/ferritic martensitic steel joining for the fabrication of the ITER test blanket module first wall, Fusion Engineering and Design, (2009) 1170-1173.
3. Youchison, D. L., Goods, S. H., Puskar, J. D., Delong, W. A., Martin, T. T., Narula, M., et al. (2009). Thermal Fatigue Cycling of Be/Cu Joining Mockups. *Fusion Engineering and Design* , 2008-2014.
4. P. Sherlock, Application of a diffusion bonding methodology to develop a Be/Cu HIP bond suitable for the ITER blanket, Fusion Engineering and Design, (2003) 425-429.
5. N. Baluc, et al, Status of reduced activation ferritic/martensitic steel development, Journal of Nuclear Materials, (2007) 33-41.
6. S.H. Goods, Cu-SS Joining-12-10-08. Livermore, CA : s.n., 2008.
7. B.C. Odegard, Beryllium-Copper reactivity in an ITER joining environment, Fusion Engineering and Design, 41 (1998) 63-71.
8. B.C. Odegard, C. H. Cadden, N. Y. C. Yang, R. D. Watson, and D. L. Youchison, Failure analysis of beryllium tile assemblies following high heat flux testing for the ITER program, Fusion Engineering and Design, (2000) 309-316.
9. C.H. Cadden, and B.C. Odegard, Aluminum-assisted joining of Beryllium to Copper for fusion application, Fusion Engineering and Design, 37 (1997) 287-298.
10. H. Kawamura, M. Kato, E. Ishitsuka, S. Hamada, K. Nishida, and M. Saito, Compatibility test between beryllium and ferritic stainless steel (F82H), Fusion Engineering and Design, (1995) 475-480.
11. M. Enoeda, et al., Overview of design and R&D of test blankets in Japan, Fusion Engineering and Design, (2006) 415-424.
12. P. Sherlock, A.T. Peacock, and A.D. McCallum, Development of a copper alloy to beyllium HIP bonding technology for the ITER first wall, Fusios Engineering and Design, (2005) 377-381.
13. P.C. Zhang, B. Bai, L. Shen, and J.S. Zhou, Distribution of the composition and micromechanical properties of Be/316L stainless steel following diffusion bonding, Surface and Interface Analysis, (2001) 88-90.
14. S. Kundu, Diffusion Bonding of commercially pure titanium to 304 stainless steel using copper interlayer, Materials Science and Engineering, A, Structural Materials, 407(1-2) (2005) 154-160.
15. T. Hatano, Development of Be/DSCu HIP bonding and thermo-mechanical evaluation, Journal of Nuclear Materials, 437(2) (2002) 430-435.
16. H. Okamoto, Cu-Be Binary Phase Diagram, ASM Alloy Phase Diagrams Center, P. Villars, editor-in-chief; H. Okamoto and K. Cenzual, section editors; http://www.asminternational.org/AsmEnterprise/APD, ASM International, Materials Park, OH, 2002.
17. Lee, D W, et al. "Current Status and R&D Plan on ITER TBMs of Korea." *Journal of the Korean Physical Society*, 2006: 340-344

23. On monitoring the tritium breeder in ITER Test Blanket Module

V.Kapyshev, I. Kartashov, V.Kovalenko, V.Poliksha, Yu.Strebkov, N.Yukhnov.

Open Joint-Stock Company "Dollezhal Research and Development Institute of Power Engineering".
P.O.Box 788, Moscow 101000, Russian Federation, e-mail: nikiet@nikiet.ru

Tritium breeder is a most process among controlled fusion reactor engineer problems. Tritium Breeding Ratio (TBR) is a main parameter characterizing of the process. TBR can be submitted as a ratio of the amount tritium produced in the fusion reactor to the amount of tritium that burned up in the reactor plasma. A concept and block-schema of tritium breeding monitoring and experimental estimation of the tritium-breeding ratio in DEMO and ITER are discussed. Systems for experimental estimation of the TBR and the tritium-breeding dynamic parameters in a Tritium Breeding Modules (TBM) of the ITER are proposed.

The systems are based on tritium and neutron flux measurements under ITER plasma experiments and use lithium ortho-silicate and lithium carbonate as tritium detectors and the neutron detectors. Beryllium and differences isotopes lithum-6 and lithium-7 are applied. The detectors are delivered to tritium breeding zone (TBZ) of the TBM on channels connected the TBM and an operating zone of ITER. Pneumatic and mechanic methods are applied to deliver the samples to the TBZ of the TBM and to extract the samples using monitor channels during plasma operational pauses.

Results of the channel parameter calculations and comparison of the pneumatic and mechanic systems are presented in the paper.

Corresponding Author: Vicor K. Kapyshev
kapyshev@nikiet.ru
Open Joint-Stock Company "Dollezhal Research and Development Institute of Power Engineering",
P.O.Box 788, Moscow 101000, Russian Federation, e-mail: kapyshev@nikiet.ru
Tel.: +7-499-763-0314; fax: +7-499-788-2052

Introduction

ITER has to demonstrate the possibility of controlled fusion for power generating. New technologies are applied in the reactor and must be tested under ITER operation [1].

At final stage of ITER operation D-T plasma will be and tritium processes for chemical purification and isotope separation of plasma gas and technology of tritium breeder in Test Blanket Modules (TBM) will be tested [2,3,4].

The most important parameter characterizing the tritium cycle of the reactors is tritium breeding ratio (TBR).

In general TBR is defined as:

$$TBR = Q_{reactor} / Q_{plasma} \quad (1)$$

where: $Q_{reactor}$ – tritium amount bred in plasma and in reactor blanket and Q_{plasma} - tritium amount burned-up in plasma.

TBR for Russian DEMO with ceramic blanket has to be no less than 1.05 [5]. Experimental demonstration of TBR definition with necessary accuracy is clear taking into account the importance of the value for normal reactor operation and exceeding of this value over a one. Operation for experimental definition of TBR was begun else in SU in 80-th [6] and followed in frame development of Russian ceramic TBM for ITER [7].

To investigate a numerator of the formula (1) a tritium production in tritium breeding zone (TBZ) of the TBM has to be measured under ITER plasma experiments.

Tritium and neutron monitoring system with some lithium and neutron sensors are proposed

Conceptual of tritium breeding monitoring in ITER is discussed.

2. Conception of tritium breeding monitoring and material irradiation using Test Breeding Modules of ITER

Conception of TBR monitoring for reactor includes measurement of numerator and denominator in formula (1) and calculation analysis for both of them. Experimental definition of tritium amount burned in plasma (denominator in formula (1)) is proposed to realize by measurement of neutron quantity arisen in result of D+T nuclear fusion reaction. Numerator demonstrates tritium breeder in a reactor blanket under neutron interaction with lithium and beryllium isotopes but neutrons from D-D reaction and possibly (γ,n) acceleration processes have to be accounted not only from D-T reaction.

Simultaneously ITER will be the power neutron source and also the material researches can be carried out.

The conceptual diagram of TBR monitoring in Fusion Reactor and irradiation material system is presented on Fig. 1.

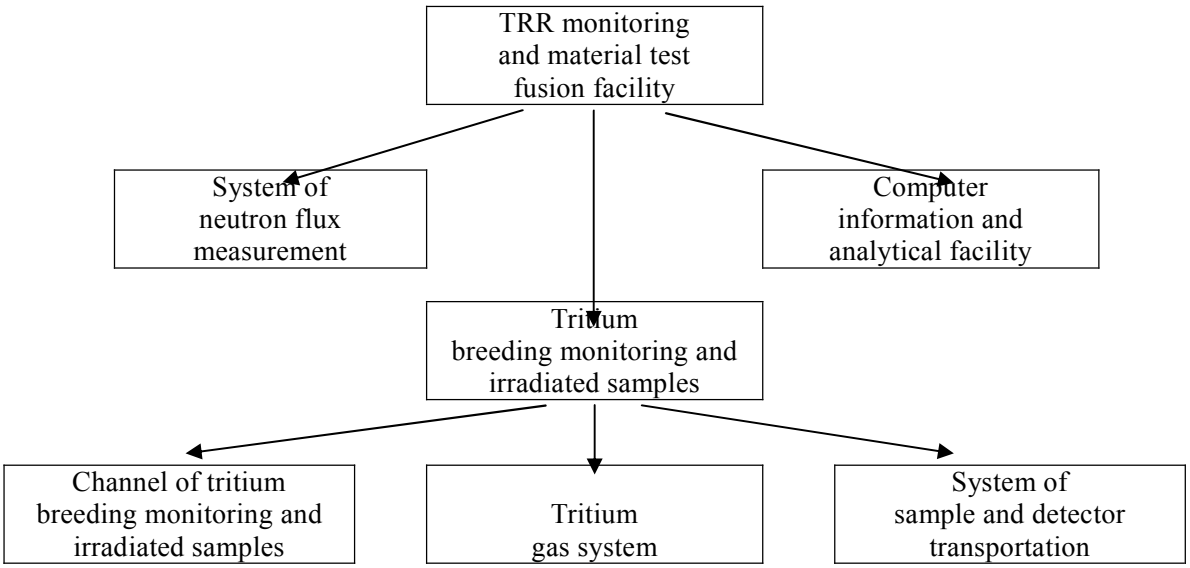

Fig. 1. Conceptual diagram of TBR monitoring in Fusion Reactor and irradiation of material

Complex of tritium breeding ratio monitoring and fusion structural material irradiation systems (TMMC) contains three components.

1. System of tritium breeder monitoring and material samples irradiation (TBMS) including:
   - channel for irradiation of samples (TMC),
   - tritium gas system providing tritium operation,
   - transport system for samples delivering to TBM and take out after irradiation and transportation to tritium and material laboratory.
2. System of neutron measurement arising in plasma on (D+T) и (D+D) fusion reactions.
3. Computer-information and analyzing facility (CIAF) includes:
   - tritium and structural material laboratories for investigation of tritium and material samples after irradiation in TMC,
   - information center for analyses of data from TBM's tritium system and calculation of neutron fluxes in ITER.

Proposed TBMS is useful to test using TBM of reactor ITER. Tritium breeder and material samples can be located for single/several plasma pulse periods.

The diagram of the proposed TBMS in ITER is shown on Fig. 2.

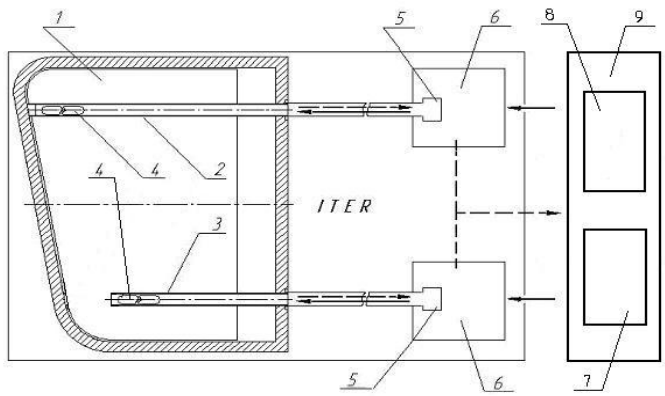

Fig. 2. The diagram of TBMS in ITER
1- TBZ of TBM, 2- channel (TMC) for irradiated samples, 3- channel (TMC) for tritium detectors, 4- casks with samples under irradiation, 5-load-in chamber, 6- transporter room, 7- tritium laboratory, 8- material laboratory, 9- tritium building
⟶ delivery of casks with samples;
- - → extraction of irradiated casks

A target of present research stage is development of TMC.

In order to estimate tritium breeding amount in TBZ of TBM (numerator in formula (2)) detectors of neutron irradiation and samples of tritium breeding materials are proposed.

Fission chamber and metal foil for further activation analysis and dielectrics for the fluencies determination via the structure analysis (diamond, special glasses) can be applied as these detectors. Lithium Orthosilicate (Li_4SiO_4) and lithium carbonate Li_2CO_3 are proposed as tritium breeding materials. Orthosilicate has same composition as breeder material of TBM TBZ but different amount of isotope lithium-6. Taking into account tritium breeding both on isotope mixture (^6Li + ^7Li) takes place for all neutron energies (from 14MeV to thermal) there are six samples with different lithium isotope content developed with availability /absence of thermal neutrons absorption (Table 1. in [8]) . In this case the channel is used for TBR monitoring only.

Transportation of the casks to the Module and back is proposed to realize by two methods: pneumatic with gas cooling and mechanical one.

3. Pneumatic conceptual method of sample convey to TBM

The canal (TMC) for irradiation materials is thought as two coaxial pipes (Ø 14x1 mm and Ø 20x1 mm). Coolant movement through the canal is possibly both straight and reveres. This depends on a mode of a TBMS operation.

The canal surrounded by TBZ beryllium contains three parts (Fig.3) [8]:

"operation" part with length ~ 0.55 m locating in TBM;

part between TBM back plate and operation room;

"leader" part with length ~ 0.5m for loading and unloading containers.

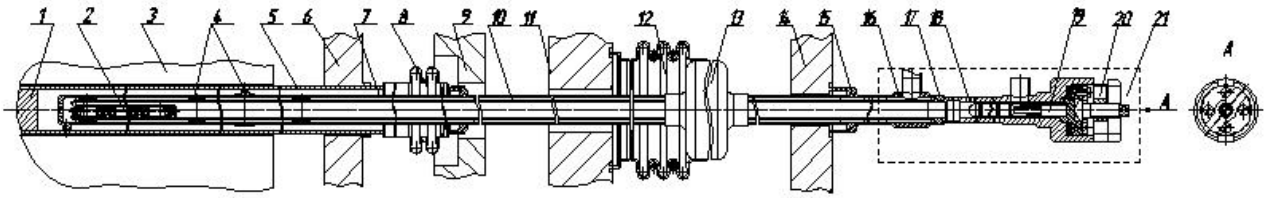

Fig. 3. Cross-section of MTBSM canal
1- beryllium plug, 2- container, 3- beryllium multiplyer, 4- separation elements, 5- of TBM shell, 6- back plate of TBM shell, 7- out side of canal pipe, 8- bellow, 9- frame, 10- inner pipe of canal, 11- shield plug, 12- armored bellows, 13- heat shield, 14- biological shield, 15- fastening unit ofcanal,16- union, 17- adapter, 18- load chamber, 19- fingered bushing, 20- bolt, 21- transporter.

Coaxial placement of the canal "operation" part in a rigid rib and fixing of an inner pipe to an outside pipe are provided by separating elements located along the canal with equal distance.

Monitoring and irradiated system contains the canal with samples, ancillary units and utility systems providing necessary modes of operations: cooling, sample transportation and blow- through of the canal. The blow-through is needed after load of containers with samples to remove air and before unload of the containers to remove a coolant which may contain tritium. These operations are carried-out during reactor pause between plasma pulses.

The diagram of the ancillary systems is shown in Fig. 4.

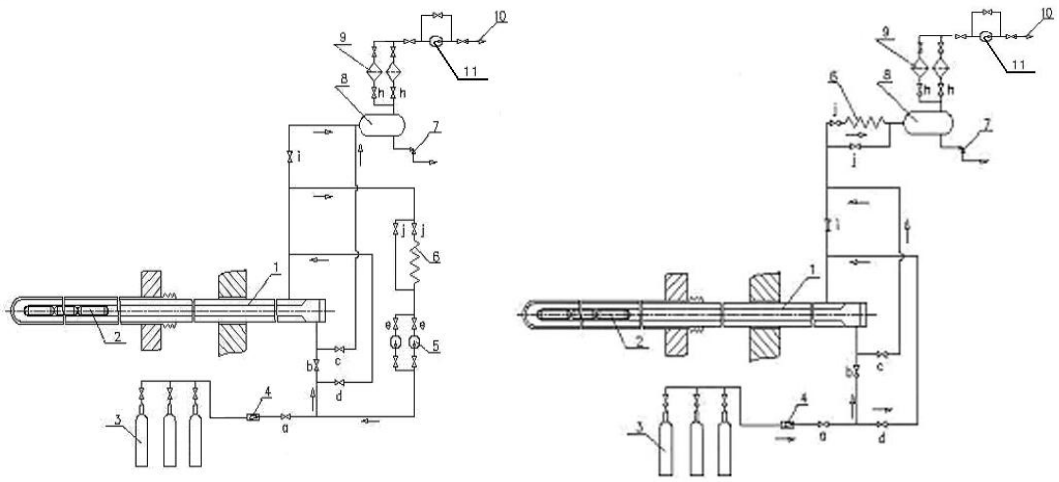

а б

Fig. 4. Conceptual diagram of TBMS system: with gas circulator (a) and more simple (b).
1- TMC of TMMS, 3- cask with tritiumbreeding samples, 3- gas cylinders, 4- pressure regulator, 5- circulator pumps, 6-heat exchanger, 7- safety valve, 8- tank, 9- purification system, 10- way to ventilation; a-h – close and control devices, 11- vacuum pump

There are two gas loops:

-open loop for operations with the containers to deliver and remove the samples by gas pulse using the tank (3),

- closed loop to cool the canal.

Gas is directed to the tank (8) under modes of transportation and blow- through of the canal and then passes through the purification unit (9) to the ventilation system (10). Using vacuum pump (10) is used for decontamination process and can provide necessary sample temperature. Safe valve (7) is in the tank (8) to prevent from gas pressure excess. The gas circulator (5) and the heat exchanger (6) are in the system to maintain of a canal temperature mode. Vacuum pump (11) can provide decontamination process and controlled temperature of a cask.

The capsule set is located in the cask to be delivered to the TMC and removed from it after plasma pulse.

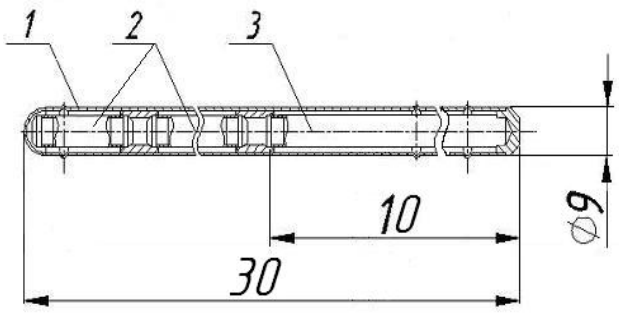

Fig. 5. Location of capsules with material samples in cask
1- container, 2- capsule, 3- material sample

Tritium breeder detector is initial main item under development of canal design. This is a capsule presenting hermetic cylinder cask closed by plugs to each end (Fig. 5). Sample for material irradiation is in the cask in contrast to initial variant. The sample (3) has 10 mm length.

Results of singl-dimension thermohydraulic calculation of the canal operation part are shown in Table 1.

Table 1.Thermohydraulic parameters of canal cooling system

Parameters	value
Power of heat sources removed from canal parts by cooler (Wt)	605
Maximum temperature of capsule shell (°C)	128,3
Cooler temperature on out-let of operation canal part (°C)	132,4
Cooler velocity on cask part of canal (m/c)	24,7

Calculation temperature in tritiumbreeding detector core is in limits 116,4 -152,4 °C under cooler temperature 87,3 - 97,3 °C on capsule places. More detail calculations are shown in [7].

4. Mechanical conceptual method of sample convey to TBM

Pneumatic method demands cooling system to provide necessary temperature for samples. This makes the system more complex and possibility of accidents more height. To simply system mechanical

method of sample convey to TBM is proposed.

The method is based on using of transport metal rods connected in consecutive order during delivery of container with samples to TBM. They are moved toward Module TBZ in pipe O18x1 mm (Fig.6).

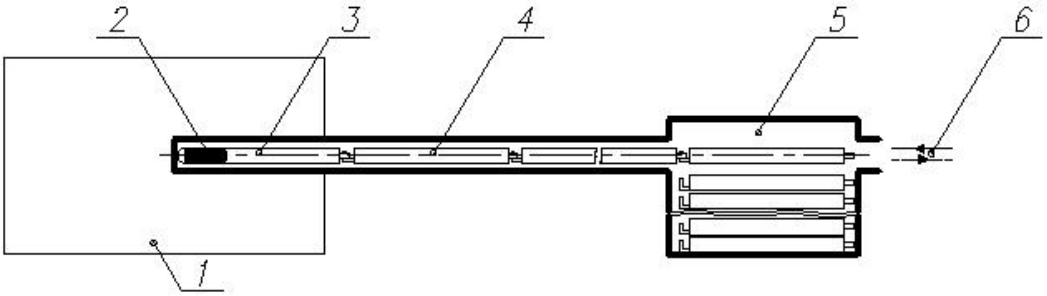

Fig. 6. Conception block-diagram of mechanical method of sample convey to TBM

1-ЗВТ ИБМ, 2- container with samples, 3-"operation" part of TBMS, 4- rod, 5- leader part of TBMS, 6-material sample

The canal contains three parts:

- "operation" part with length ~ 0.55 m locating in TBM;
- part between TBM back plate and operation room;
- "leader" part with length ~ 0.5m for loading and unloading containers.

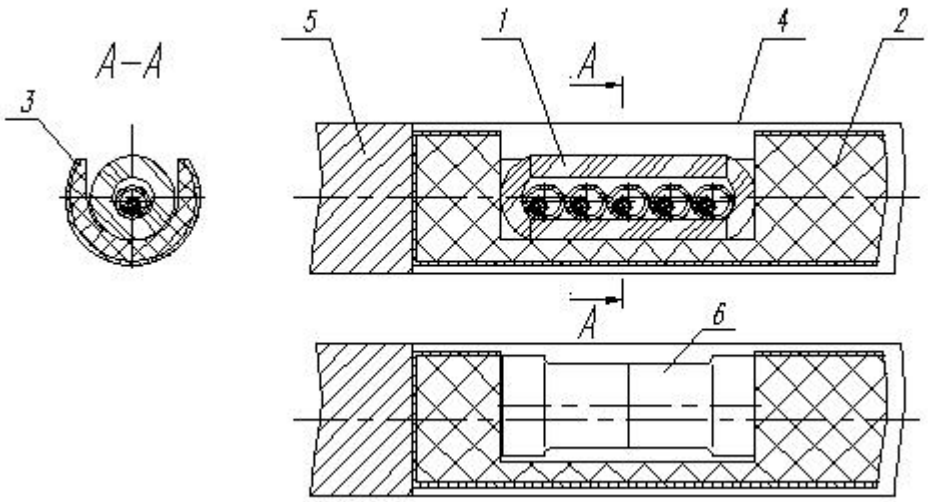

Fig. 7. Cross section of "operation" part of TBMS with lithium ceramic and/or material sample 1- cask with capsules, 2- graphite, 3- stainless steal shell, 4- inner pipe of CMMS, 5- Be inset

Material of the first rod (diameter 10 mm) with samples belonging "operation" part is graphite. Outside of shell is zirconium. Material of other rods (second part of system) can serve as shield on neutron and γ-irradiations.

"Operating" part contains lithium ceramic and/or material samples (Fig. 7). Material capsules for

samples are quartz glass.

The canal system contains only one gas system for tritium monitoring in the canal.

Neutron calculation was carried-out to estimate of heat distribution in the rod materials under reactor irradiation. The canal is in beryllium cylinder irradiated to face (Fig. 8)

Neutron source has reactor energy spectrum and isotropic distribution. Power of the source provides neutron load is equal the load for first wall of ITER – 0.8 Mwt/sm2 at total fusion power – 500 Mwt. Total density of heat generation in beryllium first wall is 5.36 Wt/sm3

Density of stainless steal is 7.39 g/sm^3, graphite – 2.25 g/sm^3, porous beryllium – 1.48 g/sm^3.

A gas gape between rod and beryllium takes into account.

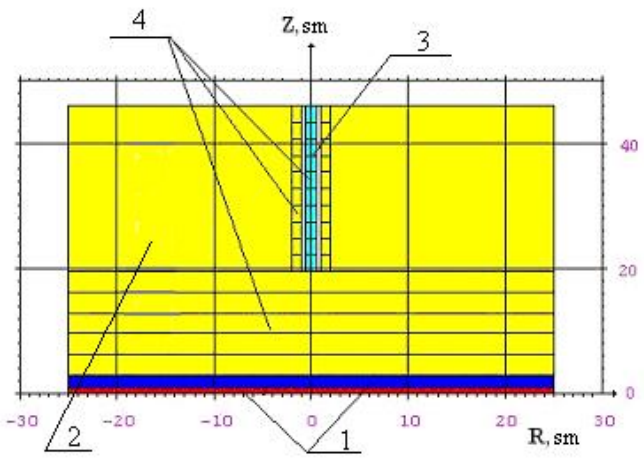

Fig. 8 Calculation model for R-Z space
1 –first wall, 2 – beryllium, 3 – steel/graphite rod, 4 – points to measure of heat generation

Results of heat and neutron calculations are in Table 2. Generate heat (q_v), porous beryllium temperature(T_{be}) and graphite temperature(T_{Gr}) on lengths of the hall. Coordinate (Z) is from back of Module.

Table 2. Temperature and heat generation on model height

Z, м	q_v, вт/м^3	T_{be}, °C	T_{Gr}, °C
0.000	6.29E04	500.0	500.3
0.024	8.97E04	502.9	503.5
0.047	11.9E04	505.9	506.6
0.071	15.7E04	508.8	509.8
0.094	20.5E04	511.8	513.2
0.118	26.6E04	514.7	516.7
0.141	34.2E04	517.7	520.0
0.165	44.8E04	520.0	522.3

Fig .9 demonstrates change of porous beryllium (1) and graphite temperature (2) as a function of distance from module back.

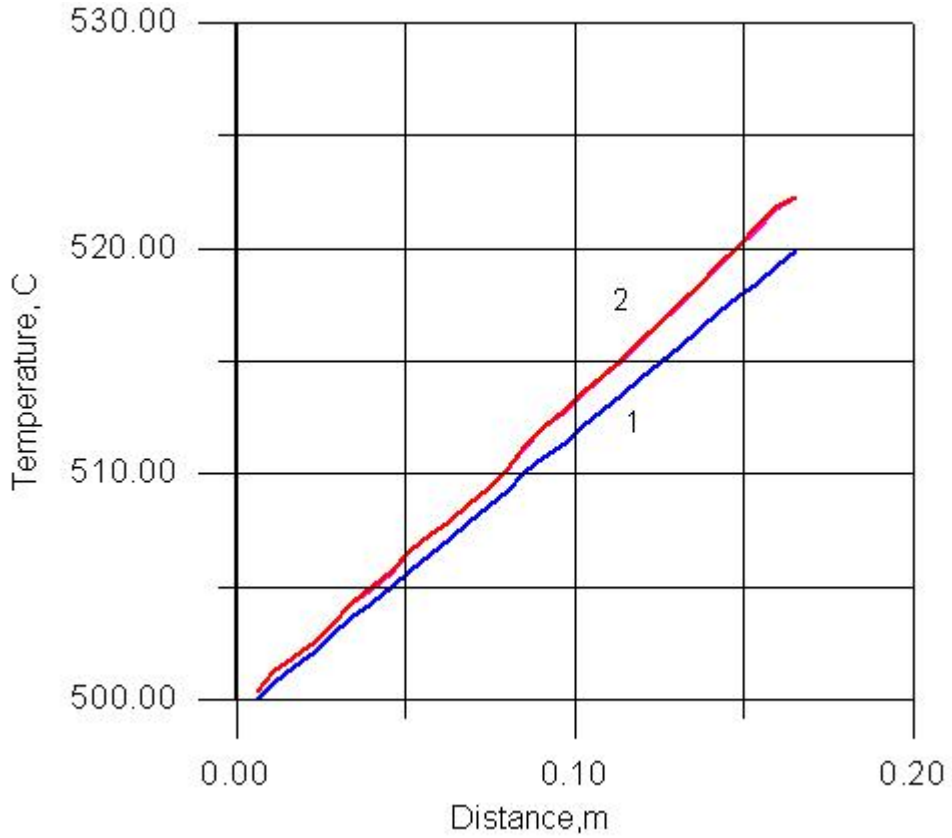

Fig. 9. Temperature of porous beryllium and graphite rod in core as function of distance from module back (m).

1 – temperature of porous beryllium;
2 – temperature in graphite rod.

Results of the calculations demonstrate temperature in a graphite core is equal porous beryllium temperature (maximum a difference is less 2.5^{o}C). Maximum temperature is 522.3 ^{o}C and doesn't exceed the limit for graphite operation (~1000 ^{o}C) and for stainless steal (~600 ^{o}C) too.

Conclusion

1. Conception of tritium breeding ratio measurement and irradiation of material samples has been proposed to irradiate of the samples and to estimate tritium breeder rate in ceramic ITER TBM by experimental method under ITER normal operation.
2. Canal design is developed for irradiation of ceramic lithium, neutron detector, material samples during plasma pulse in ITER and for fast its transportation to analytical laboratory.
4. Carried-out calculations demonstrated cooling system for pneumatic method provides necessary temperature mode of canal operations and transport system provides fast extraction and deliver of tritium detectors.
5. Calculation investigation for mechanical variant of TBMS has demonstrated that the system meets the requirements of the canal temperature modes. Structural materials of TMC can operate under reactor irradiation.

References

1. V.Barabash, The ITER International Team, A.Peacock, et al. Materials challenges for ITER – Current status and future activities. J.Nucl. Mater. 367-370 (2007) 21-32

2. L.Giancarli, V.Chuyanov, M.Abdu, et al. The blanket modulus in ITER: An overview on proposed designs and required DEMO-relevant materials. J.Nucl. Mater. 367-370 (2007) 1271-1280.

3. C.P.C.Wong, V.Chernov, A.Kimura, et al. ITER-Test blanket module functional materials. J.Nucl. Mater. 367-370 (2007) 1287-1292.

4. Yu.A.Sokolov. Overview of the Russian DEMO Plant Study. Fus. Eng. and Des., 29 (1995), p. 18-27.

5. D.I. Evgrafova, Z.V. Ershova, V.K, Kapyshev, V.I. Sascharov, Tritium measurement arisen under lithium irradiation by neutrons with fissile spectrum using Cf-252, Proceeding of All Union conference for Engineering Problem of Controlled Fusion Reactors, Leningrad 28-30 June 1977, v. 2, p. 309, NII EFD, L., 1977

6. V.Kapyshev, N. Ychnov, V. Poliksha, A. Sidorov Experimental estimation of tritium breeder parameters in Experimental Breeding Submodule of ITER blanket. VANT vol.4 (2005) p.19-29

7. V.Kapyshev, V. Kovalenko, V. Poliksha, A. Sidorov, Yu. Strebkov and N. Yuchnov
On monitoring the tritium-breeding ratio in a fusion reactor
Plasma Devices and Operations, Volume 16, Issue 2, June 2008, p.135-145

8. V.Kapyshev*, V.Kovalenko, V.Poliksha, A.Sidorov, Yu.Strebkov, N.Yukhnov “Experimental Estimate of Tritium Production Parameters for RF Test Blanket Module” Fusion Eng. Des. 83 (2008) 1204-1207

On monitoring the tritium breeder in ITER Test Blanket Module

V.Kapyshev, V.Kovalenko, V.Poliksha, Yu.Strebkov, N.Yukhnov

Federal State Unitary Enterprise "Dollezhal Research and Development Institute of Power Engineering",
PO Box 788, Moscow 101000, Russian Federation

Tritium breeder is a most process among controlled fusion reactor engineer problems. Tritium Breeding Ratio (TBR) is a main parameter characterizing of the process. TBR can be submitted as a ratio of the amount tritium produced in the fusion reactor to the amount of tritium that burned up in the reactor plasma. A concept and block-schema of tritium breeding monitoring and experimental estimation of the tritium-breeding ratio in DEMO and ITER are discussed. Systems for experimental estimation of the TBR and the tritium-breeding dynamic parameters in a Tritium Breeding Modules (TBM) of the ITER are proposed.

The systems are based on tritium and neutron flux measurements under ITER plasma experiments and use lithium ortho-silicate and lithium carbonate as tritium detectors and the neutron detectors. Beryllium and differences isotopes lithum-6 and lithium-7 are applied. The detectors are delivered to tritium breeding zone (TBZ) of the TBM on channels connected the TBM and an operating zone of ITER. Pneumatic and mechanic methods are applied to deliver the samples to the TBZ of the TBM and to extract the samples using monitor channels during plasma operational pauses.

Results of the channel parameter calculations and comparison of the pneumatic and mechanic systems are presented in the paper.

Corresponding Author: Vicor K. Kapyshev
kapyshev@nikiet.ru
Federal State Unitary Enterprise "Dollezhal Research and Development Institute of Power Engineering"
Moscow 101000, Russian Federation
Tel.: +7-499-763-0314; fax: +7-499-788-2052

On Monitoring the Tritium Breeder in ITER Test Blanket Module

V.Kapyshev, V.Kovalenko, V.Poliksha, Yu.Strebkov, N.Yukhnov.

Presented by V.K. Kapyshev

Open Joint-Stock Company "Dollezhal Research and Development Institute of Power Engineering".

P.O.Box 788, Moscow 101000, Russian Federation, e-mail: nikiet@nikiet.ru

Ceramic Breeder Blanket Interactions (CBBI-15)
3-5 September 2009, Sapporo, Japan

Content

1. Tritium Breeding Ratio (TBR) of DEMO / ITER

The most important tritium cycle parameters :

-tritium breeding ratio (TBR),

- amount of tritium in the reactor,

- radiation safety parameters.

In general TBR is defined as:

$$TBR = Q_{reactor} / Q_{plasma} \qquad (1)$$

$Q_{reactor}$ – tritium amount breaded in plasma and in reactor blanket,

Q_{plasma} - tritium amount burned-up in plasma.

1.1 Proposals for TBR monitoring in DEMO and test of its in ITER

1. TBR - constant
2. Tritium is breaded in tritium breeding zone (TBZ) of TBM on lithium-6 (Q_{Li-6}), lithium-7 (Q_{Li-7}), beryllium (Q_{Be})

$$Q_{reactor} = Q_{Li-6}+Q_{Li-7}+Q_{Be}$$

3. $Q_{plasma} = Q_{(D,T)}$ - tritium amount burned-up in plasma on reaction D-T

TBR - number per 1 pulse accordingly formula (1)

$$TBR=(Q_{Li-6}+Q_{Li-7}+Q_{Be})/ Q_{(D,T)} \qquad (2)$$

1.2 Conception of TBR monitoring using Test Breeding Modules of ITER

Conception of **TBR** monitoring in reactor includes:

- measurements of numerator and denominator in formula (1),
- calculation both.

Experimental definition of tritium amount burned in plasma (denominator in formula (1)) is proposed to realize by measurement of neutrons number arisen in result (D-T) nuclear fusion.

Numerator demonstrates tritium breeder in a reactor blanket under neutron interaction with lithium and beryllium isotopes

---

TBR for the DEMO with ceramic blanket ~1.05.

Sufficiently accuracy definition of tritium amounts breaded in a module (numerator in (1)) isn't really possibly by continue measurements in purge-gas system.

The most accuracy measurements can be done in case of tritium breeder and neutron detectors location in TBZ for short time and follow remove of its from TBZ after plasma pulse, delivery to an analytical laboratory for analyzing.

Detectors can be located for one plasma pulse period

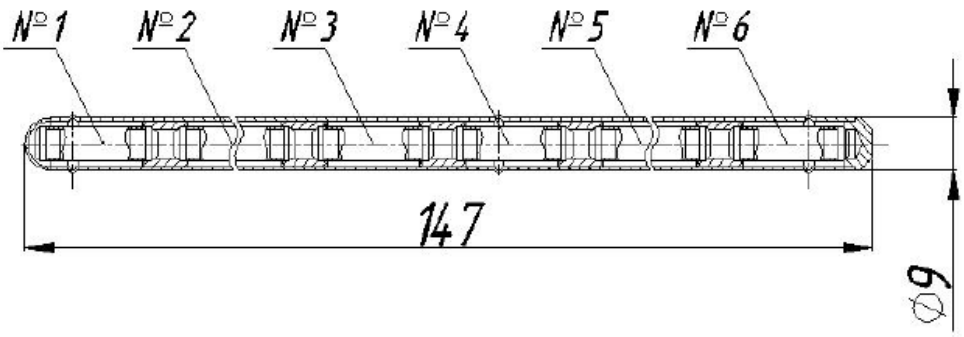

Fig. 1. Location of capsules with material samples in cask

This is a capsule presenting hermetic cylinder cask closed by plugs to each end.

Table 1. Content of samples in cask

№ capsule	Tritium breeder material	Isotope ratio (^6Li / ^7Li)	absorbers of thermal neutrons
1	Li_2CO_3	natural	–
2	Li_4SiO_4	natural	+
3	Li_4SiO_4	natural	–
4	Li_4SiO_4	~ 1	–
5	Li_4SiO_4	~ 1	+
6	Li_4SiO_4	~ 10	–

"+" –yes, "-"- no

Operation for experimental definition of TBR was begun else in SU in 80-th.

Isotope **Cf-252** was chosen as neutron source and lithium oxide carbonate as tritium breeder material

Perfect of tritium breeder methods were followed in 90-th in a frame of reactor experiments for investigations of effects of neutron irradiation on lithium ceramic properties and tritium balance carrying out

---

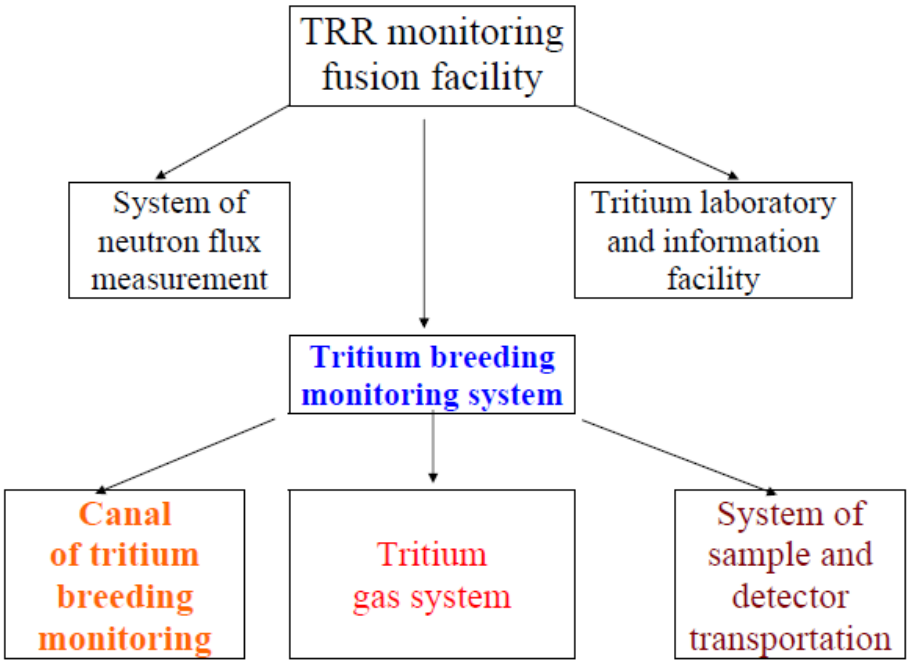

Fig. 2. Conceptual diagram of TBR monitoring in Fusion Reactor

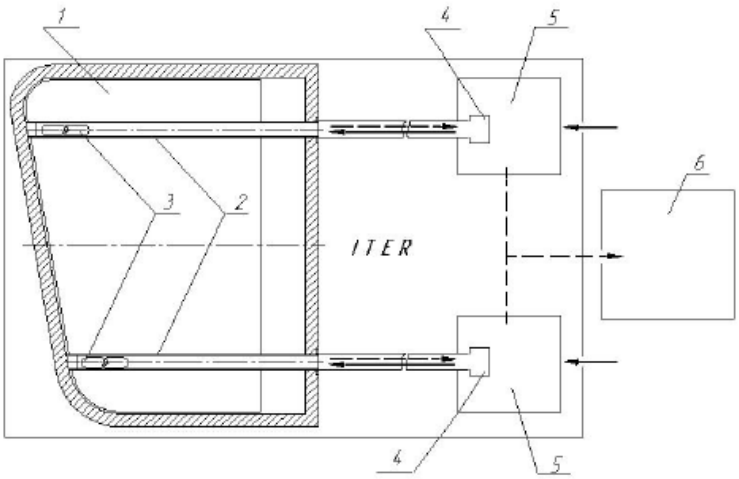

Fig. 3. Concept of TBR monitoring using TBM of ITER

1- TBZ of TBM, 2- Tritium Breeding Canals (TBC) for samples, 3- casks with samples under irradiation, 4-in-put chamber, 5- transporter room, 6- tritium laboratory

→ delivery of casks with samples;

--→ extraction of irradiated casks

---

2. Pneumatic and mechanical systems of transportation the casks to the Module

The canal (TBC) contains three parts:

- "operation" part with length ~ 0.55 m locating in TBM;
- part between TBM back plate and operation room;
- "leader" part with length ~ 0.5m for loading and unloading casks.

Transportation of the cask to the Module and back is proposed to do by two methods: pneumatic with gas cooling and mechanical.

2.1 Initial Design of Pneumatic Tritium Breeding Canal (TBC)

The canal (TMC) for irradiation materials is thought as two coaxial pipes (Ø 14x1 mm and Ø 20x1 mm). Coolant movement through the canal is possibly both straight and reveres.

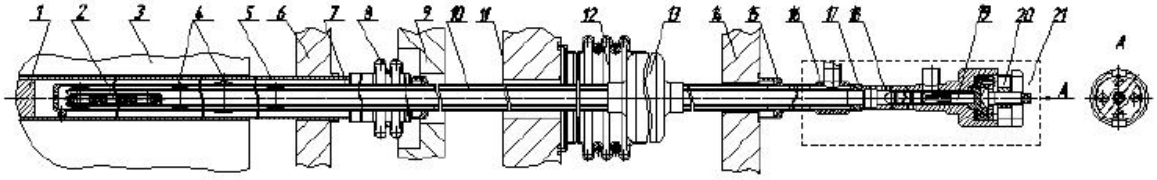

Fig. 6. Longitudinal section of TBC

1- beryllium plug, 2- container, 3- beryllium multiplier, 4- separation elements, 5- rib of TBSM case, 6- back plate of TBM case, 7- out side of canal pipe, 8- bellow, 9- frame, 10- inner pipe of canal, 11- shield plug, 12- armored bellows, 13- heat shield, 14- biological shield, 15- fastening unit of canal,16- union, 17- adapter, 18- load chamber, 19- fingered bushing, 20- bolt, 21- transporter.

Monitoring and irradiated system contains:

- canal with samples,
- ancillary units,
- utility systems providing necessary modes of operations (cooling, sample transportation and blow- through of the canal).

The blow-through is needed after load of containers with samples to remove air and before unload of the containers to remove a coolant which may contain tritium.

These operations are carried-out during reactor pause between plasma pulses.

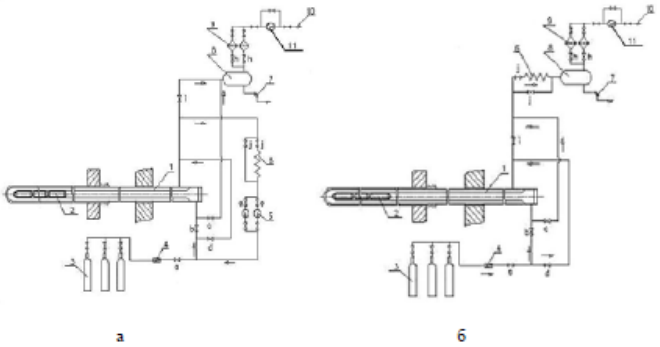

Fig. 3. Conceptual diagram of ancillary systems: with gas circulator (a) and simpler (b).

1- TMC, 3- cask with tritium breeding samples, 3- gas cylinders, 4- pressure regulator, 5- circulator pumps, 6-heat exchanger, 7- safety valve, 8- tank, 9- purification system, 10- way to ventilation; a-h – close and control devices, 11- vacuum pump

---

Table 1.Thermohydraulic parameters of canal cooling system

Parameters	value
Power of heat sources removed from canal parts by cooler (Wt)	605
Maximum temperature of capsule shell (°C)	128,3
Cooler temperature on out-let of operation canal part (°C)	132,4
Cooler velocity on cask part of canal (m/c)	24,7

Calculation temperature in tritium breeding detector core is in limits 116.4 -152.4 °C under cooler temperature 87.3 – 97.3 °C on capsule places.

2.2 Initial Design of Mechanical Tritium Breeding Canal (TBC)

2.2.1 Initial design of TBC

Pneumatic method demands cooling system to provide necessary temperature for samples. This makes the system more complex and possibility of accidents more.

The method is based on using of transport metal rods connected in consecutive order during delivery of container with samples to TBM. They are moved toward Module TBZ in pipe Ø18x1 mm (Fig.5).

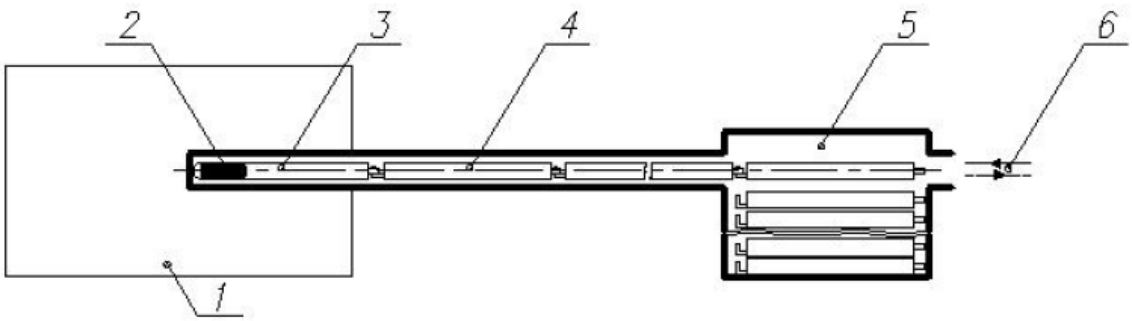

Fig. 5. Conceptual diagram of mechanical TBC
1-TBZ TBM, 2- cask with samples, 3-"operation" part of TBMS, 4- rod, 5- leader part of TBMS, 6-material sample

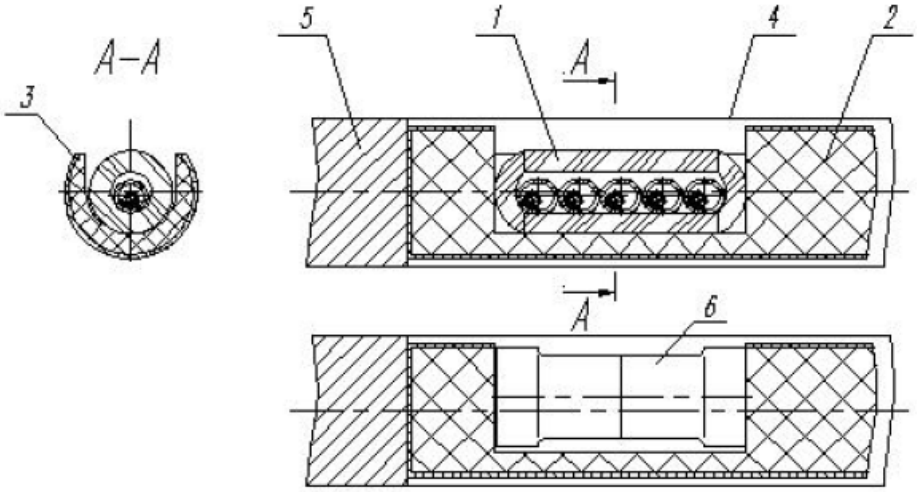

Fig. 6. Cross section of "operation" part of TBMS with lithium ceramic and/or material sample
1- cask with capsules, 2- graphite, 3- stainless steel shell, 4- inner pipe of CMMS, 5- Be inset

---

2.2.2 Neutron calculation of heat distribution in the rod materials

neutron load for first wall of ITER – 0.8 Mwt/cm2

total fusion power – 500 Mwt.

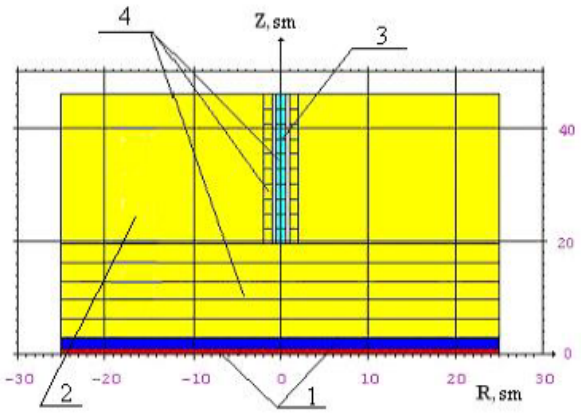

Fig. 7 Calculation model for R-Z space
1 –first wall, 2 – beryllium, 3 – steel/graphite rod, 4 – points to measure of heat generation

Table 2. Temperature and heat generation on model height

Z, м	q_v, вт/м^3	T_{be}, °C	T_{Gr}, °C
0.000	6.29E04	500.0	500.3
0.024	8.97E04	502.9	503.5
0.047	11.9E04	505.9	506.6
0.071	15.7E04	508.8	509.8
0.094	20.5E04	511.8	513.2
0.118	26.6E04	514.7	516.7
0.141	34.2E04	517.7	520.0
0.165	44.8E04	520.0	522.3

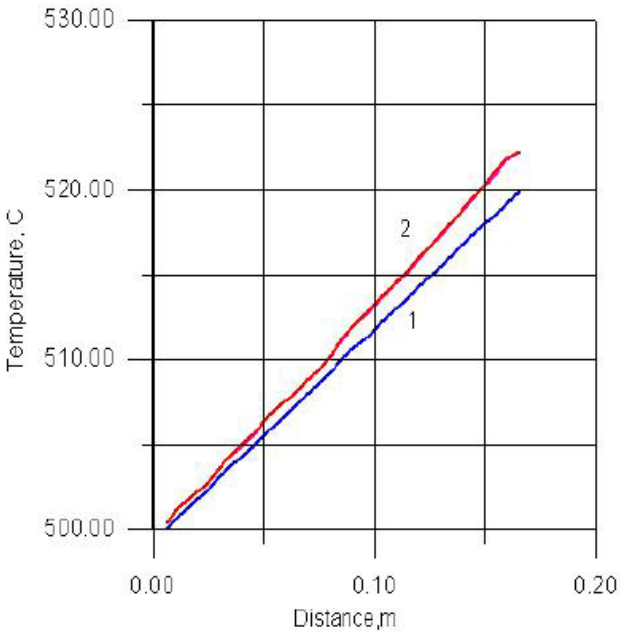

Fig. 8. Temperature of porous beryllium and graphite rod in core as function of distance from module back (m).
1 – temperature of porous beryllium, 2 – temperature in graphite rod.

R&D

1. Laboratory devices for investigation of pneumatic systems
2. Selection and irradiation of neutron detectors in IVV-2M nuclear reactor
3. Development of analytical methods for measurement of tritium breaded in lithium detectors under irradiation in IVV-2M nuclear reactor

---

Conclusion

1. Conception of tritium breeding ratio measurement and irradiation of material samples has been proposed to irradiate the samples and estimate tritium breeder rate in ceramic ITER TBM by experimental method under ITER normal operation.

2. Canal design is developed for irradiation of ceramic lithium, neutron detector, material samples during plasma pulse in ITER and for fast its transportation to analytical laboratory.

4. Carried-out calculations demonstrated cooling system for pneumatic method provides necessary temperature mode of canal operations and transport system provides fast extraction and deliver of tritium detectors.

5. Calculation investigation for mechanical variant of TBMS has demonstrated that the system meets the requirements of the canal temperature modes. Structural materials of TMC can operate under reactor irradiation.

Appendix 1

List of Participants of CBBI-15

Name	e-mail	Institute
Kisaburo Azuma	E-Mail:azuma@flanker.q.t.u-tokyo.ac.jp	the University of Tokyo
Lorenzo V. Boccaccini	lorenzo.boccaccini@inr.fzk.de	Karlsruhe Institute of Technology (KIT)
Paritosh Chaudhuri	paritc@gmail.com	Institute for Plasma Research
Mikio Enoeda	enoeda.miki@jaea.go.jp	Blanket Tech Gr., JAEA
Alexander V. Fedorov	fedorov@nrg.eu	NRG Petten
Tomoki Hanada	hanada@nucl.kyushu-u.ac.jp	Kyushu University
Tomoaki Hino	tomhino@qe.eng.hokudai.ac.jp	Hokkaido Univ.
Takanori Hirose	hirose.takanori@jaea.go.jp	Blanket Tech Gr., JAEA
Masaki Honda	honda@nfi.co.jp	Nuclear Fuel Industries, LTD.
Tuyoshi Hoshino	hoshino.tsuyoshi@jaea.go.jp	Blanket Irradiation G., JAEA
Ryan Hunt	rhunt@fusion.ucla.edu	UCLA
Kenichiro Ikuno	ikuno@flanker.q.t.u-tokyo.ac.jp	the University of Tokyo
Victor Kapyshev	kapyshev@nikiet.ru	Federal State Unitary Enterprise “Dollezhal Research and Development Institute of Power Engineering”
Regina Knitter	regina.knitter@imf.fzk.de	Karlsruhe Institute of Technology (KIT)
Rainer Laesser	rainer.laesser@f4e.europa.eu	Fusion for Energy
A. J. Magielsen	magielsen@nrg.eu	NRG, Petten
D. Mandal	dmandal@barc.gov.in	Chemical Engineering Division, Bhabha Atomic Research Centre
Daisuke Masuyama	masuyama@flanker.q.t.u-tokyo.ac.jp	the University of Tokyo
Masabumi Nishikawa	nishikaw@nucl.kyushu-u.ac.jp	Kyushu University
Takuji Oda	oda@flanker.q.t.u-tokyo.ac.jp	the University of Tokyo
Fumiaki Oikawa	oikawa.fumiaki@jaea.go.jp	Blanket Irradiation G., JAEA
D. Saithyamoorthy	dsathiyamoorthy@gmail.com	BARC
Hisashi Tanigawa	tanigawa.hisashi@jaea.go.jp	Blanket Tech Gr., JAEA
Hiroki Tsuchihira	tsuchihira@flanker.q.t.u-tokyo.ac.jp	the University of Tokyo
Daisuke Yamauchi	yamauchi@flanker.q.t.u-tokyo.ac.jp	the University of Tokyo
Alice Ying	ying@fusion.ucla.edu	UCLA
Milan Zmitko	milan.zmitko@f4e.europa.eu	Fusion for Energy

This is a blank page.

国際単位系（SI）

表１．SI 基本単位

基本量	SI 基本単位	
	名称	記号
長さ	メートル	m
質量	キログラム	kg
時間	秒	s
電流	アンペア	A
熱力学温度	ケルビン	K
物質量	モル	mol
光度	カンデラ	cd

表２．基本単位を用いて表されるSI組立単位の例

組立量	SI 基本単位	
	名称	記号
面積	平方メートル	m^2
体積	立法メートル	m^3
速さ，速度	メートル毎秒	m/s
加速度	メートル毎秒毎秒	m/s^2
波数	毎メートル	m^{-1}
密度，質量密度	キログラム毎立方メートル	kg/m^3
面積密度	キログラム毎平方メートル	kg/m^2
比体積	立方メートル毎キログラム	m^3/kg
電流密度	アンペア毎平方メートル	A/m^2
磁界の強さ	アンペア毎メートル	A/m
量濃度[a]，濃度	モル毎立方メートル	mol/m^3
質量濃度	キログラム毎立法メートル	kg/m^3
輝度	カンデラ毎平方メートル	cd/m^2
屈折率[b]	（数字の）　1	1
比透磁率[b]	（数字の）　1	1

(a) 量濃度（amount concentration）は臨床化学の分野では物質濃度（substance concentration）ともよばれる。
(b) これらは無次元量あるいは次元１をもつ量であるが、そのことを表す単位記号である数字の１は通常は表記しない。

表３．固有の名称と記号で表されるSI組立単位

組立量	SI 組立単位			
	名称	記号	他のSI単位による表し方	SI基本単位による表し方
平面角	ラジアン[b]	rad	1 [b]	m/m
立体角	ステラジアン[b]	sr[c]	1 [b]	m^2/m^2
周波数	ヘルツ[d]	Hz		s^{-1}
力	ニュートン	N		$m\ kg\ s^{-2}$
圧力，応力	パスカル	Pa	N/m^2	$m^{-1}\ kg\ s^{-2}$
エネルギー，仕事，熱量	ジュール	J	N m	$m^2\ kg\ s^{-2}$
仕事率，工率，放射束	ワット	W	J/s	$m^2\ kg\ s^{-3}$
電荷，電気量	クーロン	C		s A
電位差（電圧），起電力	ボルト	V	W/A	$m^2\ kg\ s^{-3}\ A^{-1}$
静電容量	ファラド	F	C/V	$m^{-2}\ kg^{-1}\ s^4\ A^2$
電気抵抗	オーム	Ω	V/A	$m^2\ kg\ s^{-3}\ A^{-2}$
コンダクタンス	ジーメンス	S	A/V	$m^{-2}\ kg^{-1}\ s^3\ A^2$
磁束	ウエーバ	Wb	Vs	$m^2\ kg\ s^{-2}\ A^{-1}$
磁束密度	テスラ	T	Wb/m^2	$kg\ s^{-2}\ A^{-1}$
インダクタンス	ヘンリー	H	Wb/A	$m^2\ kg\ s^{-2}\ A^{-2}$
セルシウス温度	セルシウス度[e]	℃		K
光束	ルーメン	lm	cd sr[c]	cd
照度	ルクス	lx	lm/m^2	$m^{-2}\ cd$
放射性核種の放射能[f]	ベクレル[d]	Bq		s^{-1}
吸収線量, 比エネルギー分与, カーマ	グレイ	Gy	J/kg	$m^2\ s^{-2}$
線量当量, 周辺線量当量, 方向性線量当量, 個人線量当量	シーベルト[g]	Sv	J/kg	$m^2\ s^{-2}$
酸素活性	カタール	kat		$s^{-1}\ mol$

(a)SI接頭語は固有の名称と記号を持つ組立単位と組み合わせても使用できる。しかし接頭語を付した単位はもはやコヒーレントではない。
(b)ラジアンとステラジアンは数字の１に対する単位の特別な名称で、量についての情報をつたえるために使われる。実際には、使用する時には記号rad及びsrが用いられるが、習慣として組立単位としての記号である数字の１は明示されない。
(c)測光学ではステラジアンという名称と記号srを単位の表し方の中に、そのまま維持している。
(d)ヘルツは周期現象についてのみ、ベクレルは放射性核種の統計的過程についてのみ使用される。
(e)セルシウス度はケルビンの特別な名称で、セルシウス温度を表すために使用される。セルシウス度とケルビンの単位の大きさは同一である。したがって、温度差や温度間隔を表す数値はどちらの単位で表しても同じである。
(f)放射性核種の放射能（activity referred to a radionuclide）は、しばしば誤った用語で"radioactivity"と記される。
(g)単位シーベルト（PV,2002,70,205）についてはCIPM勧告2（CI-2002）を参照。

表４．単位の中に固有の名称と記号を含むSI組立単位の例

組立量	SI 組立単位		
	名称	記号	SI 基本単位による表し方
粘度	パスカル秒	Pa s	$m^{-1}\ kg\ s^{-1}$
力のモーメント	ニュートンメートル	N m	$m^2\ kg\ s^{-2}$
表面張力	ニュートン毎メートル	N/m	$kg\ s^{-2}$
角速度	ラジアン毎秒	rad/s	$m\ m^{-1}\ s^{-1}=s^{-1}$
角加速度	ラジアン毎秒毎秒	rad/s^2	$m\ m^{-1}\ s^{-2}=s^{-2}$
熱流密度，放射照度	ワット毎平方メートル	W/m^2	$kg\ s^{-3}$
熱容量，エントロピー	ジュール毎ケルビン	J/K	$m^2\ kg\ s^{-2}\ K^{-1}$
比熱容量，比エントロピー	ジュール毎キログラム毎ケルビン	J/(kg K)	$m^2\ s^{-2}\ K^{-1}$
比エネルギー	ジュール毎キログラム	J/kg	$m^2\ s^{-2}$
熱伝導率	ワット毎メートル毎ケルビン	W/(m K)	$m\ kg\ s^{-3}\ K^{-1}$
体積エネルギー	ジュール毎立方メートル	J/m^3	$m^{-1}\ kg\ s^{-2}$
電界の強さ	ボルト毎メートル	V/m	$m\ kg\ s^{-3}\ A^{-1}$
電荷密度	クーロン毎立方メートル	C/m^3	$m^{-3}\ sA$
表面電荷	クーロン毎平方メートル	C/m^2	$m^{-2}\ sA$
電束密度，電気変位	クーロン毎平方メートル	C/m^2	$m^{-2}\ sA$
誘電率	ファラド毎メートル	F/m	$m^{-3}\ kg^{-1}\ s^4\ A^2$
透磁率	ヘンリー毎メートル	H/m	$m\ kg\ s^{-2}\ A^{-2}$
モルエネルギー	ジュール毎モル	J/mol	$m^2\ kg\ s^{-2}\ mol^{-1}$
モルエントロピー, モル熱容量	ジュール毎モル毎ケルビン	J/(mol K)	$m^2\ kg\ s^{-2}\ K^{-1}\ mol^{-1}$
照射線量（X線及びγ線）	クーロン毎キログラム	C/kg	$kg^{-1}\ sA$
吸収線量率	グレイ毎秒	Gy/s	$m^2\ s^{-3}$
放射強度	ワット毎ステラジアン	W/sr	$m^4\ m^{-2}\ kg\ s^{-3}=m^2\ kg\ s^{-3}$
放射輝度	ワット毎平方メートル毎ステラジアン	$W/(m^2\ sr)$	$m^2\ m^{-2}\ kg\ s^{-3}=kg\ s^{-3}$
酵素活性濃度	カタール毎立方メートル	kat/m^3	$m^{-3}\ s^{-1}\ mol$

表５．SI 接頭語

乗数	接頭語	記号	乗数	接頭語	記号
10^{24}	ヨタ	Y	10^{-1}	デシ	d
10^{21}	ゼタ	Z	10^{-2}	センチ	c
10^{18}	エクサ	E	10^{-3}	ミリ	m
10^{15}	ペタ	P	10^{-6}	マイクロ	μ
10^{12}	テラ	T	10^{-9}	ナノ	n
10^{9}	ギガ	G	10^{-12}	ピコ	p
10^{6}	メガ	M	10^{-15}	フェムト	f
10^{3}	キロ	k	10^{-18}	アト	a
10^{2}	ヘクト	h	10^{-21}	ゼプト	z
10^{1}	デカ	da	10^{-24}	ヨクト	y

表６．SIに属さないが、SIと併用される単位

名称	記号	SI 単位による値
分	min	1 min=60s
時	h	1h =60 min=3600 s
日	d	1 d=24 h=86 400 s
度	°	1°=(π/180) rad
分	’	1’=(1/60)°=(π/10800) rad
秒	”	1”=(1/60)’=(π/648000) rad
ヘクタール	ha	$1ha=1hm^2=10^4m^2$
リットル	L，l	$1L=11=1dm^3=10^3cm^3=10^{-3}m^3$
トン	t	$1t=10^3\ kg$

表７．SIに属さないが、SIと併用される単位で、SI単位で表される数値が実験的に得られるもの

名称	記号	SI 単位で表される数値
電子ボルト	eV	$1eV=1.602\ 176\ 53(14)\times10^{-19}J$
ダルトン	Da	$1Da=1.660\ 538\ 86(28)\times10^{-27}kg$
統一原子質量単位	u	1u=1 Da
天文単位	ua	$1ua=1.495\ 978\ 706\ 91(6)\times10^{11}m$

表８．SIに属さないが、SIと併用されるその他の単位

名称	記号	SI 単位で表される数値
バール	bar	$1\ bar=0.1MPa=100kPa=10^5Pa$
水銀柱ミリメートル	mmHg	1mmHg=133.322Pa
オングストローム	Å	$1\ Å=0.1nm=100pm=10^{-10}m$
海里	M	1 M=1852m
バーン	b	$1\ b=100fm^2=(10^{-12}cm)2=10^{-28}m^2$
ノット	kn	1 kn=(1852/3600)m/s
ネーパ	Np	SI単位との数値的な関係は、対数量の定義に依存。
ベル	B	
デジベル	dB	

表９．固有の名称をもつCGS組立単位

名称	記号	SI 単位で表される数値
エルグ	erg	$1\ erg=10^{-7}\ J$
ダイン	dyn	$1\ dyn=10^{-5}N$
ポアズ	P	$1\ P=1\ dyn\ s\ cm^{-2}=0.1Pa\ s$
ストークス	St	$1\ St\ =1cm^2\ s^{-1}=10^{-4}m^2\ s^{-1}$
スチルブ	sb	$1\ sb\ =1cd\ cm^{-2}=10^4cd\ m^{-2}$
フォト	ph	$1\ ph=1cd\ sr\ cm^{-2}\ 10^4lx$
ガル	Gal	$1\ Gal\ =1cm\ s^{-2}=10^{-2}ms^{-2}$
マクスウェル	Mx	$1\ Mx\ =1G\ cm^2=10^{-8}Wb$
ガウス	G	$1\ G\ =1Mx\ cm^{-2}\ =10^{-4}T$
エルステッド[c]	Oe	$1\ Oe \triangleq (10^3/4\pi)A\ m^{-1}$

(c) ３元系のCGS単位系とSIでは直接比較できないため、等号「 ≙ 」は対応関係を示すものである。

表10．SIに属さないその他の単位の例

名称	記号	SI 単位で表される数値
キュリー	Ci	$1\ Ci=3.7\times10^{10}Bq$
レントゲン	R	$1\ R = 2.58\times10^{-4}C/kg$
ラド	rad	$1\ rad=1cGy=10^{-2}Gy$
レム	rem	$1\ rem=1\ cSv=10^{-2}Sv$
ガンマ	γ	1 γ =1 nT=10-9T
フェルミ		1フェルミ=1 fm=10-15m
メートル系カラット		1メートル系カラット = 200 mg = 2×10-4kg
トル	Torr	1 Torr = (101 325/760) Pa
標準大気圧	atm	1 atm = 101 325 Pa
カロリー	cal	1cal=4.1858J（「15℃」カロリー），4.1868J（「IT」カロリー）4.184J（「熱化学」カロリー）
ミクロン	μ	1 μ =1μm=10^{-6}m

（第8版，2006年改訂）